

NASA/CR-2009-215932



Damage Arresting Composites for Shaped Vehicles

Phase 1 Final Report

*Alex Velicki
The Boeing Company, Huntington Beach, California*

September 2009

NASA STI Program . . . in Profile

Since its founding, NASA has been dedicated to the advancement of aeronautics and space science. The NASA scientific and technical information (STI) program plays a key part in helping NASA maintain this important role.

The NASA STI program operates under the auspices of the Agency Chief Information Officer. It collects, organizes, provides for archiving, and disseminates NASA's STI. The NASA STI program provides access to the NASA Aeronautics and Space Database and its public interface, the NASA Technical Report Server, thus providing one of the largest collections of aeronautical and space science STI in the world. Results are published in both non-NASA channels and by NASA in the NASA STI Report Series, which includes the following report types:

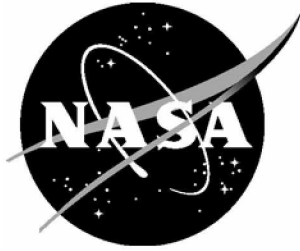
- **TECHNICAL PUBLICATION.** Reports of completed research or a major significant phase of research that present the results of NASA programs and include extensive data or theoretical analysis. Includes compilations of significant scientific and technical data and information deemed to be of continuing reference value. NASA counterpart of peer-reviewed formal professional papers, but having less stringent limitations on manuscript length and extent of graphic presentations.
- **TECHNICAL MEMORANDUM.** Scientific and technical findings that are preliminary or of specialized interest, e.g., quick release reports, working papers, and bibliographies that contain minimal annotation. Does not contain extensive analysis.
- **CONTRACTOR REPORT.** Scientific and technical findings by NASA-sponsored contractors and grantees.
- **CONFERENCE PUBLICATION.** Collected papers from scientific and technical conferences, symposia, seminars, or other meetings sponsored or co-sponsored by NASA.
- **SPECIAL PUBLICATION.** Scientific, technical, or historical information from NASA programs, projects, and missions, often concerned with subjects having substantial public interest.
- **TECHNICAL TRANSLATION.** English-language translations of foreign scientific and technical material pertinent to NASA's mission.

Specialized services also include creating custom thesauri, building customized databases, and organizing and publishing research results.

For more information about the NASA STI program, see the following:

- Access the NASA STI program home page at <http://www.sti.nasa.gov>
- E-mail your question via the Internet to help@sti.nasa.gov
- Fax your question to the NASA STI Help Desk at 443-757-5803
- Phone the NASA STI Help Desk at 443-757-5802
- Write to:
NASA STI Help Desk
NASA Center for AeroSpace Information
7115 Standard Drive
Hanover, MD 21076-1320

NASA/CR-2009-215932



Damage Arresting Composites for Shaped Vehicles

Phase 1 Final Report

Alex Velicki
The Boeing Company, Huntington Beach, California

National Aeronautics and
Space Administration

Langley Research Center
Hampton, Virginia 23681-2199

Prepared for Langley Research Center
under Contract NNL07AA48C

September 2009

The use of trademarks or names of manufacturers in this report is for accurate reporting and does not constitute an official endorsement, either expressed or implied, of such products or manufacturers by the National Aeronautics and Space Administration.

Available from:

NASA Center for AeroSpace Information
7115 Standard Drive
Hanover, MD 21076-1320
443-757-5802

FOREWORD

This document summarizes the work performed by Boeing Phantom Works, Huntington Beach, California under the NASA Subsonic Fixed Wing Project – Materials and Structures for Wing Components and Non-Circular Fuselage Phase I contract, entitled *Damage Arresting Composites for Shaped Vehicles*. It documents the development work that was performed to support the vehicle-level trade studies and structural testing. It also outlines a proposed Phase II effort.

The NASA technical monitor was Dawn Jegley of the Mechanics and Durability Branch, Langley Research Center.

This document was written by the following Boeing personnel:

Mr. Alex Velicki	Principal Investigator
Ms. Nicolette Yovanof	Program Manager
Mr. Victor Li	Structural Analysis
Mr. Patrick Thrash	Manufacturing Engineering
Mr. Arthur Hawley	Structural Analysis
Mr. Frederick F. Shen	Loads & Dynamics

Acknowledgment is also made to the following individuals for their technical contributions: Mr. Jaime Baraja, Mr. Steve DeCoux, Mr. Bruce Kimoto, Mr. Robert Pickell, and Mr. Robert Turley of The Boeing Company, as well as Professor Lorenzo Valdevit of the University of California, Irvine and Mr. Bruce Sauer of OCM Test Labs for their contribution to the test program.

TABLE OF CONTENTS

Introduction	1
1.0 Phase I Work Completed.....	2
1.1 Analytical Trades	2
1.1.1 Structural Definition.....	2
1.1.2 Material Requirements	14
1.1.3 Manufacturing and Process Requirements	21
1.1.4 Load Case Development.....	28
1.1.5 FEM-based Structural Sizing	34
1.1.6 Weights Summary	51
1.2 Compression Specimens.....	53
1.2.1 Streamwise Single-Stringer Compression Panel.....	53
1.2.2 Spanwise Single-Frame Compression Panel	57
1.2.3 Fatigue Cycled Specimens.....	60
1.3 Phase I Conclusions and Metrics	62
1.3.1 Metric A.....	62
1.3.2 Metric B	64
2.0 Phase II Proposal.....	66
2.1 Phase II Plan	66
References	74
Appendix A – Panel and Specimen Drawings	75
Appendix B – Fatigue Profile Development Notes	78
Appendix C – Single-Stringer Specimen Test Data	81
Appendix D - Single-Frame Specimen Test Data	83

LIST OF FIGURES

Figure 1. Phase I Schedule.....	1
Figure 2. Baseline Aircraft Design Features.....	2
Figure 3. Evolution of BWB Fuselage Design.....	4
Figure 4. BWB Baseline Material/Structural Breakdown	4
Figure 5. PrSEUS Structural Concept	5
Figure 6. PRSEUS Panel Design Notes.....	6
Figure 7. Nominal PRSEUS Stringer Geometry.....	6
Figure 8. Nominal PRSEUS Frame Geometry.....	7
Figure 9. Structural Planview (Outboard Wings Removed).....	7
Figure 10. Fuselage Inboard Profile (at Side Pressure Panel).....	8
Figure 11. Typical Pressure Cabin Cross-Section.....	8
Figure 12. Cabin Corner Detail.....	9
Figure 13. Baseline Longitudinal Panel Splice Concept	9
Figure 14. Redefining Ultimate Load.....	10
Figure 15. Panel Repair Philosophy	12
Figure 16. Outboard Wing Structural Arrangement.....	12
Figure 17. Wing Box Structural Details	13
Figure 18. Winglet Structural Layout.....	13
Figure 19. Fiber Orientation Guidelines	14
Figure 20. Hybrid Warp-knit Fabrics	15
Figure 21. PRSEUS Panel.....	21
Figure 22. CAPRI (Controlled Atmospheric Pressure Resin Infusion).....	21
Figure 23. Single Thread Modified Chain Stitch Seam.....	22
Figure 24. Frame Detail Preform Assembly	23
Figure 25. Stringer and Frame Warp-knit Fabric Details	23
Figure 26. Placement of Stringer and Frame Details.....	24
Figure 27. Preform Panel Assembly Stitching and Tool Removal	24
Figure 28. Free-Standing Preform Lifted Off Tool.....	25
Figure 29. Resin Infusion and Oven Cure Operation	25
Figure 30. Panel 1 After Peel Ply Removal Prior to Post Cure.....	26
Figure 31. Panel 2 Surface Void Locations	26
Figure 32. Panel 2 Repair and Edge Trim.....	27
Figure 33. Panel 2 with Fatigue Specimens Cut from Panel 1 (shipped to NASA).....	27
Figure 34. BWB Shear/Moment/Torque Diagrams.....	32
Figure 35. BWB Finite Element Model Contains Over 44,000 Elements.....	34
Figure 36. Global-Local Optimization Approach	35
Figure 37. Global-Local Process Flow	36
Figure 38. 2.5-g Limit Load Streamwise Direction (Nx) lbs/in.....	37
Figure 39. 2.5-g Limit Load Spanwise Direction (Ny) lbs/in.....	38
Figure 40. -1.0-g Limit Load Streamwise Dirction (Nx) lbs/in	39
Figure 41. -1.0-g Limit Load Spanwise Direction (Ny) lbs/in.....	40
Figure 42. 1.33P Limit Load Streamwise Direction (Nx) lbs/in.....	41
Figure 43. 1.33P Limit Load Spanwise Direction (Ny) lbs/in.....	42
Figure 44. HyperSizer Optimization Processes.....	43

Figure 45. Typical HyperFEA.....	43
Figure 46. PRSEUS Stringer Modeling.....	45
Figure 47. Laminate Selection Input Screen.....	45
Figure 48. PRSEUS Minimum Gauge Dimensions	46
Figure 49. Upper Skin Design Regions and Number of Skin Stacks.....	47
Figure 50. Lower Skin Design Regions and Number of Skin Stacks.....	48
Figure 51. Upper Frame Design Regions and Gauges	49
Figure 52. Lower Frame Design Regions and Gauges	50
Figure 53. BWB Pressurized Region.....	51
Figure 54. Second Panel and Specimens Shipped to NASA-LaRC.....	52
Figure 55. Single-Stringer Compression Specimen Design.....	53
Figure 56. Test Set-Up at Univ of California Santa Barbara.....	54
Figure 57. Single-Stringer Specimen Strain Gage Placement	54
Figure 58. Panel Failure Load and Skin Buckling Pattern.....	55
Figure 59. Replicate 1 - Single-Stringer Failure Summary	56
Figure 60. Replicate 2 - Single-Stringer Failure Summary	56
Figure 61. Single-Frame Compression Specimen Design.....	57
Figure 62. Single-Frame Compression Panel Specimen	57
Figure 63. Test Set-Up at OCM	58
Figure 64. Single-Frame Specimen Strain Gage Placement.....	59
Figure 65. Replicate 1 and 2 - Single-Frame Failure Summary.....	59
Figure 66. Replicate 1 and 2 - Single-Frame Failure Summary.....	60
Figure 67. Fatigue Specimens Shipped to NASA-LaRC.....	60
Figure 68. Compression Fatigue Spectrum for Element Panels.....	61
Figure 69. Metric A - Normalized Weight Comparison.....	63
Figure 70. Metric B - Comparison of Compression Design Parameters	65
Figure 71. Key Elements of Phase II Plan	66
Figure 72. Phase II Work Statement.....	67
Figure 73. Pressure Box Test Specimen	68
Figure 74. Streamwise Tension Panel Geometry (inches).....	69
Figure 75. Spanwise Compression Panel Geometry (inches).....	71
Figure A1. Specimen Panel Blank Drawing	75
Figure A2. Single-Stringer Specimen Drawing	76
Figure A3. Single-Frame Specimen Drawing.....	77
Figure B1. Available Strain Data – Four Options.....	78
Figure B2. Axial Compression Strain from Maneuver.....	78
Figure B3. Axial Tensile Strain from 2P Load Case.....	79
Figure B4. Maximum Repeated Compression Strain Calculation	79
Figure B5. Fatigue Loading Profile for Specimens.....	80
Figure C1. Load-vs-Deflection Plot - Single-Stringer Replicate 1	81
Figure C2. Strain Gage Readings - Single-Stringer Replicate 1	81
Figure C3. Load-vs-Deflection Plot - Single-Stringer Replicate 2	82
Figure C4. Strain Gage Readings - Single-Stringer Replicate 2.....	82
Figure D1. Load-vs-Deflection Plot - Single-Frame Replicate 1.....	83
Figure D2. Strain Gage Readings - Single-Frame Replicate 1	83
Figure D3. LDVT Displacement – Frame Web	84

Figure D4. LDVT Displacement - Skin.....	84
Figure D5. Load-vs-Deflection Plot - Single-Frame Replicate 2.....	85
Figure D6. Strain Gage Readings - Single-Frame Replicate 2	85
Figure D7. LDVT Displacement – Frame Web	86
Figure D8. LDVT Displacement - Skin.....	86

LIST OF TABLES

Table 1. Configuration Baseline Weight Summary.....	3
Table 2. Wing Material Specifications	16
Table 3. Fuselage Material Specifications	16
Table 4. Stack Architecture.....	16
Table 5. Laminate Stiffness.....	17
Table 6. Laminate Unnotched Strengths [ksi].....	17
Table 7. Laminate CAI Strength for BWB Covers (100 ft-lb impact)	17
Table 8. Laminate CAI Strength for BWB Spars/Ribs (20 ft-lb impact)	18
Table 9. Rohacell Minimum Properties	18
Table 10. Rod Mechanical Properties.....	19
Table 11. Environmental Correction Ratios (R_{env}).....	20
Table 12. Estimated Maximum Control Deflection Limits	29
Table 13. Load Survey - Gust Cases	30
Table 14. Sorted Gust Load Cases by Component.....	30
Table 15. Load Survey - Maneuver Cases	31
Table 16. Sorted Maneuver Load Cases by Component	31
Table 17. Maneuver Load Cases Used For Global Optimization	33
Table 18. HyperSizer Major Functions.....	44
Table 19. Panel Design Limit & Frame Design Limits	46
Table 20. Pressurized Center Body Weight Comparison	52

ACRONYMS

2P	2 times Max Internal Pressure
BHD	Bulkhead
BWB	Blended Wing Body
CAI	Compression After Impact
CD	Cold Dry
CAPRI	Controlled Atmospheric Pressure Resin Infusion
CG	Center of Gravity
D&DT	Durability and Damage Tolerance
EVM	Earned Value Management
FAR	Federal Aviation Regulations
FEM	Finite Element Model
H/W	Hot/Wet
IML	Inner Moldline
IWNG	Inboard Wing
IRAD	Independent Research and Development
KEAS	Knots Equivalent Airspeed
KIPS	Thousand Pounds
KSI	Thousand Pounds Per Square Inch
L/D	Lift-to-Drag Ratio
MLG	Main Landing Gear
MTOGW	Maximum Takeoff Gross Weight
MZFW	Maximum Zero Fuel Weight
NDE	Nondestructive Evaluation
NDI	Nondestructive Inspection
N_x	Axial Load in x-direction
N_{xy}	Shear Load in xy-plane
N_y	Axial Load in y-direction
OB	Outboard
OEW	Operator Empty Weight
OCM	Orange Country Materials (Test Lab)
OML	Outer Moldline
OWNG	Outboard Wing
OHC	Open Hole Compression
OML	Outer Moldline
PRSEUS	Pultruded Rod Stitched Efficient Unitized Structure
PMC	Polymer Matrix Composite
PSI	Pounds per Square Inch
SQ-IN	Square Inches
UCI	University of California, Irvine
UCSB	University of California, Santa Barbara
VARTM	Vacuum-Assisted Resin Transfer Molding

INTRODUCTION

This work focuses on the development of a novel structural solution that addresses the demanding fuselage loading requirements for the Hybrid Wing or Blended Wing Body (BWB) configurations that are described in the NASA NRA Subtopic A.2.4.3, “Materials & Structures for Wing Components and Non-Circular Fuselage.”

The funded Phase I portion of the contract is a comprehensive Finite Element Model (FEM)-based structural sizing exercise performed using the BWB airplane configuration to generate internal loads and fuselage panel weights for an advanced Pultruded Rod Stitched Efficient Unitized Structure (PRSEUS) structural concept. An accompanying element-level test program was also conducted to establish basic compressive structural responses under static loadings to substantiate the analytical results and calculation methods used in the trade study. The primary subtasks of this one-year Phase I study are outlined in the schedule below (Figure 1) and described in detail in Section 1.0 of this final written report.

	Phase I												Phase II							
	FY08																			
Phase I Schedule	CY07				CY08															
	O	N	D		J	F	M	A	M	J	J	A	S	O	N	D				
Phase I																				
3.1 Analytical Trades																				
3.1.1 General Design Reqmts	█																			
3.1.2 Vehicle-level Sizing Studies					█															
3.1.2.1 Load Case Devmt					█															
3.1.2.2 Non-optimum Factors					█															
3.1.2.3 Update BWB FEM					█															
3.1.2.4 FEM-based Structural Sizing					█				█											
3.1.2.5 Develop Wts Statement									█											
3.1.2.6 Document Sizing Results													█							
3.2 Compression Specimens																				
3.2.1 Chordwise Single Stringer (4 Reps)					█															
3.2.2 Spanwise Single Frame (4 Reps)					█															
3.3 Phase II Planning																				
3.3.1 Update Technical Approach					█								█							
3.4 Phase I Status Reporting																				
3.4.1 Program Management	█				█															
3.4.2 Monthly Reports	█				█															
3.4.3 Oral Briefings	█				█								█							
3.4.4 Final Written Report													█							

FIGURE 1. PHASE I SCHEDULE

The funding for the two-year Phase II portion of the study has yet to be committed by NASA. The proposed Phase II work plan is described in Section 2.0 of this report per the requirements of the Phase I contract. The Phase II plan maintains the continuity of Phase I activities by extending the building-block development approach to encompass more technically demanding analysis and testing tasks. Over the course of Phase II, three large subcomponent specimens will be fabricated and tested to better understand the structural responses for axially and pressure-type loadings. Improved analytical methods tailored for the PRSEUS design approach will also be developed and then ultimately rolled in the vehicle-level sizing task to improve the airframe weight estimates generated during Phase I.

1.0 PHASE I WORK COMPLETED

To assess the weight savings potential of the PRSEUS structural concept on the BWB airframe, an existing airplane configuration and finite element model (that was developed outside the Phase I contract with Boeing funding) were adapted for this study. The baseline dataset had been used for prior studies comparing Sandwich, J-frame, and Hat-stiffened fuselage structural concepts (Reference 1). In this Phase I study, although some improvements were made to the overall dataset, the primary emphasis was on remodeling the pressurized area of the fuselage and then resizing the new airplane arrangement to generate a new fuselage weight that could be compared to prior results. In addition to the analytical work, a small four-element test program was completed to assess the PRSEUS structural concept under axial compression loading, while additional elements and panels were also provided to NASA for future analysis and testing.

1.1 Analytical Trades

The study baseline used for the analyses makes extensive use of stitching and resin infusion to provide a cost-competitive damage-tolerant airframe with an emphasis on simplifying fabrication and assembly for the compound curvatures of the BWB airframe. The design features large unitized wing and fuselage components that offer efficient continuous load paths, higher notched design properties, larger allowable damage levels, along with enhanced levels of survivability beyond those currently possible using conventional materials/designs. The study aircraft configuration and design parameters are described in the following sections.

1.1.1 Structural Definition

The BWB aircraft employs advanced technologies to achieve a highly integrated airframe that is capable of substantial aerodynamic performance improvements (Figure 2). This design approach incorporates a twin-engine pod-mounted arrangement, and movable rudder controls on the winglets. Airframe weights are kept low through the extensive use of advanced composite materials resulting in primary wing and fuselage structures that are appreciably lighter than comparable aluminum designs.

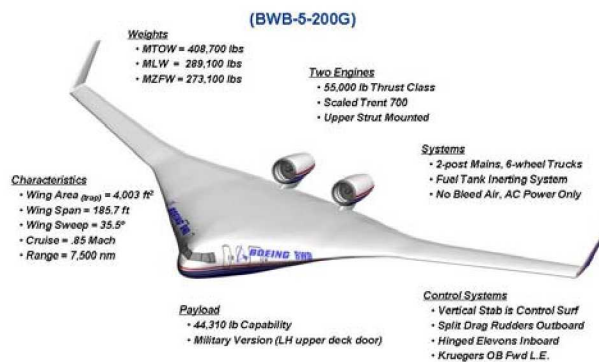


FIGURE 2. BASELINE AIRCRAFT DESIGN FEATURES

The corresponding weight distribution for the BWB-5-200G baseline configuration is summarized in Table 1. These values were used to populate the initial loads evaluation software

that determined the critical sizing load cases, and were also used to provide an initial mass distribution for the FEM-based structural sizing task.

TABLE 1. CONFIGURATION BASELINE WEIGHT SUMMARY

Baseline Weights Summary	(lbs)
Airframe	96,360
Propulsion	20,660
Systems	46,618
Equipment/Furnishings	26,632
Operational Items	19,419
Usable Fuel	154,681
Payload	44,310
TOGW	408,680

The airframe development challenge was to find a noncircular pressurized shell that would be both weight and cost effective. Due to the large secondary bending forces that are present in the near-flat fuselage panels during pressurization cycles, fatigue-sensitive materials such as metals were not a viable option. This led to the selection of composite primary structure candidates that are amenable to the compound curvatures found on the BWB. To keep fabrication costs reasonable for this geometry, the airframe will be constructed of large integral panel assemblies produced outside of a size constrained autoclave.

The airframe must also be extremely damage tolerant to maintain a higher level of safety than conventional aluminum structures to compensate for the higher intrinsic risk that is encountered in the noncircular passenger cabin design. To ensure customer acceptance, maintainability and reliability should be equivalent to that of conventional aluminum structures. The airframe must also feature significantly better repair techniques than those commonly used for prepreg composites, which are frequently criticized by the airlines as expensive and tedious.

For the flat-sided BWB cabin, the out-of-plane loads experienced during the 2P over-pressure condition are particularly harsh. This is especially true if a conventional prepreg composite material system is used, as the confluence of thin gauge skins, large diameter fasteners, countersinking, and the weak bearing properties of the resin combine to make fastener pull-through a problem. To avoid this, stitching was selected to increase the out-of-plane strength as well as permit crack arrestment without compromising the in-plane properties of the thin gauge laminates that are prevalent throughout the BWB pressure shell.

Finding the right stitched concept with the manufacturing versatility and performance attributes needed to satisfy the BWB challenge is a difficult undertaking. Even the most advanced cobonded or cocured composite fuselage designs (Figure 3) include too many fasteners through the skin to be structurally viable. In addition, the utilization of hard tooling on the inner moldline (IML) to produce net stringer shapes that would in turn be matched to thin-gauge net-molded skins makes this approach prohibitively expensive. To address this manufacturing concern, resin-infused hat-section panels were also considered. While this approach eliminated the majority of fasteners through the skin, as well as much of the IML tooling, there were still unresolved problems in the fabrication and interfaces for this concept. Recognition of these short-comings led to the development of the PRSEUS design approach.

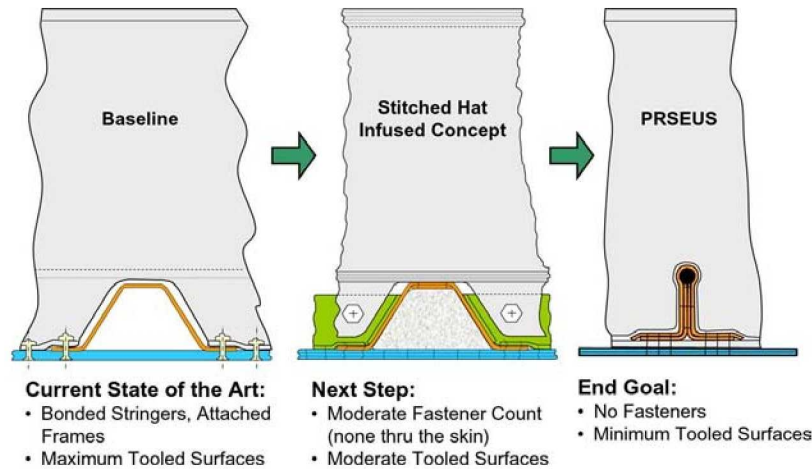


FIGURE 3. EVOLUTION OF BWB FUSELAGE DESIGN

The weights distribution (Table 1) and the material-structural concepts callouts (Figure 4) represent the starting assumptions for the reference configuration that was established for this study. It makes extensive use of stitching and resin infusion to provide a cost-competitive damage-tolerant airframe that is capable of meeting the performance and productivity challenges of the BWB airframe. This novel airframe design also features large unitized wing and fuselage components that offer efficient continuous load paths, higher notched design properties, larger allowable damage levels, and enhanced levels of survivability beyond those currently possible using conventional materials/designs.

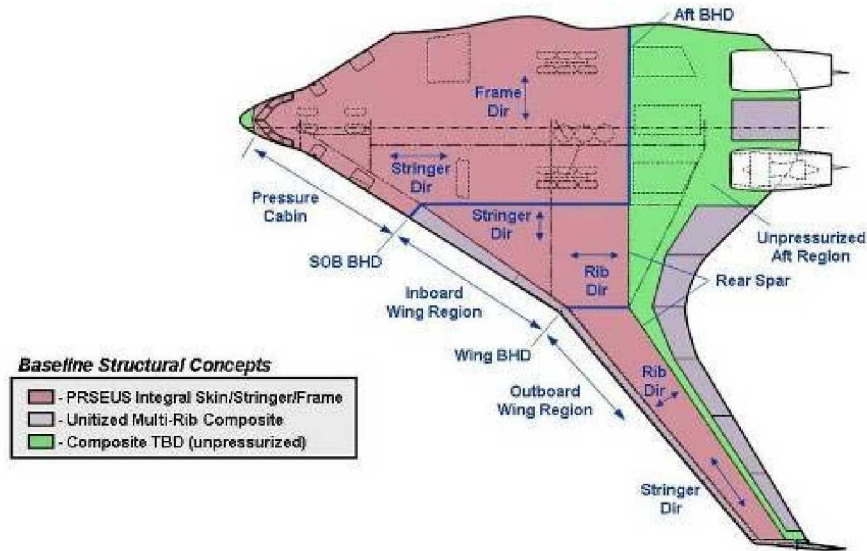


FIGURE 4. BWB BASELINE MATERIAL/STRUCTURAL BREAKDOWN

The main wing box and pressurized portion of the fuselage is an integral stitched-composite skin-stringer design (PRSEUS) and the unpressurized shell (green region) is a composite sandwich shell support by numerous rib and spar members. Initial sizing studies will assume composite sandwich concepts with composite frames or ribs, depending on the location. The aft fuselage regions around the engines would be a combination of metallic and composite components with substantial composite material usage.

Large control surfaces would be fabricated using the unitized multi-rib stitched-composite designs flying on the C-17 landing gear doors. Lightly loaded elements like fairings, gear doors, and engine nacelles would be fabricated using conventional sandwich honeycomb techniques to minimize weight. The floor structure would be conventional in nature, but would also be improved with advanced composite materials and aluminum alloys where possible to reduce weight and cost.

PRSEUS Design Details – The highly integrated nature of PRSEUS is evident in the strategic placement of the carbon fibers (Figure 5). The dry warp-knit fabric, precured rods, and foam-core materials are assembled and then stitched together to create the optimal structural geometry for the BWB fuselage loading. Load path continuity at the stringer-frame intersection is maintained in both directions. The 0-degree-fiber dominated pultruded rod increases local strength/stability of the stringer section while simultaneously shifting the neutral axis away from the skin to further enhance the overall panel bending capability. Frame elements are placed directly on the IML skin surface and are designed to take advantage of carbon fiber tailoring by placing bending and shear-conductive lay-ups where they are most effective. The stitching is used to suppress out-of-plane failure modes, which enables a higher degree of tailoring than would be possible using conventional laminated materials.

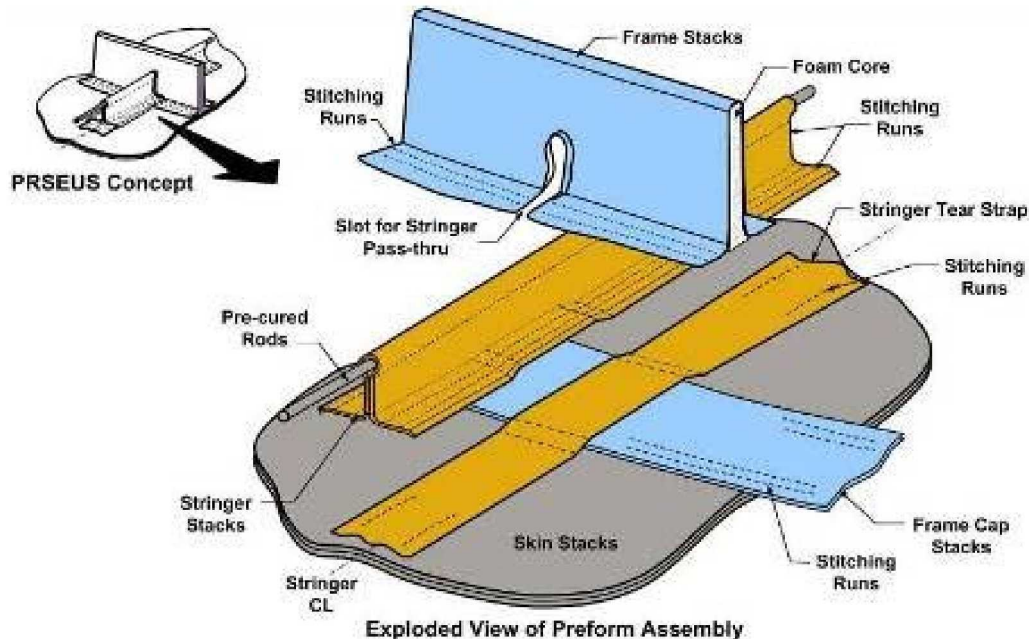


FIGURE 5. PRSEUS STRUCTURAL CONCEPT

The resulting integral structure is ideal for the BWB pressure cabin because it is a highly efficient stiffened-panel geometry in three directions (N_x , N_y , and N_z) that is damage tolerant, stitched to react against pull-off loads, and capable of operating well into the post-buckled design regime. This enables thin-gauge skin-stringer designs to be lighter than non-buckled sandwich designs.

The PRSEUS design approach combines existing technologies in a novel way. It uses a pultruded rod in the stringer cap, which passes through foam-core frames, to create a stitched preform of dry carbon fiber that can support itself during vacuum bagging and resin infusion. The result is a highly tailored stiffened panel that can be fabricated without the use of complex

interior mold tools. This approach permits the skin, stringer, and frame elements to be inexpensively resized at the point of fabrication for customized structural solutions for each aircraft model. This attribute is the enabling feature for the BWB family-of-aircraft design scenario because it also addresses the fundamental producibility problem for the compound curvatures of the BWB airframe.

Figure 6 shows a simplified summary of the geometry nomenclature for a PRSEUS panel and material callouts that were used in the trade studies. More detailed geometric information for the stringer (Figure 7) and frame elements (Figure 8) can also be found in the subsequent figures. These dimensions represent the nominal panel gauges prior to the FEM-based structural sizing exercise.

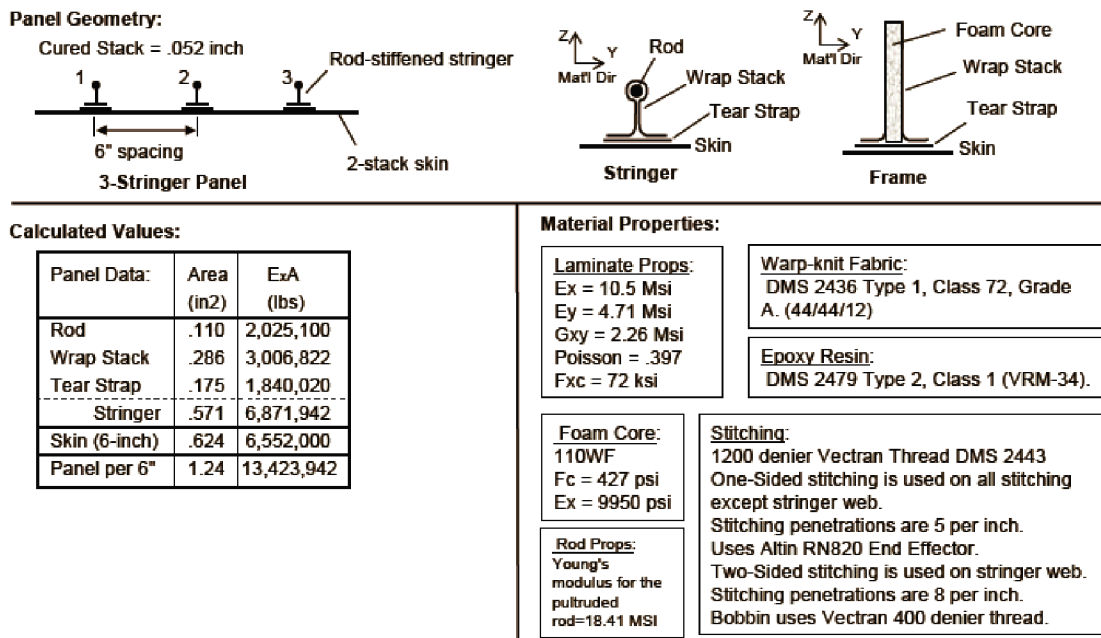


FIGURE 6. PRSEUS PANEL DESIGN NOTES

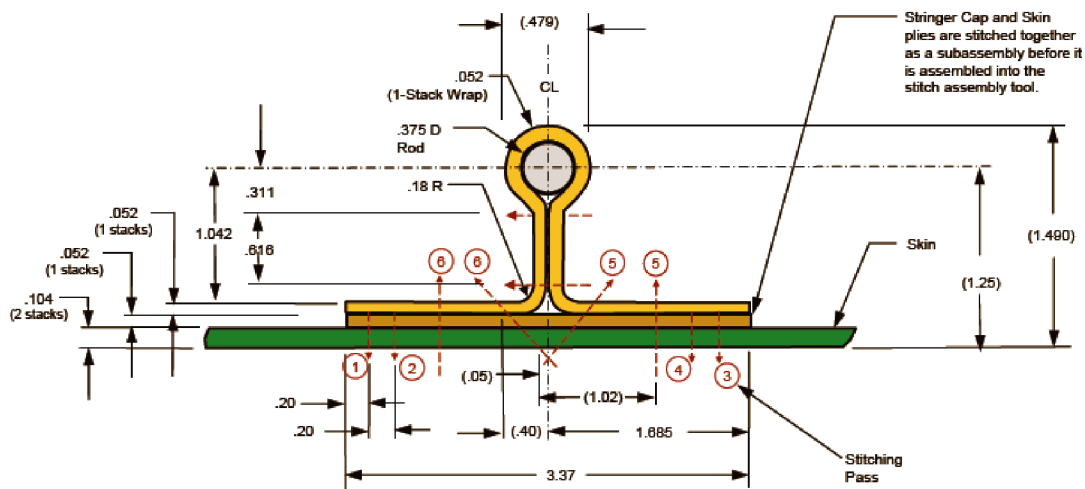


FIGURE 7. NOMINAL PRSEUS STRINGER GEOMETRY

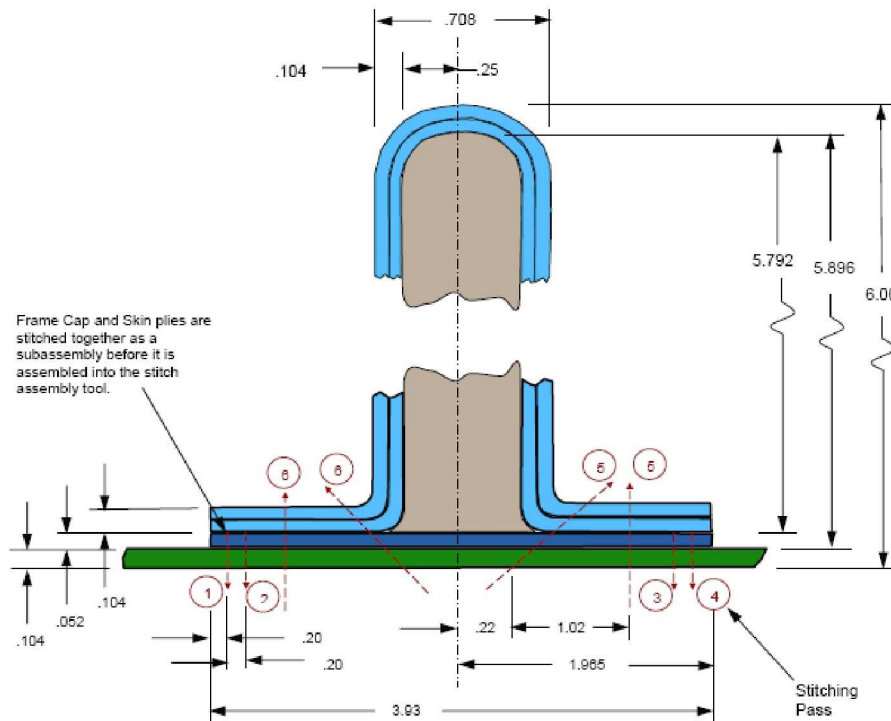


FIGURE 8. NOMINAL PRSEUS FRAME GEOMETRY

Fuselage Design - A structural arrangement drawing was created for the baseline configuration to locate the airframe primary structure and to describe typical structural features. The plan view and inboard profile are shown (Figures 9 and 10) with the pressure cabin regions highlighted in yellow. Frames run spanwise through the pressure cabin and rib and bulkhead elements run streamwise.

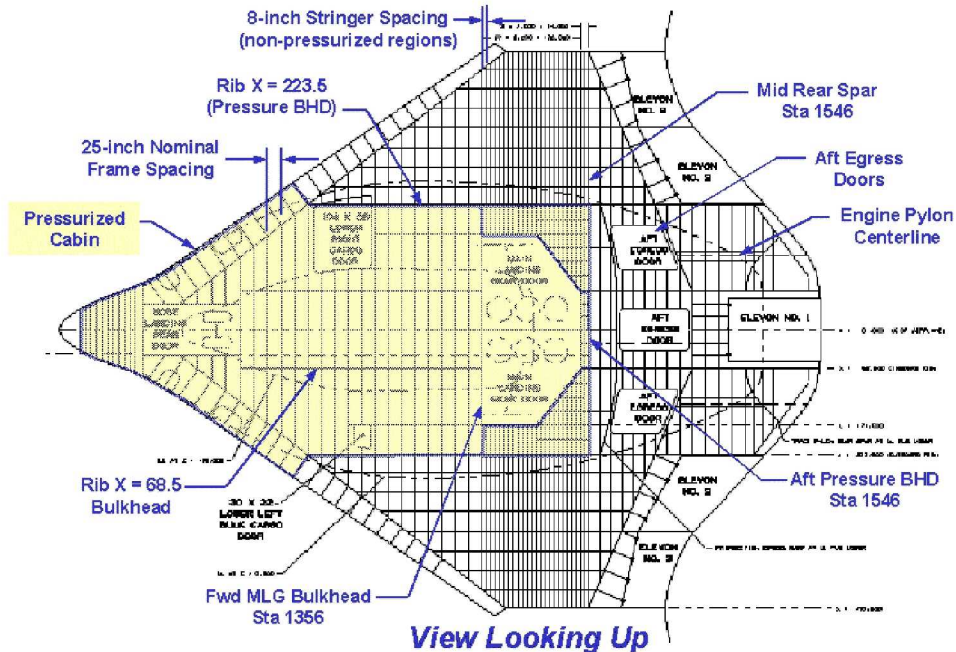


FIGURE 9. STRUCTURAL PLANVIEW (OUTBOARD WINGS REMOVED)

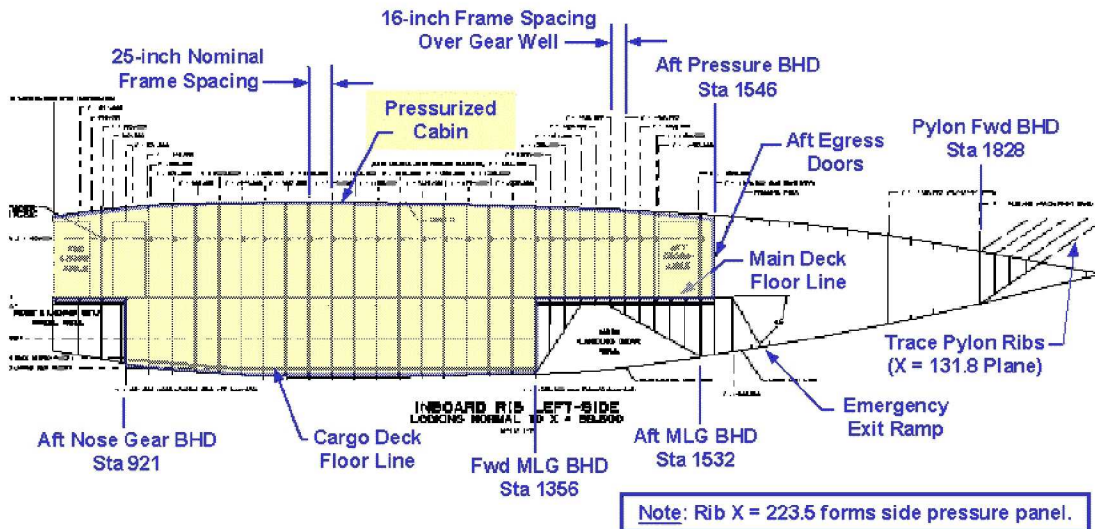


FIGURE 10. FUSELAGE INBOARD PROFILE (AT SIDE PRESSURE PANEL)

Diagonal bracing members support the frames at each longitudinal rib/bulkhead to reduce the bending moments in the covers (Figure 11). A basic frame depth of 6 inches was used. In the lower cargo region, the frames extend the entire depth between the skin and the cargo floor. Deeper frames or support bracing are used in regions of the lower shell not housing cargo containers and where landing gear and systems geometries permit.

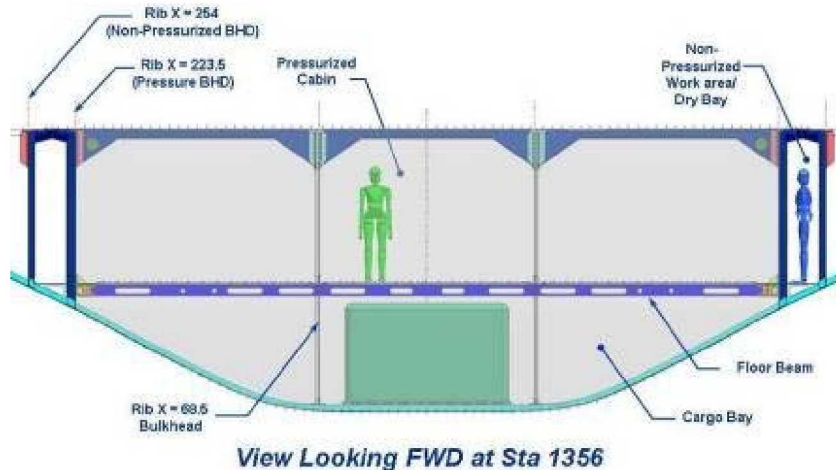


FIGURE 11. TYPICAL PRESSURE CABIN CROSS-SECTION

The passenger floor performs the same functions as other floors, but to keep the space in the under-floor cargo bays as clear as possible, there will be no intermediate struts for the floor beams between the ribs. The beams run continuously across (and through) the ribs, and are attached to the end pressure bulkheads with some degree of fixity. These end attachments will assist the bulkheads in carrying the lateral pressure loads, and in doing so, the beams themselves are subjected to a tension load from the spanwise pressure loads. The beams also pick up some spanwise bending loads, but these are small since the floor is generally not far from the neutral axis of the entire shell. The corner regions of the pressure cabin will maintain bending moment continuity using the pressure panel arrangement as depicted in Figure 12.

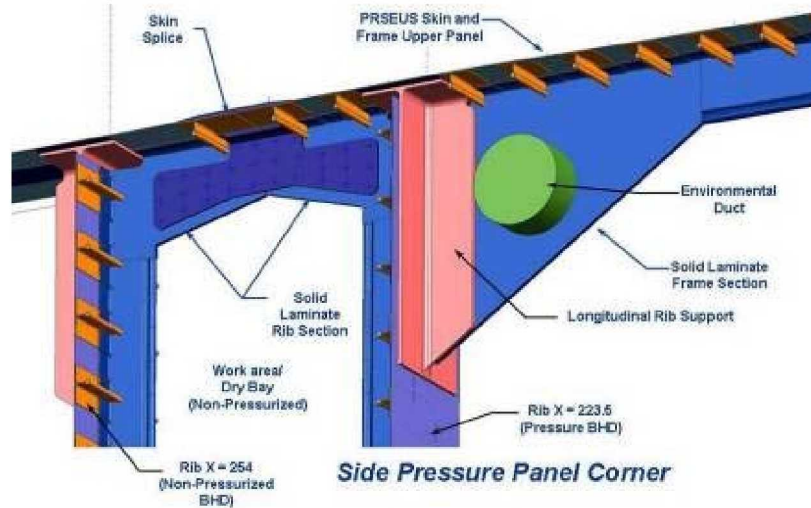


FIGURE 12. CABIN CORNER DETAIL

There are a number of regions for landing gear or systems under the passenger floor that have to be unpressurized. The floor above these regions becomes the boundary of the pressure shell and has to carry the full transverse pressure loads. In addition, there are spanwise and streamwise components of pressure in the plane of the floor itself. A portion of these in-plane loads will be due to reactions from pressures applied to the side walls of unpressurized wells. In regions where the under-floor bays are unpressurized, normal floor panels shall be used, to permit easy replacement, and pressure loads shall be taken by a separate structure. This structure shall be contained within the depth of the floor beams and will have enough strength to beam the pressure loads between the floor beams.

Splicing Concept - A baseline longitudinal panel splice concept (Figure 13) was developed to define the non-optimum factor weight penalty for panel joining. The approach is similar to conventional aluminum skin-stringer splice designs and is therefore expected to have similar non-optimum factors in the weight calculations.

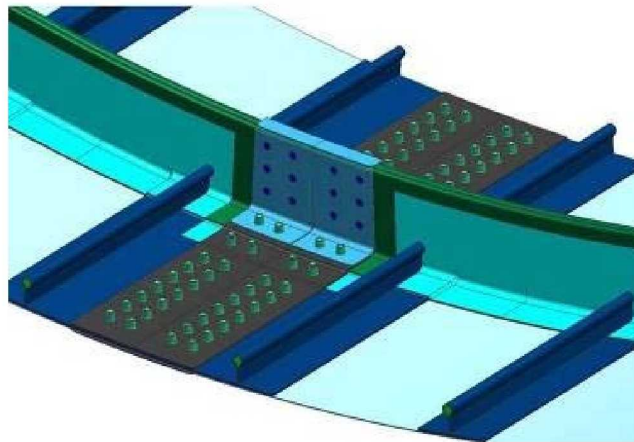


FIGURE 13. BASELINE LONGITUDINAL PANEL SPLICE CONCEPT

Faying surface seal will maintain pressure tightness. Two rows of bolts should be adequate to transfer load, however three may be needed to stop joint rotation under internal pressure. The outer lap is thicker than the inner because the outer has countersunk bolt heads that are

essentially ineffective in bearing. The splice material is titanium and could also be used for electrical grounding.

Damage Tolerance Design - The requirements specified in Federal Aviation Regulations, Part 25 (FAR 25) were used as a basis for establishing the trade study design requirements. Additional guidance was also found in FAA Advisory Circulars AC20-107A “Composite Aircraft Structure” and AC25.571-1A “Damage Tolerance and Fatigue Evaluations of Structure”.

Damage arrestment is the single most important breakthrough needed to realize the full load-carrying potential of carbon fiber based materials for large primary structures. The weak laminated interfaces have long been identified as problematic as they relied on bonded or cocured interfaces that were not particularly effective at stopping damage propagation. This has resulted in the use of safe-life design techniques rather than fail-safe designs as is common in metallic structures. This is not the case for stitched composite materials because the onset of damage propagation is no longer critical since damage can now be arrested at key structural interfaces with stitching. This characteristic failure mode now makes it possible to redefine ultimate load in a new way for composite structures.

While this approach may be new for composite structures, it is commonplace for metallic structures where limit load is typically defined as the first non-linear event (typically material yield) and then ultimate load is defined as either: 1.5 x limit load or catastrophic failure, whichever is lower (Figure 14). A similar design approach can also be used for stitched composites, where the onset of damage propagation defines limit load and ultimate load is 1.5 times higher.

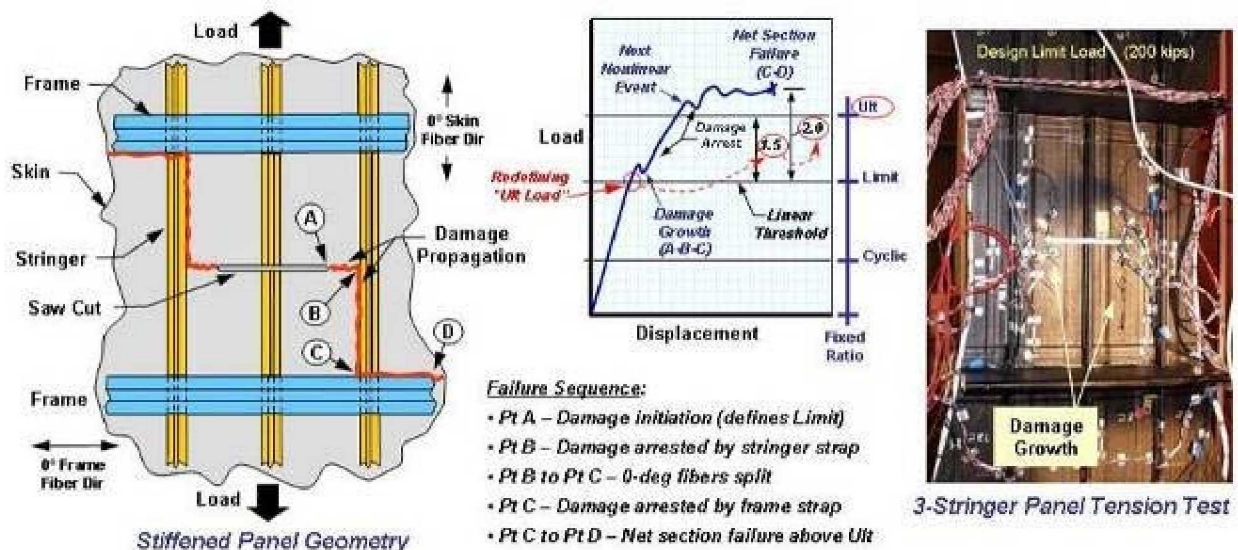


FIGURE 14. REDEFINING ULTIMATE LOAD

This damage-arrest design philosophy was demonstrated on a fuselage panel with 6-inch stringer spacing and 20-frame pitch (Reference 2). The goal of this test was to show that damage propagating from Point A-to-B would be arrested first at Point B, and then later again at Point C after propagating vertically (Figure 14). The higher load levels achieved beyond crack initiation

(growth at Point A) and final failure (Points C-to-D) would demonstrate the advantage of designing beyond conventional no-growth constraints.

The 3-stringer dog-bone tension panel with a 2-bay crack (slot across central stringer) was statically tested to failure (Figure 14). The specimen was able to arrest propagating damage in both the horizontal and vertical directions as it emanated from the slot edge. Because damage was arrested at the stitched interfaces and fully contained within the 2-bay damage zone bordered by the adjacent stringers and frames, the panel was able to continue bearing load beyond the 200,000-lb limit design requirement. The specimen ultimately exceeded the design requirement by 30% with final failure occurring at 264,000 lbs. Had a conventional no-growth composite design criterion been used, the onset of damage propagation occurred at 162,000 lbs which was 18% below the 200,000-lb design requirement. This test clearly demonstrates that substantial load-carrying improvements are possible (60% higher) when stitched interfaces are used to arrest damage and redistribute loading. This is what makes fail-safe design philosophies feasible for composite materials.

This new approach will be used to justify the higher tension allowables that were used in the structural sizing trades. The fail-safe approach is: no damage growth up to Limit Load with Ultimate Load being achieved using multi-load path damage-arrest design methodologies. This effectively increases the tension design allowable for the panel by 50% in most instances.

Damage Limits and Repair - The most important aspect of these criteria is ensuring airframe safety. For composite structures, a particularly important element of this goal is establishing damage tolerance limits where a distinction is made between detectable and nondetectable damage. Nondetectable damage is that which may be undetected or not repaired for the whole life of the aircraft. Such damage is assumed to be always present and the structure is designed for the whole range of ultimate load conditions with this damage in place. Ironically, when damage is larger than that defined as non-detectable, a lower level of load conditions (limit) is allowed. The assumption here is that this level of damage will be repaired within a period of time short enough to reduce the probability of meeting the higher loads.

The BWB allowable working stress levels were based on an indentation depth of 0.100-inch being the threshold between detectable and non-detectable damage. It has been suggested that this is too severe and that 0.050-inch (or even 0.010) could be used. Obviously, the smaller the indentation depth, the more difficult it is going to be for the operator to find the damage. But this smaller number will also result in a higher design allowable and more weight savings in the trade study.

A 0.100-inch indentation in a 0.100-inch thick skin essentially represents penetration. In a fuel tank or the pressure cabin, such damage is likely to be immediately evident and corrective action will be taken. Use of a thinner skin may not reduce the allowable stress values and it might be argued that damage tolerance is not adversely affected. However damage resistance, and the incidence of damage in-service, will be degraded and this will be reflected in higher maintenance costs and aircraft downtime.

The repair philosophy selected for PRSEUS utilizes a combined bolted-bonded repair approach (Figure 15). In order to not degrade the thin-gauge skin design allowable by accepting bolted repairs (would require open-hole design values), a bonded repair philosophy was selected for the open skin bays between the stringers and frames. In these regions repairs would be made using

simple bonded patches. For larger repairs, that include the built-up regions of the stringer and frame flanges, bolted repairs would be used. Such an approach eliminates the open-hole design penalty for the entire skin surface, while accepting it for the thicker regions of the build-ups.

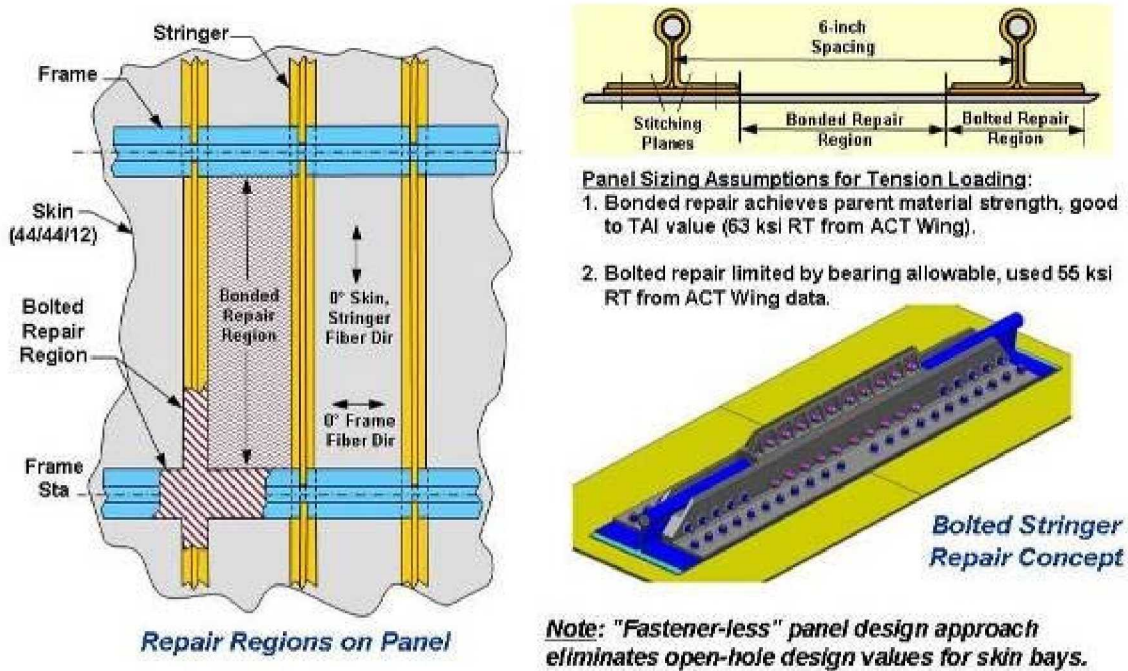


FIGURE 15. PANEL REPAIR PHILOSOPHY

Wing Design - The structural arrangement for the outboard wing is fairly conventional (Figure 16). The structural box has a front and rear spar, with 35-inch rib spacing, nominal 8-inch stringer spacing, and a row of access ports on the lower surface. The wing leading and trailing edges contain movable control surfaces, as does the winglet component, which contains a movable rudder system for directional control.

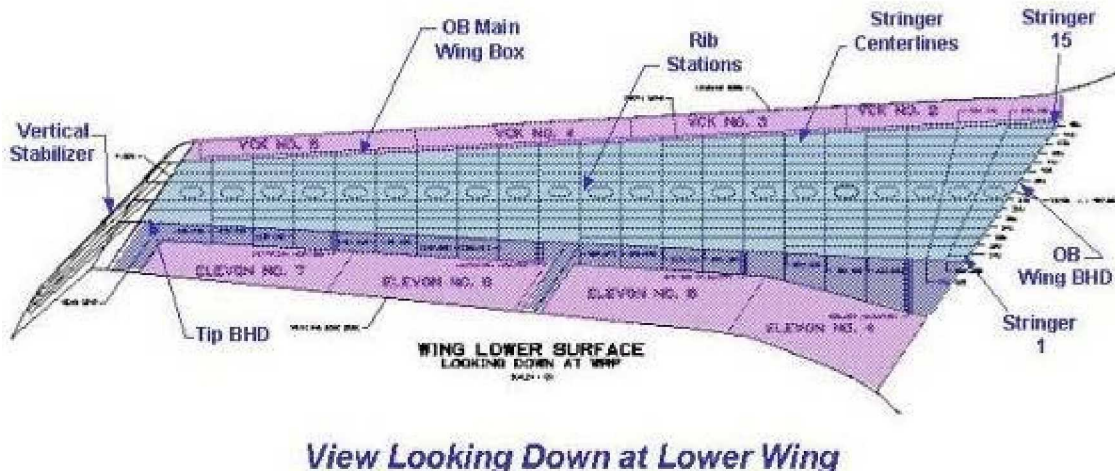


FIGURE 16. OUTBOARD WING STRUCTURAL ARRANGEMENT

The stitched-composite integral wing cover panels have blade-type stringers (that will eventually be switched over to PRSEUS in future trades), along with rib and spar caps combined into a

single stitched-and-cured panel assembly (Figure 17). Stiffened rib and spar webs are mechanically attached through the upstanding leg of the substructure cap elements during the assembly operation to complete the structural box.

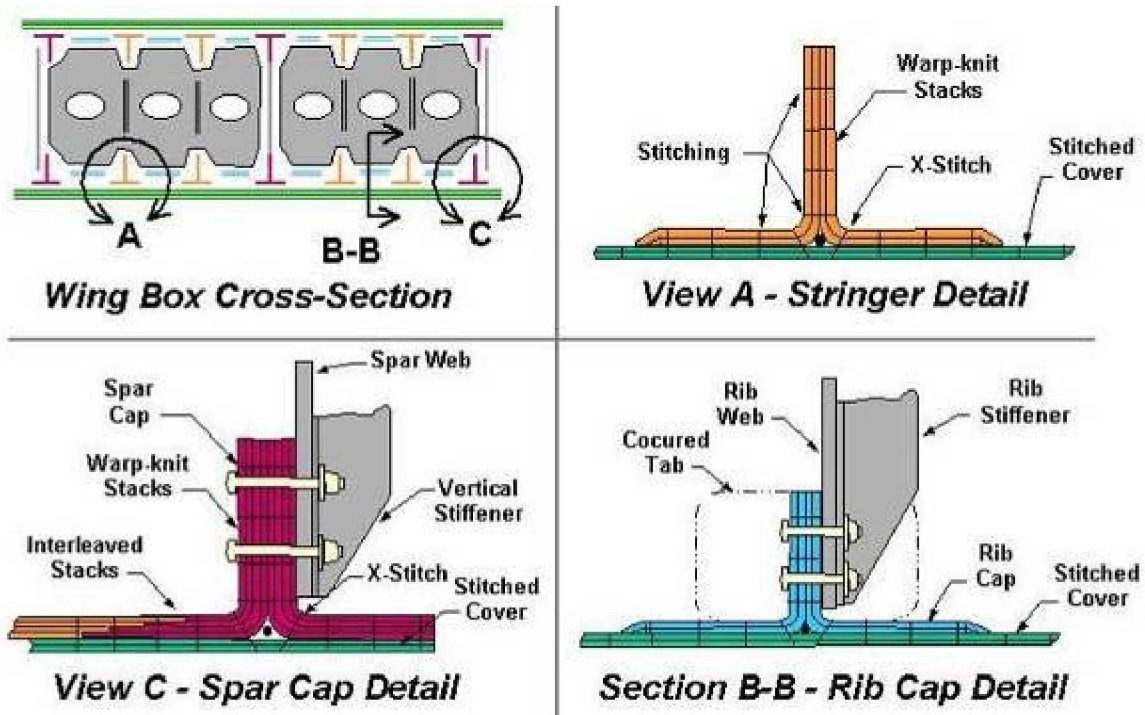


FIGURE 17. WING BOX STRUCTURAL DETAILS

The primary structure centerlines for the winglet component are shown below in Figure 18.

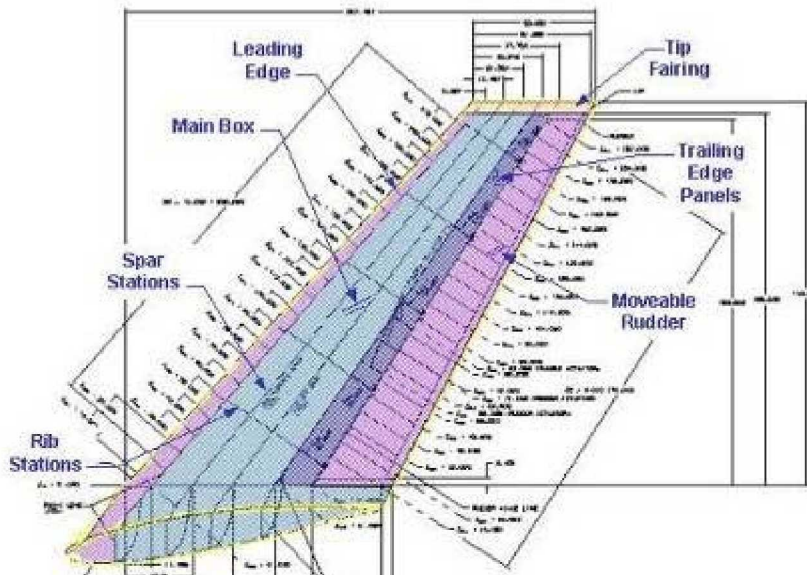


FIGURE 18. WINGLET STRUCTURAL LAYOUT

1.1.2 Material Requirements

Material properties and design values were derived from the test data developed by the ACT composite wing program (Reference 3). The fiber system was generally based on medium-performance AS-4 fibers, with some selective usage of IM-7 fibers to improve tensile performance. The influence of lay-up patterns were used as basic design guidelines. For predominately unidirectionally-loaded members like the wing structures, the ACT wing laminate fiber percentages were used. For the pressure cabin though, where skins had to work effectively with the frames in the spanwise direction and at the same time be efficient in spanning the pressure loads between frames in a streamwise direction, the cover panel skins needed more-equal capability in both the 0° and 90° directions.

Panels that were dominated by shear loading will require a higher percentage of $\pm 45^\circ$ layers. Spar and rib webs in the pressure cabin will be subjected to a combination of bi-axial loading and shear, and the percentage of fibers in each direction will have to be determined for each set of loading conditions. More development is required before the fiber percentages and stack thicknesses are optimized for the various BWB structural components.

Fiber Architecture - Prior studies on the influence of lay-up patterns were used as basic design guidelines. For predominately unidirectionally-loaded members like the wing structures, the ACT wing laminate fiber percentages were used (Figure 19). For the pressure cabin though, where skins had to work effectively with the frames in the spanwise direction and at the same time be efficient in spanning the pressure loads between frames in a streamwise direction, the cover panel skins needed more-equal capability in both the 0° and 90° directions.

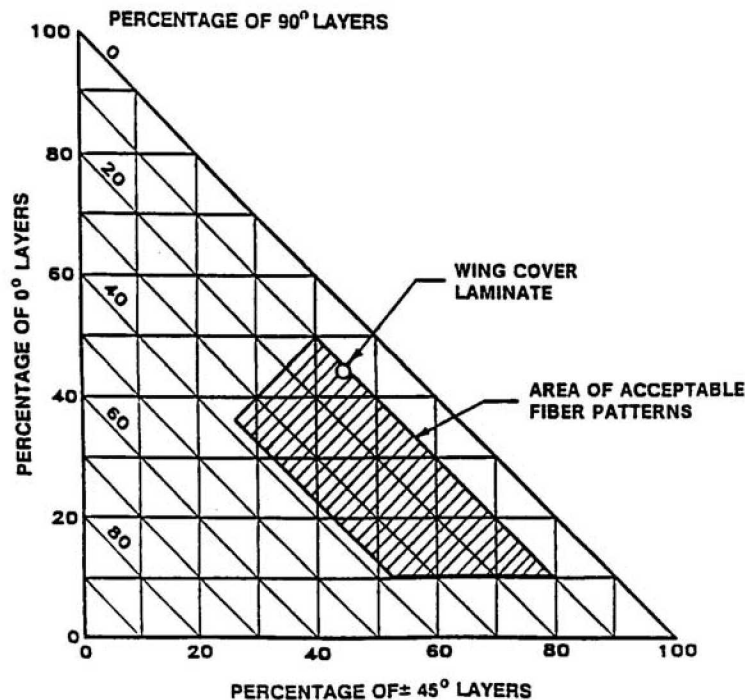


FIGURE 19. FIBER ORIENTATION GUIDELINES

Panels that were dominated by shear loading will require a higher percentage of $\pm 45^\circ$ layers. Spar and rib webs in the pressure cabin will be subjected to a combination of bi-axial loading and shear, and the percentage of fibers in each direction will have to be determined for each set

of loading conditions. More development must also be conducted before the fiber percentages and stack thicknesses are optimized for the various BWB structural components. This will include development and sizing studies on hybrid architectures (Figure 20) with fiber mixtures to promote crack-turning behavior within the laminate.

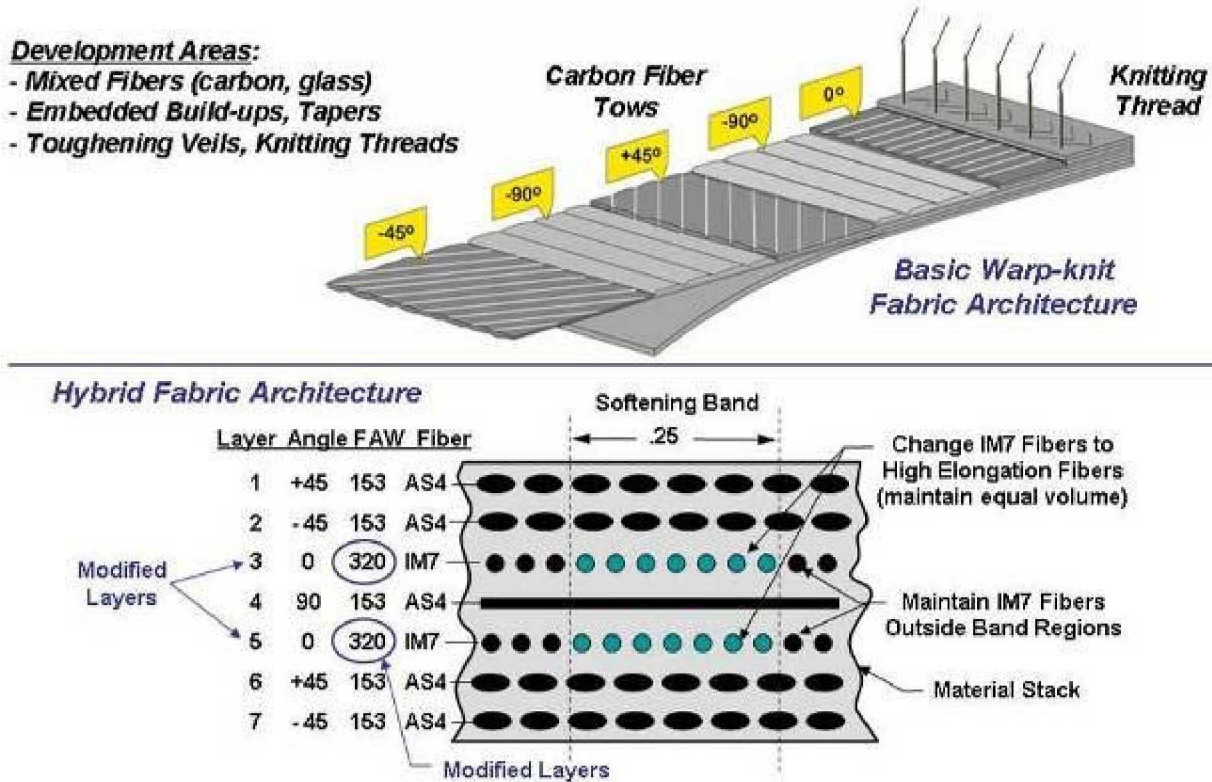


FIGURE 20. HYBRID WARP-KNIT FABRICS

Fiber Material Properties - The material properties are largely based on the results of material testing performed in support of the ACT wing program. Although the current version of the materials properties database is limited in scope and only encompasses the baseline materials proposed for use in the preliminary sizing studies, it will be continuously updated to reflect the future design and analysis needs as additional test data becomes available.

The allowables are based upon Hercules AS4 and IM7 fibers supplied in a warp-knit architecture where several layers of dry carbon fiber are oriented into single stack product forms. The following warp-knit material types were used in the trades.

TABLE 2. WING MATERIAL SPECIFICATIONS

Upper Cover Skin	DMS-2436D, TYPE 1, CLASS 72
Lower Cover Skin	DMS-2436D, TYPE 2, CLASS 72
Rib/Spar Web	DMS-2436D, TYPE 2, CLASS 74
Upper Spar Cap and Stringers	DMS-2436D, TYPE 1, CLASS 72
Lower Spar Cap	DMS-2436D, TYPE 2, CLASS 72
Intercostals	DMS-2436D, TYPE 2, CLASS 72

TABLE 3. FUSELAGE MATERIAL SPECIFICATIONS

Upper Cover Skin	DMS-2436D, TYPE 1, CLASS 72
Lower Cover Skin	DMS-2436D, TYPE 2, CLASS 72
Upper Cover Frames	DMS-2436D, TYPE 1, CLASS 72
Lower Cover Frames	DMS-2436D, TYPE 2, CLASS 72

Type 1 laminates consist of AS4 fibers only. Type 2 laminates consist of IM7 fibers in the 0° direction and AS4 fibers in the 45° and 90° directions. The laminates are further identified by their class to specify the fiber pattern. Class 72 and Class 74 have a fiber pattern of (44.9/42.9/12.2) and (30.0/59.9/10.1), respectively (Table 4).

TABLE 4. STACK ARCHITECTURE

Ply Number	Orientation	FAW-Class 72	FAW-Class 74
1	+45	153	214
2	-45	153	214
3	0	320	214
4	90	173	145
5	0	320	214
6	-45	153	214
7	45	132	214

The laminate stiffness for some typical BWB laminates is listed in Table 5, while the laminate strengths are listed in Table 6. The stitching angle for these laminates is in the X direction. The TxCy designation refers to DMS2436D type x class y definition.

TABLE 5. LAMINATE STIFFNESS

	Tension				Compression			
	E _x (msi)	E _y (msi)	G _{xy} (msi)	v _{xy}	E _x (msi)	E _y (msi)	G _{xy} (msi)	v _{xy}
T1C74 Spar	7.96	5.05	3.14	0.485	7.23	4.66	2.84	0.475
T2C74 Spar	9.21	5.16	3.14	0.486	8.07	4.73	2.84	0.475
T1C72 Upr.Cover	10.25	5.07	2.48	0.403	9.23	4.66	2.26	0.397
T2C72 Lwr.Cover	12.13	5.14	2.48	0.403	10.50	4.71	2.26	0.397

TABLE 6. LAMINATE UNNOTCHED STRENGTHS [KSI]

Laminate	B-Allowable stress				
	F _{tx}	F _{cx}	F _{ty}	F _{cy}	F _s
T1C74 Spar	75.5	61.6	44.6	38.2	42.3
T2C74 Spar	90.3	54.8	46.1	38.7	42.3
T1C72 Cover	105.1	79.2	46.5	37.9	29.9
T2C72 Cover	127.2	71.9	47.3	38.2	30.0

The compression strength was governed by the compression after impact (CAI) values which are a function of the number of stacks and the non-detectable damage levels that are used. For the external components, such as covers, the impact energy limits were 100 ft-lb, while internal components were limited to 20 ft-lb impacts. Tables 7 and 8 specify the allowable CAI strength for the BWB laminates.

TABLE 7. LAMINATE CAI STRENGTH FOR BWB COVERS (100 FT-LB IMPACT)

Stacks	Thickness [in]	Stress, longitudinal [ksi]	Stress, transverse [ksi]
2	.110	38.8	19.6
3	.165	38.8	19.6
4	.220	38.8	19.6
5	.275	38.8	19.6
6	.330	43.8	22.1
7	.385	46.2	23.3
8	.440	48.9	24.7
9	.495	52.6	26.6
10	.550	58.6	29.6
11	.605	61.1	30.8
12	.660	63.7	32.2

TABLE 8. LAMINATE CAI STRENGTH FOR BWB SPARS/RIBS (20 FT-LB IMPACT)

Stacks	Thickness [in]	Stress, longitudinal [ksi]	Stress, transverse [ksi]
2	.110	37.9	22.2
3	.165	42.0	24.6
4	.220	47.6	27.9
5	.275	53.3	31.2
6	.330	54.8	33.1
7	.385	54.8	33.3
8	.440	54.8	33.6
9	.495	54.8	33.8
10	.550	54.8	33.8
11	.605	54.8	33.9
12	.660	54.8	33.9

The allowable tension strength was, in general, a function of the impact energy and laminate thickness. Since only a limited amount of testing has been done to date to establish the tension after impact (TAI) for a range of laminates, the values shown below were used based on the results of testing a single set of 4-stack coupons with .10-inch dents (Reference 3).

Class T1C72 , Upper cover $F_{tu} = 48.6$ ksi

Class T2C72 , Lower cover $F_{tu} = 62.9$ ksi

Core Material Properties - Rohacell 110 WF foam was used in the frame. Table 9 lists the minimum stiffness and strength properties for Rohacell foam at RT.

TABLE 9. ROHACELL MINIMUM PROPERTIES

Rohacell	Density lbs/ft ³	Compressive Strength psi	Tension Modulus psi	Shear Strength psi	Shear Modulus psi	Tensile Strength psi
110 WF	6.24	407	21000	294	7950	441
200 WF	12.81 ± 2.2	928	39150	522	14500	701

Rod Material Properties - The rods were fabricated using a compression molding technique with a Toray unidirectional T800/3900-2B fiber/resin system. Since only a limited test database exists for the rods using this manufacturing approach, a representative set of mechanical properties (Table 10) was generated for the molded rods used in the PRSEUS panels.

TABLE 10. ROD MECHANICAL PROPERTIES

Laminate Mechanical Properties	Test Condition	Minimum Average
Tension		
Ultimate Strength, ksi	RT	390
Modulus, Msi	RT	22.0
Ultimate Strain, percent	RT	1.68
Notched Tension, Ultimate Strength, ksi	RT 180°F	67.5 62.0
Notched Compression, Ultimate Strength, ksi	RT 180°F	42.0 35.0
Compression		
Ultimate Strength, ksi	RT 180°F	200 176.2
Modulus, Msi	RT -75°F	18.2 18.2
Comp After Impact, Ult Strength, ksi, 270 in-lb	RT	40.5
Compression Interlaminar Shear, Ult Strength, ksi	RT 180°F	9.00 7.50

Environmental Knockdowns - All reported strength values in this document are for RTD condition. When environmental conditions are to be considered in the analysis, these RTD strength value should be multiplied by the appropriate R_{env} ratio listed in Table 11.

TABLE 11. ENVIRONMENTAL CORRECTION RATIOS (R_{ENV}).

Failure Mode	Material	Parameter	Cond.	Ratio
Unnotched tension	All	F_t	CD	0.933
Unnotched compression	All	F_c	HW	0.601
Tension after impact	All	ϵ_{tai}	CD	0.700
Compression after impact	All	ϵ_{cai}	HW	0.919
Hole net-section tension	Warp/knit	ϵ_{uht}	CD	0.954
Hole net-section tension	Braided	ϵ_{uht}	CD	0.819
Hole net-section compression	AS4 Warp/knit	ϵ_{uhc}	HW	0.823
Hole net-section compression	IM7 Warp/knit	ϵ_{uhc}	HW	0.814
Hole net-section compression	Braided	ϵ_{uhc}	HW	0.768
Hole bearing initial yield	Warp/knit	F_{bri}	HW	0.779
Hole bearing initial yield	Braided	F_{bri}	HW	0.809
Hole bearing yield	Warp/knit	F_{bry}	HW	0.776
Hole bearing yield	Braided	F_{bry}	HW	0.842
Hole bearing ultimate	Warp/knit	F_{bru}	HW	0.863
Hole bearing ultimate	Braided	F_{bru}	HW	0.908
Fastener pull-through yield	All	F_{pty}	HW	0.771
Fastener pull-through ultimate	All	F_{ptu}	HW	0.882

1.1.3 Manufacturing and Process Requirements

Using this approach (Figure 21), complex stitched panel assemblies can be built without exacting tolerances, and then accurately net-molded in a single oven-cure operation using high-precision outer moldline (OML) tooling. Since all the materials in the stitched assembly are dry, there are no out-time, or autoclave limitations as in prepreg systems, which can restrict the size of an assembly because it must be cured within a limited processing envelope. Resin infusion is accomplished using a soft-tooled fabrication method where the bagging film conforms to the inner moldline (IML) surface of the preform geometry thus eliminating costly tooling that would normally be required to form net-molded details.

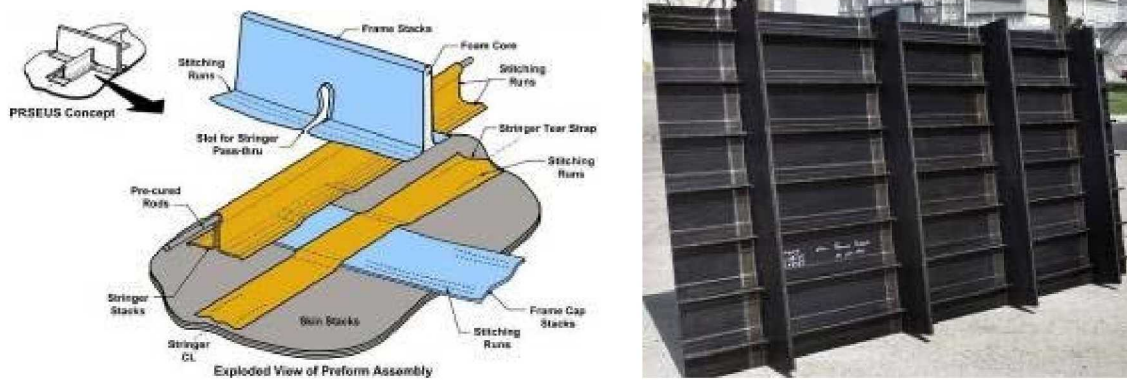


FIGURE 21. PRSEUS PANEL

Key Fabrication Technologies - Moving outside the autoclave represents an improvement over the first-generation stitching and resin infusion technologies developed by NASA-LaRC and The Boeing Company under the Advanced Composite Technology (ACT) research program. While these new fabrication techniques are better for BWB structures, the highly integrated nature of the design and manufacturing also requires a more thorough understanding of the process and its relationship to the design. (Reference 4)

PRSEUS panel fabrication utilizes a low-pressure resin infusion technique called the CAPRI (Controlled Atmospheric Pressure Resin Infusion) process. In this approach (Figure 22), the resin is pushed through the dry carbon preform by a vacuum-induced pressure differential, that not only promotes resin flow but also creates a critical pressure differential normal to the vacuum bag surface. This normal-acting force compacts the preform bulk and enables laminate fiber volumes of nearly 60%. This permits the low-pressure processing technique to achieve higher fiber volume fractions and mechanical properties that now rival those of state-of-the-art prepreg material systems that typically require autoclave processing environments.

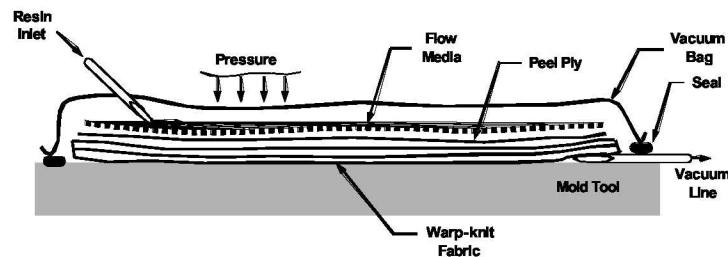


FIGURE 22. CAPRI (CONTROLLED ATMOSPHERIC PRESSURE RESIN INFUSION)

The basic building block of the PRSEUS concept is the dry warp-knit fabric. Warp-knitting technology offers the flexibility of mixing tow concentrations and material types, like carbon and glass of various tensile strengths and moduli, at various orientations and locations to create highly optimized multi-axial fabrics. These fabrics can be specifically tailored for different aircraft types and loading conditions to optimize cost and weight. This feature is particularly attractive for a BWB design because it offers an inexpensive way to optimize the weight and cost performance for the compound curvature of the airframe.

Stitching a dry-fiber preform of a 3-D structure like PRSEUS using a conventional two-sided stitching process would require extremely complex tooling. This tooling would have to support the preform, but move out of the way as the bobbin on the bottom surface passes, and then move back into position to support the preform. Although this works for assembling small panels with simple geometry, it has proven to be cost prohibitive for large complex structures.

PRSEUS preforms are fabricated using one-sided stitching technology that enables the use of stitching for joining, fastening, and stabilizing dry fabrics while accessing the material from only one side. The end effector consists of two needles, one for inserting the thread, and one for catching the loop of thread formed by the other needle. Using a single thread, the two needle system forms a modified chain stitch (Figure 23).

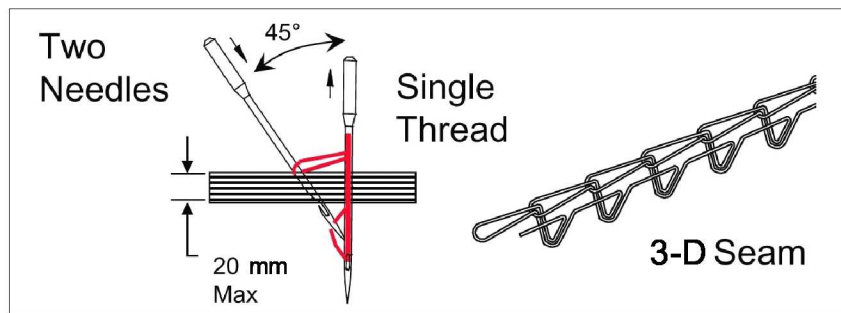


FIGURE 23. SINGLE THREAD MODIFIED CHAIN STITCH SEAM

An industrial robot arm gives the end effector six degrees of freedom for stitching in 3-D space. One-sided robotic stitching of large complex structures, like the BWB wing and fuselage components, is now possible. In addition, the design and construction of the preform support tooling for one-sided stitching is straightforward. The tool must merely replicate the inner or outer surface of the component with clearance for the sewing needles to poke through the material at seam locations. Using techniques developed by the textile industry, these highly-tailored fabrics are built up into details and assembled together with stitching.

PRSEUS Panel Fabrication— Manufacture of the dry fiber preforms for the PRSEUS panel starts with the cutting and kitting of the plies of dry material that make up the skin, stringer, and frame components. The 50-inch wide warp-knit multi-axial carbon fiber fabric were cut into individual details and placed into kits. Frame details are constructed using dry warp-knit fabric and closed-cell foam materials. The foam core was CNC machined with all the detailed features required to support the frame plies, carbon fiber rods and resin infusion processing. They were assembled by wrapping the dry fabric plies around the machined foam core by hand and then stapling the fabric in place (Figure 24).



*Frame Stack
Placement on Core*

*Frame Stacks
Stapled in Place*

*Frame Stacks
Over Wrapped*

FIGURE 24. FRAME DETAIL PREFORM ASSEMBLY

Stringer details are initially assembled using dry fabric and a leader wire. The precut stringer pieces were folded in half length-wise and then stitched in two locations. One seam defines the bulb feature at the top of the stringer while the other establishes the fold line for the stringer flange. (Figure 25)

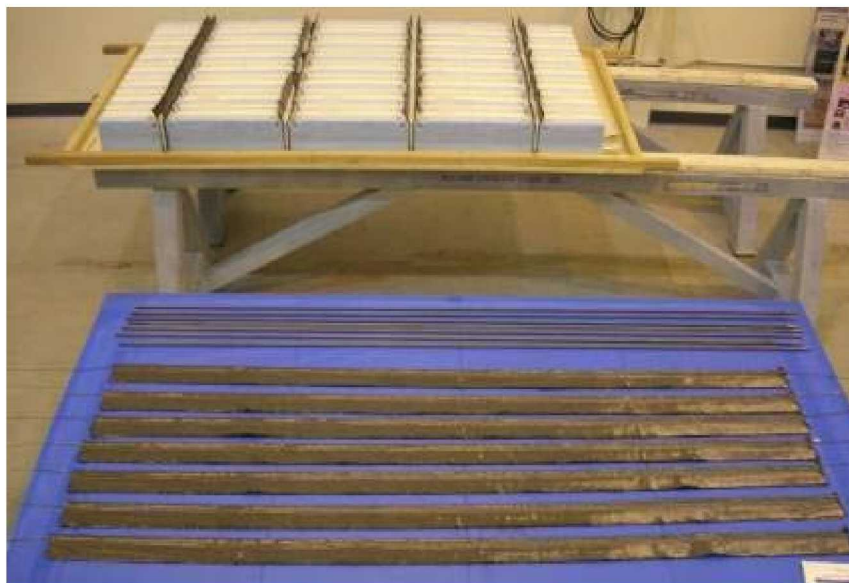


FIGURE 25. STRINGER AND FRAME WARP-KNIT FABRIC DETAILS

The individual details were then located in the preform assembly fixture (Figure 26) prior to the stitching operation. The frames were installed into the assembly tool first by simply dropping the stapled foam core preform into the corresponding slot for each frame station, and then the stringers were installed next in between the matching sets of plastic mandrels working from one side of the panel to the other. Next, the flanges were folded down, tear straps were laid over the stringer and frame flanges, and then covered by the skin stacks.

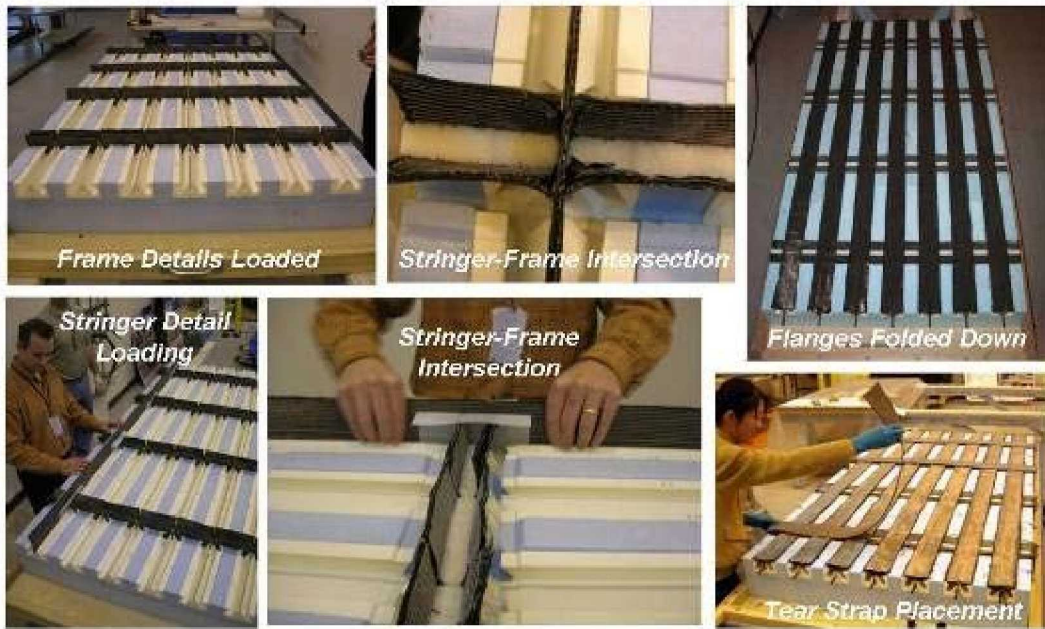


FIGURE 26. PLACEMENT OF STRINGER AND FRAME DETAILS

The details were then joined by stitching to create a preform assembly (Figure 27). The preform assembly tool has slots positioned at stitching seam locations to let the sewing needles penetrate through that region of the preform. The stringers and the frames were stitched to the skin using the single-sided stitching operation where two rows of stitching were placed along all the edges of the stringer and frame flanges. The completed preform assembly was then transferred to a rigid OML tool where the stitching tool was removed. (Figure 27)



FIGURE 27. PREFORM PANEL ASSEMBLY STITCHING AND TOOL REMOVAL

At this point the stitched preform maintains a rigid shape and can easily be handled. The stringer rods are firmly locked into the rough edges of the foam-core frames providing a rigid backbone for the dry carbon fabric to cling to. The sturdiness of the self-supporting preform design is apparent in Figure 28, where the preform was lifted off the cure tool by grasping the stringer ends in only four locations.



FIGURE 28. FREE-STANDING PREFORM LIFTED OFF TOOL

The free-standing preform can now be vacuum bagged from the IML side (Figure 29). By integrating the tool and the part being fabricated, the formation or molding of critical internal design features of the structure is possible without hard metal tooling. Such tooling typically requires a large amount of touch labor to clean, release, install and remove. Eliminating it reduces the manufacturing cost and substantially accelerates the overall assembly of the fuselage.



FIGURE 29. RESIN INFUSION AND OVEN CURE OPERATION

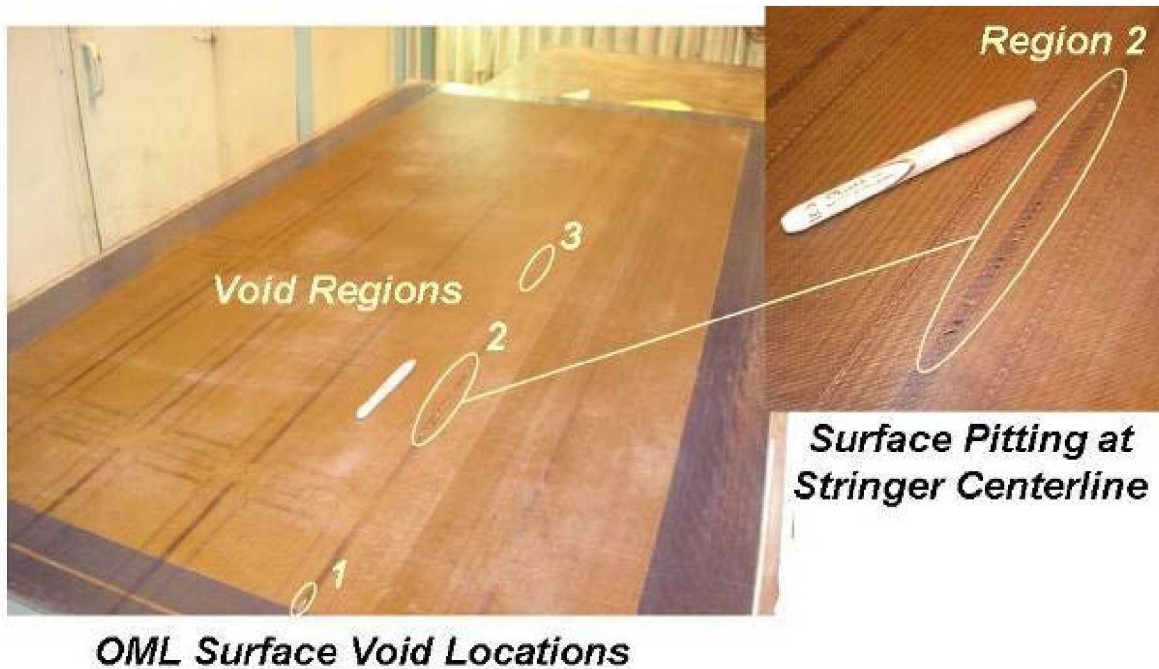
Once a vacuum was established, the resin was introduced into the flow media (which rests on the inner surface of the part) where it rapidly moved across the part surface before finally migrating through the thickness. Once the part was filled with resin, a 250° F oven-cure operation was

completed (Figure 30), which was then followed by a 350° F free-standing post-cure cycle with the bagging materials removed.



FIGURE 30. PANEL 1 AFTER PEEL PLY REMOVAL PRIOR TO POST CURE

Two 42-inch-by-80-inch panels were fabricated under the Phase I contract. Panel 1 was successfully infused, cured, and then cut up to make four single-stringer and four single-frame compression test specimens. Panel 2 was successfully infused and cured although it had some small surface imperfections (Figure 31), caused by operator error during the resin infusion cycle (exceeded resin infusion processing time limit).



OML Surface Void Locations

FIGURE 31. PANEL 2 SURFACE VOID LOCATIONS

Since the pitting was confined to skin surface and contained within the stitch rows, a simple resin-fill repair was completed. A summary of the repair considerations is summarized in Figure 32. The repaired panel (Panel 2), along with the fatigue specimens that were cut from Panel 1

were shipped to NASA-LaRC for future testing outside the scope of the Phase I contract. (Figure 33)

Summary:

- Complete fiber wet-out
- Confined to single stringer
- Between stitch rows
- Less than CAI criterion
- No effect on strength
- Resin fill repair

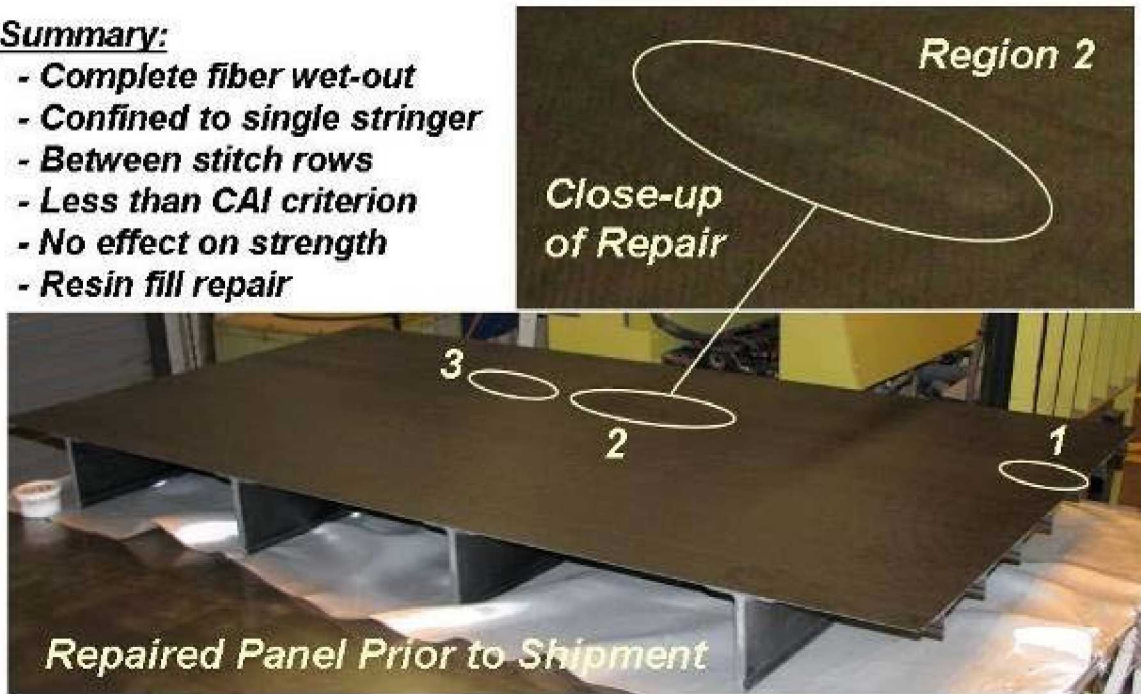


FIGURE 32. PANEL 2 REPAIR AND EDGE TRIM



FIGURE 33. PANEL 2 WITH FATIGUE SPECIMENS CUT FROM PANEL 1 (SHIPPED TO NASA)

1.1.4 Load Case Development

The loads assessment used the BWB-5-200G baseline with a TOGW of 408,700 lbs at the forward CG limit. Table 1 (page 3) summarizes the take-off gross weight (TOGW) distribution.

FAR-25 (Federal Aviation Regulations Part 25 - Airworthiness Standards: Transport Category Aircraft) was used as a guideline in defining the loads criteria for this study. Results of previous loads analyses of BWB aircraft configurations were used to aid in the identification of critical load cases of this configuration for vehicle-level sizing. Since the margins of safety calculated in the sizing process were based on limit load values, a factor of safety of 1.50 was used to obtain ultimate loads.

The process of determining the critical load cases for the structural optimization is iterative and is based on the initial aircraft stiffness, mass distribution, and flight envelope. Critical conditions are determined by simulating the required maneuvers across the flight envelope using a loads model. Once the maximum internal forces are isolated for particular components on the aircraft, a simplified subset of these cases can then be used for the structural optimization.

Flight Envelope

The limiting airspeeds were provided for two weights at the forward c.g. limit of 34.85% mac:

- (1) $1.07 \text{ OEW} + 0.35 \text{ max payload} = 246,572 \text{ lbs}$
- (2) $\text{MTOGW} = 408,680 \text{ lbs}$

The 1-g stall speeds were based on a BWB-5-200G maximum lift coefficient derived from low-speed wind tunnel data adjusted for flight Reynolds number, with a Mach number correction applied. The speeds apply to the slats retracted “clean” configuration and were calculated to an altitude of 43,000 ft.

Additional specifications of the flight envelope were as follows:

- $V_B = 305 \text{ KCAS}$
- $V_C = 355 \text{ KCAS} (M_C = 0.88)$
- $V_D = 405 \text{ KCAS} (M_D = 0.95)$
- $V_F = 280 \text{ KCAS}$ (maximum slats extended speed)

The estimated maximum control deflection limits are shown in Table 12. These limits were based on maximum deflection estimates for the BWB 450-1L airplane configuration at 355 KEAS and then ratioed to lower and higher airspeeds as a function of dynamic pressure for the 5-200G configuration used in the this study.

TABLE 12. ESTIMATED MAXIMUM CONTROL DEFLECTION LIMITS

elev 1-5 TED		elev 1-5 TEU		elev 6,7 (U or L)		winglet rudders-ob		winglet rudders-ib	
Ve (kt)	δ_{LIMIT} (deg)	Ve (kt)	δ_{LIMIT} (deg)	Ve (kt)	δ_{LIMIT} (deg)	Ve (kt)	δ_{LIMIT} (deg)	Ve (kt)	δ_{LIMIT} (deg)
200	30.00	200	-40.00	200	60.00	200	-40.00	200	30.00
205	30.00	205	-40.00	220	60.00	220	-40.00	220	30.00
210	28.58	210	-38.10	240	60.00	240	-40.00	240	30.00
220	26.04	220	-34.72	251	60.00	251	-40.00	251	30.00
240	21.88	230	-31.76	260	55.93	260	-37.29	260	27.96
260	18.64	240	-29.17	280	48.22	280	-32.15	280	24.11
280	16.07	260	-24.86	300	42.01	300	-28.01	300	21.00
300	14.00	280	-21.43	320	36.92	320	-24.61	320	18.46
320	12.31	300	-18.67	340	32.71	340	-21.80	340	16.35
340	10.90	320	-16.41	367	28.07	367	-18.71	367	14.04
367	9.36	340	-14.54	380	26.18	380	-17.45	380	13.09
380	8.73	367	-12.48	405	23.05	405	-15.37	405	11.52
405	7.68	380	-11.64						
		405	-10.24						

The maximum angle-of-attack for incipient outer wing stall (slats extended) was 26 deg. This was the angle assumed for C_{Lmax} . For the clean (slats retracted) configuration, the corresponding angle of attack at C_{Lmax} was 10 deg.

Approximately eighty loading conditions were evaluated to determine the critical cases. After the loads analysis, fourteen cases were determined to be critical for the optimization and sizing exercises on this configuration of the aircraft. The load cases used in the vehicle-level sizing analyses came from a simplified assessment of cabin pressure, taxi bump, crash, and maneuver loads as follows:

Cabin Pressure - For the non-curved design of the BWB airplane, pressurization of the shell is expected to drive some of the sizing of the skin where other loads are low. For this reason, a cabin over-pressurization load case was analyzed with an internal pressure equal to twice the maximum allowable cabin pressure differential. This internal pressure load case does not include any aerodynamic, inertial or other external loads. For the FEM, a pressure differential of 18.4 psi ultimate was used for the 2P pressurization load case.

Taxi Bump - This ground handling case was run by applying a downward 2.0 g inertial load to the entire structure and to all of the mass in the model. The ground loads analyses for landing impact and taxi only calculate the nose and main landing gear applied loads to be used in future landing & taxi aircraft loads analysis.

Crash Loads - These ultimate load cases were run by applying two separate ultimate inertial loads to the entire structure and to all of the mass in the model. These were a forward 9.0 g and a lateral 4.5 g inertial load to meet the requirements for an ultimate crash load case.

Maneuver Loads - Loads were evaluated for the symmetric maneuver, yaw maneuver, roll maneuver (with and without cabin pressure) and gust conditions. An initial loads survey was run to determine the critical set of maneuver cases that defined the edges of the flight envelope. Asymmetric maneuvers as well as symmetric maneuvers were considered. These limit load conditions for gust and maneuver loading are summarized in Tables 13 and 15.

TABLE 13. LOAD SURVEY - GUST CASES

CASE No.	G.W (lbs)	C.G (%)	SPEED (Knots)	ALT(ft)	q(psi)	Mach No.	Ude	DEFINITION
10001	408 680	36.74	305.0	0.0	2.1871	0.461	41.222	Vertical Up Gust
10002	408 680	36.74	355.0	0.0	2.9629	0.537	41.222	Vertical Up Gust
10004	408 680	36.74	380.2	25337.0	3.3985	0.950	17.245	Vertical Up Gust
10005	408 680	36.74	334.8	27627.0	2.6353	0.880	33.968	Vertical Up Gust
10006	408 680	36.74	284.9	34663.0	1.9083	0.880	32.154	Vertical Up Gust
10007	408 680	36.74	305.0	0.0	2.1871	0.461	41.222	Vertical Down Gust
10008	408 680	36.74	355.0	0.0	2.9629	0.537	41.222	Vertical Down Gust
10009	408 680	36.74	405.0	0.0	3.8563	0.612	20.611	Vertical Down Gust
10010	408 680	36.74	380.2	25337.0	3.3985	0.950	17.245	Vertical Down Gust
10012	408 680	36.74	284.9	34663.0	1.9083	0.880	32.154	Vertical Down Gust
20001	408 680	36.74	305.0	0.0	2.1871	0.461	41.222	Right Lateral Gust
20006	408 680	36.74	284.9	34663.0	1.9083	0.880	32.154	Right Lateral Gust
20011	408 680	36.74	305.0	0.0	2.1871	0.461	41.222	Left Lateral Gust
20013	408 680	36.74	405.0	0.0	3.8563	0.612	20.611	Left Lateral Gust

The results of the gust load survey were then used to assess the maximum forces acting on major components of the airplane; where VS = vertical stabilizer, OWNG = outer wing, IWNG = inboard wing, and OCB = pressurized cabin, in Table 14.

TABLE 14. SORTED GUST LOAD CASES BY COMPONENT

GUST(2005)	Max Fz	Case No.	Min Fz	Case No.	Max Mx	Case No.	Min Mx	Case No.	Max My	Case No.	Min My	Case No.	
VS	1141.22	-3.07713	10008	-49.5129	10002	1597.72	10002	137.62	10008	108.288	20001	-1128.55	10004
VS	1136.85	91.9103	10010	-68.1775	10001	10491.2	10002	-390.074	10008	-2801.15	10007	-15657.3	10004
VS	1130.33	817.828	10004	246.323	20011	15230.4	10001	-24671.4	10010	-2835.85	10007	-29400.7	10004
VS	1124.59	1443.87	10004	418.877	20011	-20580.1	20011	-82247.8	10004	7931.98	10008	-407495	10002
OWNG	1113.69	3311.1	10004	1322.03	10007	-362588	10007	-1241270	10004	-188268	10008	-787944	10004
OWNG	1049.98	12975.4	10005	325.795	10008	-536943	10007	-1767940	10004	-73969.5	10008	-968767	10005
OWNG	990.7	14639.8	10005	1209.71	10008	-628324	10008	-2790980	10004	-40151.4	10008	-886365	10005
OWNG	931.43	21365.5	10006	-3220.61	10008	-389045	10008	-4237820	10005	189732	10008	-886002	10006
OWNG	872.15	34167.1	10006	-17314.3	10009	251063	10008	-6149060	10005	1012770	10009	-876302	10008
OWNG	812.88	34393.9	10006	-16799.7	10009	1462150	10008	-8547310	10006	1064970	10009	-803839	10008
OWNG	753.6	47817.2	10006	-28205.4	10009	3030450	10008	-11575800	10006	1993000	10009	-918438	10008
OWNG	694.33	56351.1	10006	-34583.6	10009	5010300	10008	-15235700	10006	2801940	10009	-957932	10008
OWNG	635.05	64069.5	10006	-28309.6	10008	7321140	10008	-19540100	10006	3150840	10009	-409559	10008
OWNG	575.78	70460.3	10006	-36170.8	10008	9999500	10008	-24604800	10006	3824250	10009	-539923	10008
OWNG	497.5	92437.9	10006	-29196.6	10008	13448100	10008	-32238600	10006	8662150	10009	-833262	10008
IWNG	429.5	86656.5	10006	-49328.4	10008	16604200	10008	-34098000	10006	19100100	10006	-5773710	10008
IWNG	360.5	90549.6	10006	-34516.7	10008	19349000	10008	-40472200	10006	18957700	10006	-5153860	10008
IWNG	289.5	95117.3	10006	-25711.5	10008	21386000	10008	-47179600	10006	17467900	10006	-5480980	10008
IWNG	223.5	72231.4	10001	-16296.7	10008	22613900	10008	-53018900	10006	15036100	10006	-3647530	10008
OCB	160	88815.8	10002	-4645.47	10008	23437800	10008	-57218300	10006	9200640	10006	-2920190	10008
OCB	80	63770.6	10002	-4325.58	10008	23929200	10008	-61748800	10006	-4215480	10012	-17653100	10002
OCB	1	750.7	10006	-6355.1	10009	24129500	10008	-63415100	10006	1576350	20006	-2436650	20013

CASE DEFINITION :

CASE NO : 100XX

CASENO : 200XX

XX : 01 - 06 - Up Gust



XX : 01 - 06 - Right Lateral Gust



07 - 12 - Down Gust



11 - 16 - Left Lateral Gust



TABLE 15. LOAD SURVEY - MANEUVER CASES

CASE No.	G.W (lbs)	C.G (%)	SPEED (K _{ess})	ALT(ft)	C.P(psi)	L.F (G)	DEFINITION
100106	408 680	36.74	355.0	0.0	0.00	-1.00	Pushovers
160005	408 680	36.74	304.2	35000.0	8.00	2.50	2.5G
101205	408 680	36.74	304.2	35000.0	0.00	1.67	Checked RWU Roll COORD
101239	408 680	36.74	380.1	25337.0	0.00	0.00	Checked LWU Roll COORD
161005	408 680	36.74	304.2	35000.0	8.00	1.67	Intial RWU Roll COORD
161025	408 680	36.74	304.2	35000.0	8.00	0.00	Intial RWU Roll COORD
102119	408 680	36.74	380.1	25337.0	0.00	1.00	Dynamic Overswing RWF
102209	408 680	36.74	380.1	25337.0	0.00	1.00	Rudder Reversal LWF
162213	408 680	36.74	293.1	20000.0	4.75	1.00	Rudder Reversal RWF

The results of the maneuver load survey were also used to assess the maximum forces acting on major components of the airplane; where VS = vertical stabilizer, OWNG = outer wing, IWNG = inboard wing, and OCB = pressurized cabin, in Table 16.

TABLE 16. SORTED MANEUVER LOAD CASES BY COMPONENT

MANEUVER(2005)	Max Fz	Case No.	Min Fz	Case No.	Max Mx	Case No.	Min Mx	Case No.	Max My	Case No.	Min My	Case No.	
VS	1141.22	173216	102209	-219.039	161005	5799.74	161005	-4265.51	161025	18553.3	102119	-18013.2	102119
VS	1136.85	791699	161025	-686.079	161005	49343.1	161005	-42876.9	161025	48597.2	102119	-71100.3	102119
VS	1130.33	3761.73	102209	-1529.69	162213	160037	161005	-209778	102209	309142	102119	-294391	102119
VS	1124.59	5912.66	102209	-2247.98	162213	512653	161025	-678465	102209	1427890	161025	-1684690	161005
OWNG	1113.69	8766.26	102209	-1562.32	162213	960967	162213	-3676770	102209	415853	162213	-2022590	102209
OWNG	1049.98	25892.8	160005	-10737.4	100106	1154050	162213	-4700610	102209	609822	100106	-2112020	102209
OWNG	990.7	28344.4	160005	-18485.8	162213	1886150	162213	-6246330	102209	633515	101239	-2601580	102119
OWNG	931.43	45099	160005	-24267.4	100106	2952940	162213	-8098480	160005	1367590	101239	-2830530	102119
OWNG	872.15	76644	160005	-56398.7	100106	5721270	100106	-12503500	160005	3144320	101239	-3873210	101205
OWNG	812.88	77075.4	160005	-55955.7	100106	9763390	100106	-18006200	160005	3463130	101239	-4163890	101205
OWNG	753.6	107132	160005	-83981.9	100106	14831900	100106	-24767500	160005	5492740	101239	-5779840	101205
OWNG	694.33	125815	160005	-100789	100106	21044500	100106	-32887500	160005	6664680	101239	-6572170	101205
OWNG	635.05	136387	160005	-97978.6	100106	28271300	100106	-42315200	160005	8003030	101239	-7043830	101205
OWNG	575.78	150303	160005	-114482	100106	36635800	100106	-53196900	160005	9809930	101239	-8595540	101205
OWNG	497.5	179210	160005	-116745	100106	48277700	100106	-69258600	160005	15549500	101239	-11532500	101205
IWNG	429.5	186307	160005	-143890	100106	54287700	100106	-73859600	160005	42710100	161005	-27431700	161025
IWNG	360.5	182793	160005	-123318	100106	63513500	100106	-86918200	160005	44298100	161005	-28766900	161025
IWNG	289.5	186655	160005	-113379	100106	71835600	100106	-100125000	160005	42569400	161005	-28229200	161025
IWNG	223.5	137657	161005	-92088.6	161025	78042700	100106	-111644000	160005	42281300	161005	-25158900	161025
OCB	160	162959	161005	-72589.6	100106	82424000	100106	-125036000	160005	30363300	161005	-25652500	161025
OCB	80	150274	161005	-92309.6	161025	86759400	100106	-145942000	160005	16669000	161025	-30983600	161005
OCB	0.1	99634.9	161005	-98403.8	162213	88373800	100106	-150254000	160005	24670600	102119	-23794600	161025

CASE DEFINITION :

CASENO: 1 X Y ##

X : 0 - Without Cabin Pressure 6 - With Cabin Pressure

Y : 0 - Symmetric Maneuver



1 - Roll Maneuver



2 - Yaw Maneuver



The maximum limit loads were then plotted to create the load envelopes shown in Figure 34.

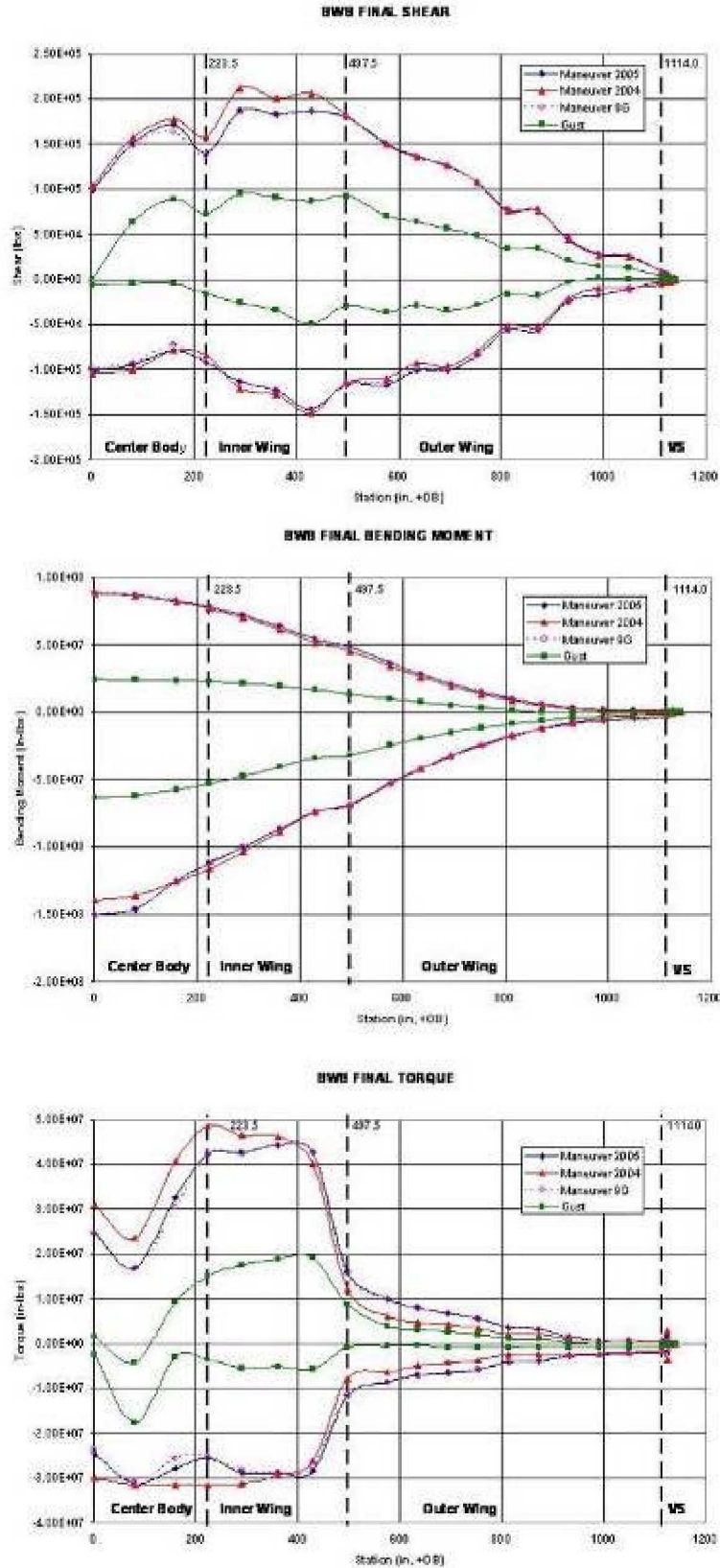


FIGURE 34. BWB SHEAR/MOMENT/TORQUE DIAGRAMS

Once the critical set of maneuver cases defining the loads envelope were found, they were used in the sizing process. All of the cases included in sizing were run without cabin pressure. A NASTRAN vortex lattice model was used to produce the aeroelastic loads for the structural FEM.

The final maneuver load cases that were used in the global optimization are summarized in Table 17.

TABLE 17. MANEUVER LOAD CASES USED FOR GLOBAL OPTIMIZATION

SYMMETRIC BALANCE MANEUVERS								
(trim solves for alpha, longitudinal load factor and control surface 1-3 deflections)								
COND	Mach	SPEED	Altitude	Nz	C.P			
		(KEAS)	ft	(G's)	(psi)			
100106	0.54	355(Vc)	0	-1	0			
160005	0.95(Md)	304(VptA)	35	2.5	8			
DYNAMIC OVERSWING								
Max Sideslip, Max Subtracting Rudder deflection, Max drag rudder forces								
(trim solves for side load factor, yaw acceleration and control surface 4 and 5 deflection)								
COND	Mach	SPEED	Altitude	Nz	C.P	Beta	LH Rudder	RH Rudder
		(KEAS)	ft	(G's)	(psi)	(Deg)	(Deg)	(Deg)
102119	0.95(Md)	380(vd)	25,337	1	0	5	17.4	-13.1
RUDDER REVERSAL								
Max Sideslip, Max Adding Rudder deflection, Max drag rudder forces								
(trim solves for side load factor, yaw acceleration and control surface 4 and 5 deflection)								
COND	Mach	SPEED	Altitude	Nz	C.P	Beta	LH Rudder	RH Rudder
		(KEAS)	ft	(G's)	(psi)	(Deg)	(Deg)	(Deg)
102209	0.95(Md)	380(Vd)	25,337	1	0	5	-13.1	17.4
102211	0.41	274(VptA)	0	1	0	-7.36	33.8	-25.34
162213	0.65	293(VptA)	20,000	1	4.75	-5.6	29.4	-22.1
INITIAL ROLL MANEUVERS								
Roll Rate = 0, Sideslip = 0, Control Surfaces 4-7 maximum deflection								
(trim solves for side load factor, roll acceleration and rudder deflection)								
COND	Mach	SPEED	Altitude	Nz	C.P	LH CS	RH CS	
		(KEAS)	ft	(G's)	(psi)	(Deg)	(Deg)	
161005	0.95(Md)	304(VptA)	35,000	1.67	8	-18.2	13.6	
161025	0.95(Md)	304(VptA)	35,000	0	8	-18.2	13.6	
CHECKED ROLL MANEUVERS								
Roll Rate set to Steady roll rate, Control Surfaces 4-7 maximum deflection								
(trim solves for side load factor, roll acceleration and rudder deflection)								
COND	Mach	SPEED	Altitude	Nz	C.P	LH CS	RH CS	
		(KEAS)	ft	(G's)	(psi)	(Deg)	(Deg)	
101205	0.95(Md)	304(VptA)	35,000	1.67	0	-18.2	13.6	
101239	0.95(Md)	380(Vd)	25,337	0	0	8.7	-11.6	

One taxi bump load case, two crash load cases, ten maneuver cases, and one cabin pressure load case make up the fourteen cases that were used for the vehicle-level sizing studies to meet the goals of the Phase I statement of work.

1.1.5 FEM-based Structural Sizing

The vehicle-level BWB-5-200G finite element model was originally developed using Boeing IRAD funding and then modified for this study to include the basic sizing requirements for the PRSEUS structural concept in the pressurized region. The updated model was first used to size a baseline sandwich pressure cabin, and then repeated with a PRSEUS pressure cabin for comparison. The major changes include implementation of the PRSEUS concept on the upper and lower fuselage skin panels and the new frame design. The final FEM model (Figure 35) features the vehicle's fuselage skins, frames, ribs, spars and floors, wing skins, spars and ribs, vertical stabilizer, movable control surfaces and high-lift devices, and bulkheads. Structural cutouts were included for landing gear doors and cargo doors. The total number of elements in the vehicle model is approximately 44,000, which represents more than 142,000 degrees of freedom.

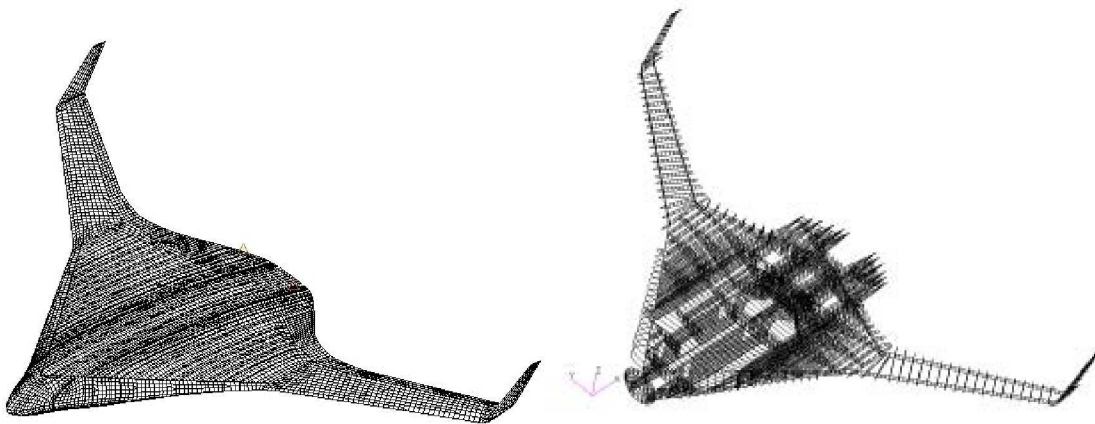


FIGURE 35. BWB FINITE ELEMENT MODEL CONTAINS OVER 44,000 ELEMENTS

Three- and four-node bending plate elements were used for skin, spar, and rib webs. Bending bar elements were used to represent frames, and floor beams. Axial rod elements were used to represent spar and rib caps. Stringers in PRESUS panels were not discretely modeled but instead, were smeared as equivalent properties for the stiffened panel simulations (PSHELL/MAT2 in NASTRAN), which were then locally sized in HyperSizer as true skin-stringer geometries.

Principal concentrated masses, including landing gear, engines, and major systems, were included to account for internal and external subsystems. The weight of furnishings and payload was applied to passenger and cargo floors/beams as distributed non-structural masses.

Structural Sizing - To conduct vehicle-level optimization efficiently, a two-stage global-local optimization approach was implemented (Figure 36). The FEM-based global sizing step constrains the overall vehicle-level stiffness and internal load distributions in order to satisfy vehicle-level, or airplane, design requirements. While a local panel-level analysis code checks whether local panel-level design parameters, such as panel stability or panel strength, are violated using the overall global stiffness requirements calculated from the vehicle-level analyses.

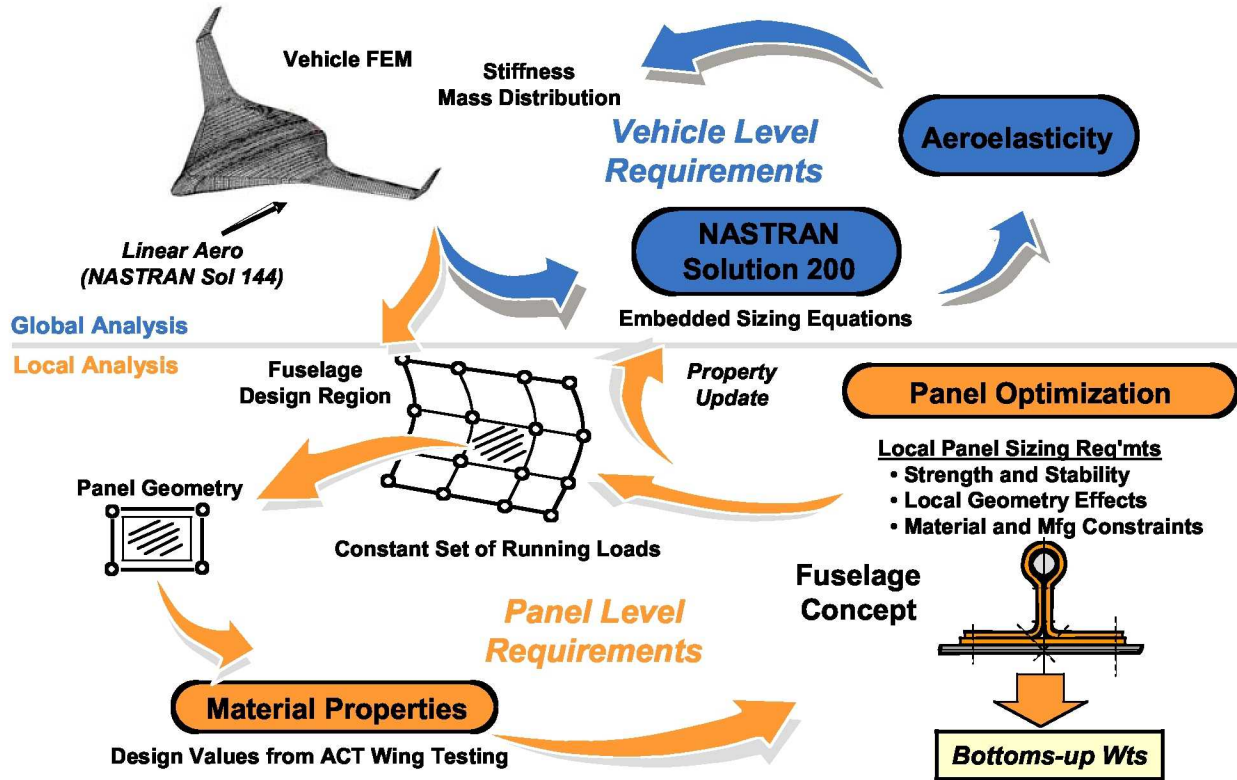


FIGURE 36. GLOBAL-LOCAL OPTIMIZATION APPROACH

Starting with the vehicle finite element model, loads, boundary conditions, and design constraints/requirements, a global optimization was performed using the optimization capabilities of MSC/NASTRAN (Sol 200) and local panel optimization was completed using the commercial analysis code HyperSizer. Over a series of iterations, the NASTRAN internal loads were imported back and forth into HyperSizer until a convergence of mass and stiffness was achieved. The HyperSizer code performed the local structural optimization using pre-defined material/structural properties and geometric design constraints to assess panel suitability for strength and stability constraints.

The resulting panel cross-sections were then idealized and exported back to the NASTRAN model as equivalent plate elements to simulate a PRSEUS fuselage panel response at the airplane level. Each time, the resized elements were used to create an updated NASTRAN design model for maneuver-load sizing (Figure 37). Once the models converged, the final sized weights were multiplied by non-optimum factors to generate a final “as-fabricated” weights distribution needed to balance the model. This final step was conducted outside the automated FEM optimization process.

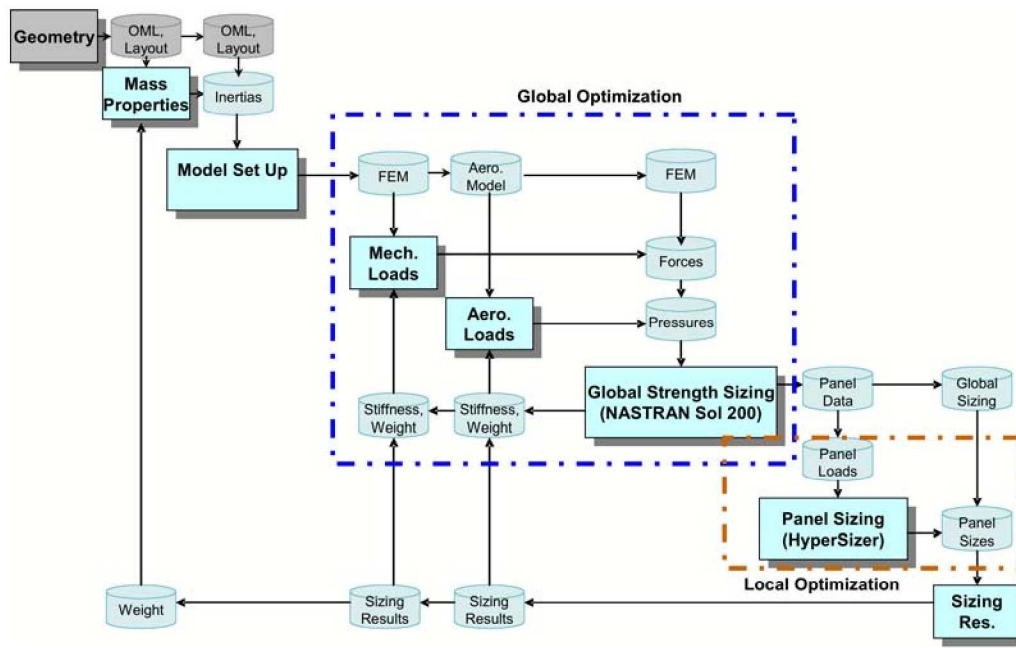


FIGURE 37. GLOBAL-LOCAL PROCESS FLOW

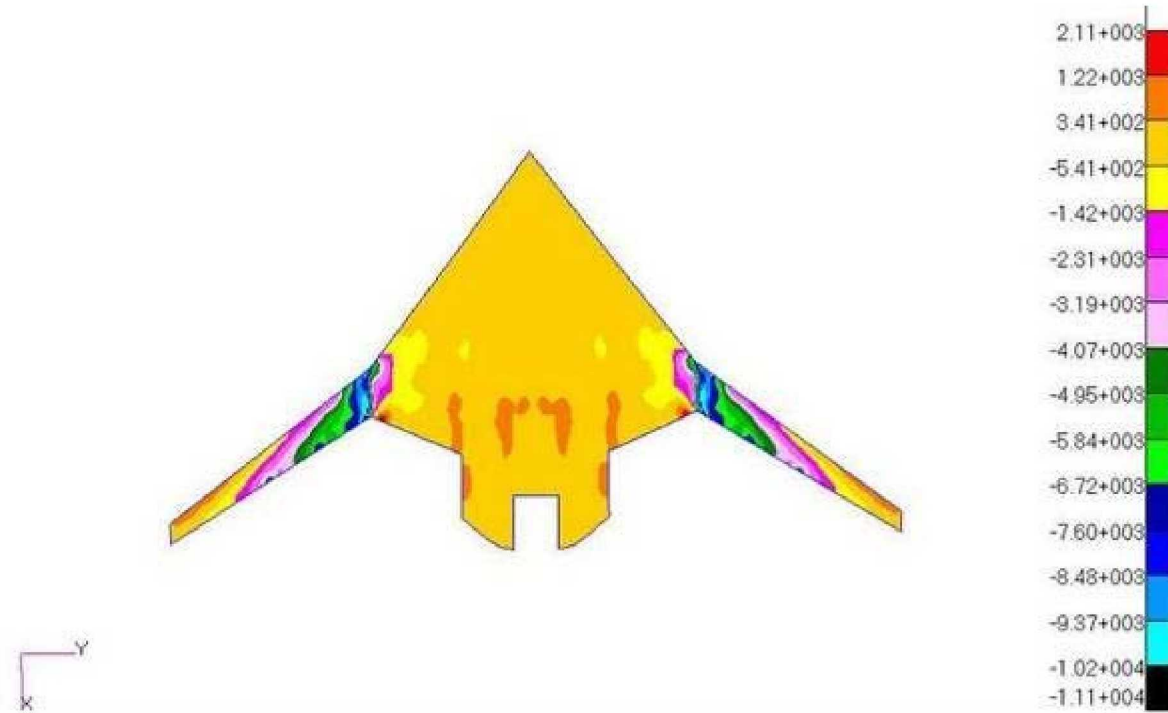
The vehicle-level structural sizing was based on a MTOGW of 408,700 lbs at the forward C.G. limit. The objective function being optimized was the overall vehicle weight. NASTRAN Sol 200 optimized the primary structure weight using global strength as the design criteria. Under this study, the optimization was limited to the pressurized fuselage cabin regions (Section 1, 2, 3, 4, 5) consisting of the upper and lower fuselage skin panels and associated frames. The bulkhead regions within the pressure cabin were held constant because their overall weights and load paths would not vary significantly as the skin panel and frame selections were changed for each of the two concepts under study. The remaining portions of the airframe, such as inboard & outboard wings and all substructures were also held constant in the sizing studies by maintaining the structural gages established from the original baseline (sandwich shell fuselage) FEM used in the prior trade study.

Internal Loads – The fourteen external load cases that were determined to be the most critical for sizing were applied to the updated finite element model in the structural optimization. A representative collection of critical running load plots is shown in the following figures (maneuver cases shown without internal pressure):

- 1) 2.5-g Limit Load Streamwise Direction (Nx) – Figure 38
- 2) 2.5-g Limit Load Spanwise Direction (Ny) – Figure 39
- 3) -1.0-g Limit Load Streamwise Direction (Nx) – Figure 40
- 4) -1.0-g Limit Load Spanwise Direction (Ny) – Figure 41
- 5) 1.33P Limit Load Streamwise Direction (Nx) – Figure 42
- 6) 1.33P Limit Load Spanwise Direction (Ny) – Figure 43

As expected, the plots show the critical maneuver loads (2.5 and -1.0-g) are dominant in the shell region adjacent to the wing, but less so moving forward. Whereas the forward portion of the fuselage shell is dominated by the 2P pressure loading ($2P = 1.33P \times 1.5$). This observation was consistent throughout the sizing process.

Upper:



Lower:

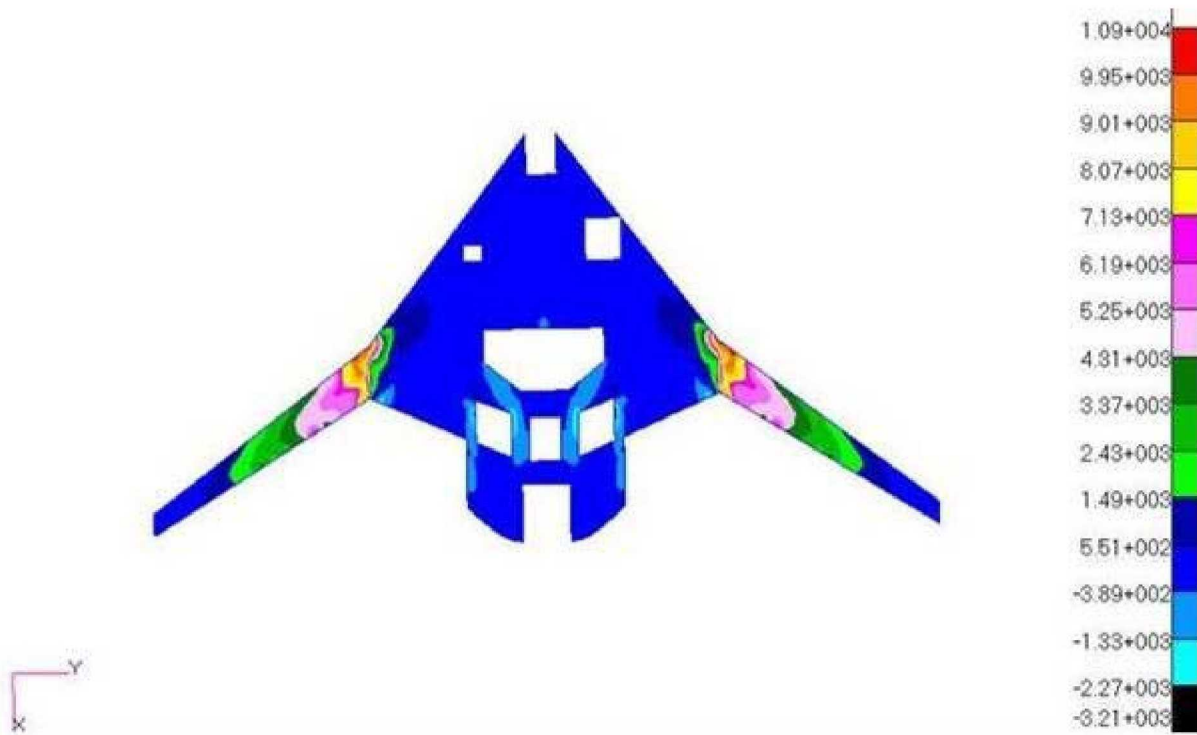
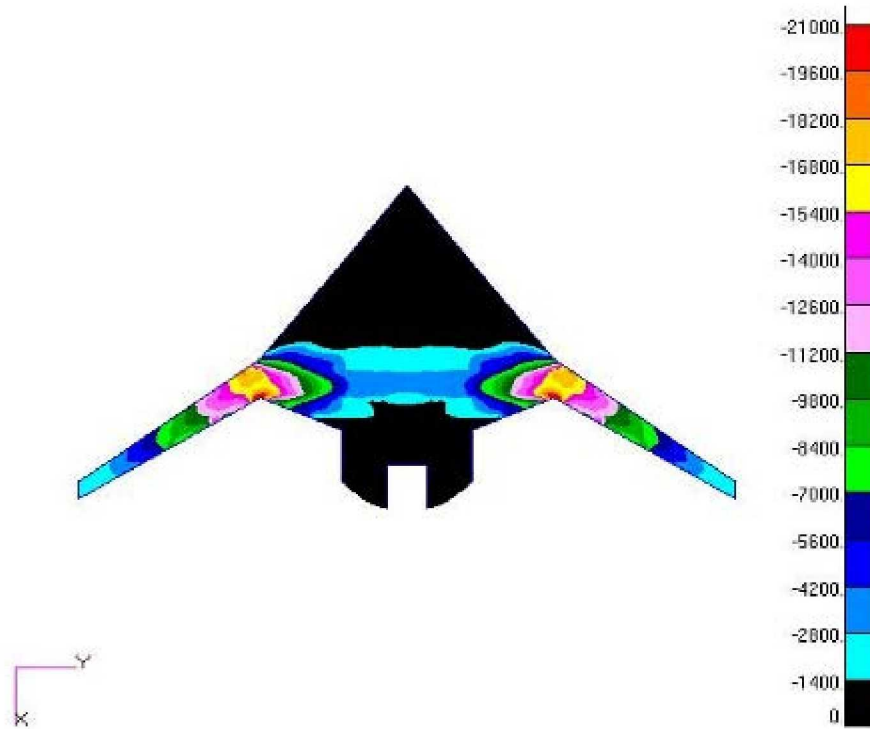


FIGURE 38. 2.5-G LIMIT LOAD STREAMWISE DIRECTION (NX) LBS/IN

Upper:



Lower:

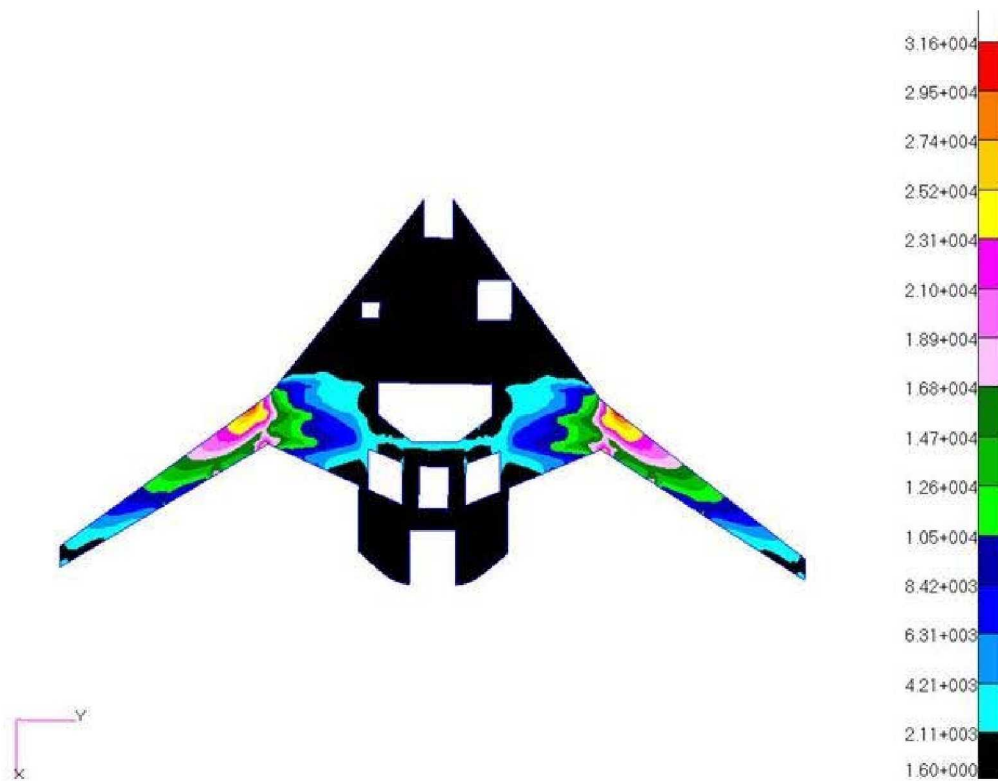
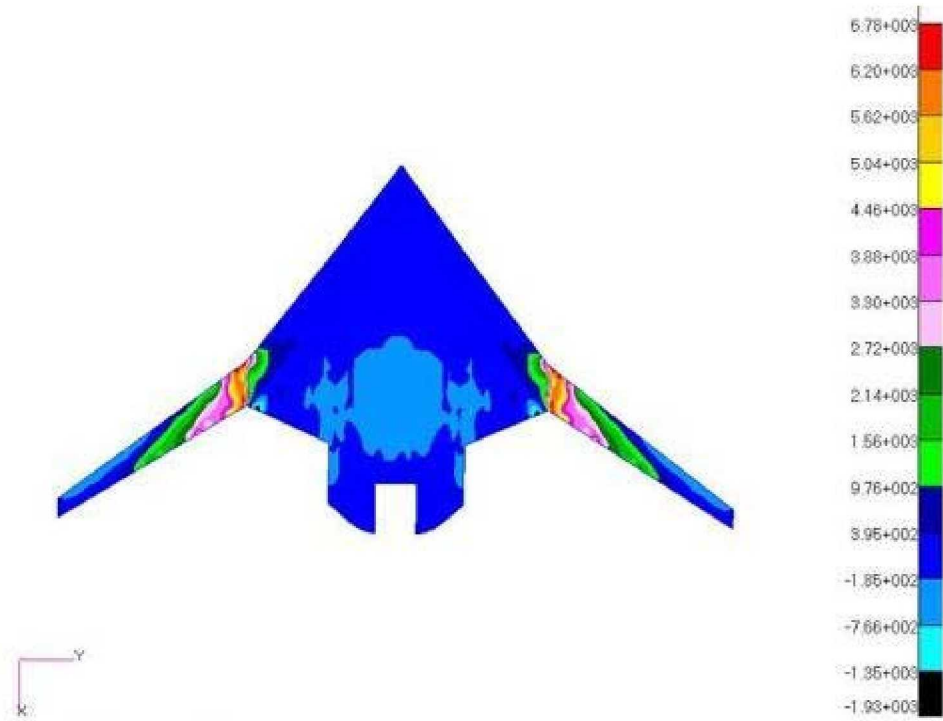


FIGURE 39. 2.5-G LIMIT LOAD SPANWISE DIRECTION (NY) LBS/IN

Upper:



Lower:

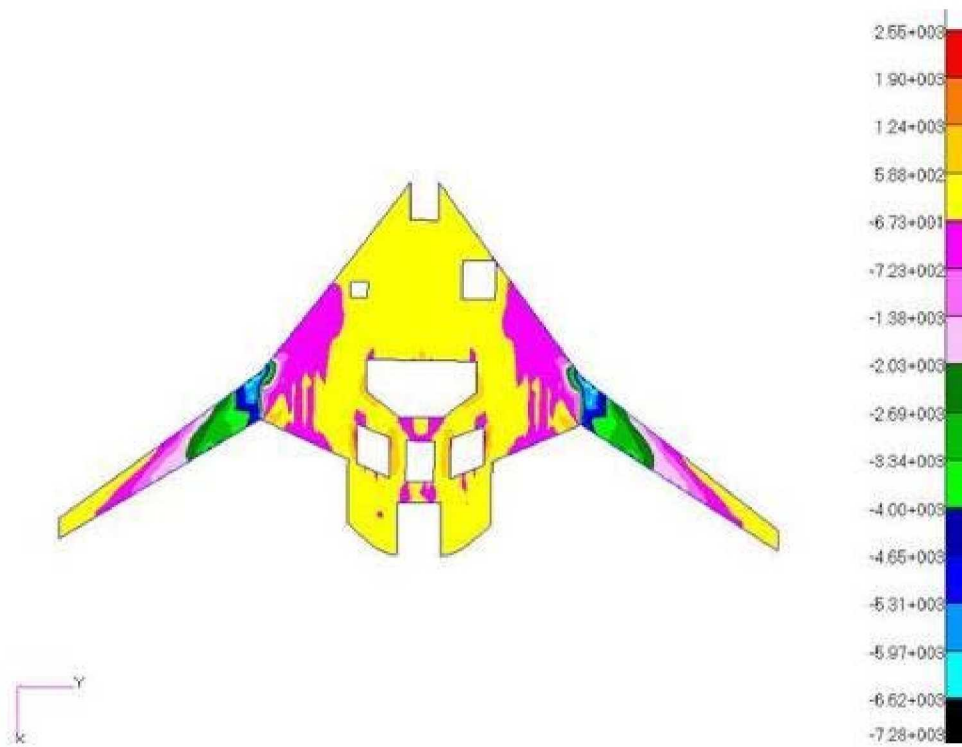
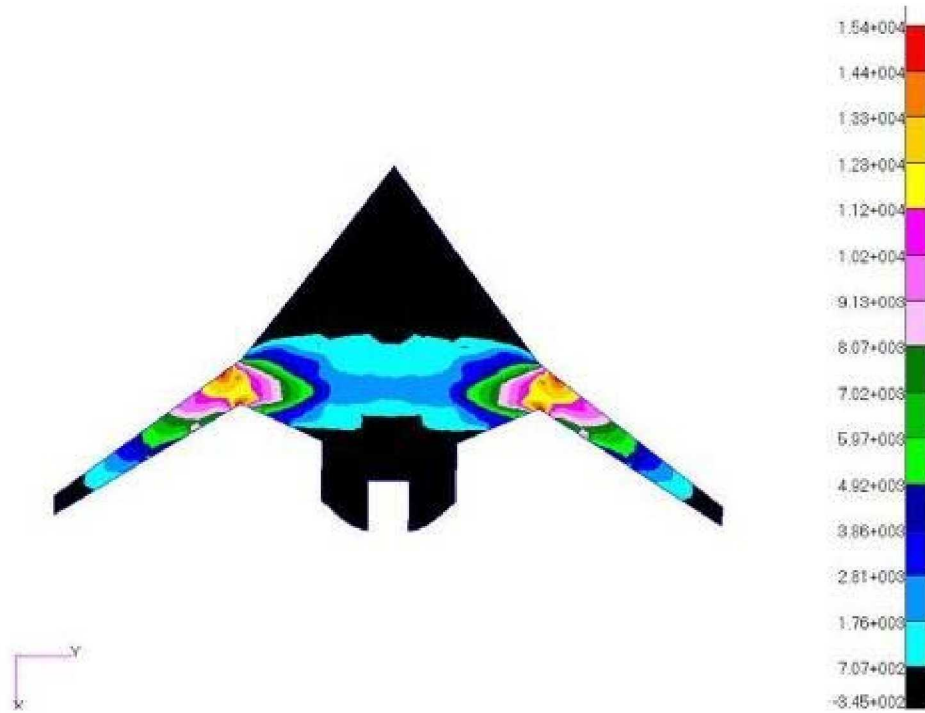


FIGURE 40. -1.0-G LIMIT LOAD STREAMWISE DIRECTION (NX) LBS/IN

Upper:



Lower:

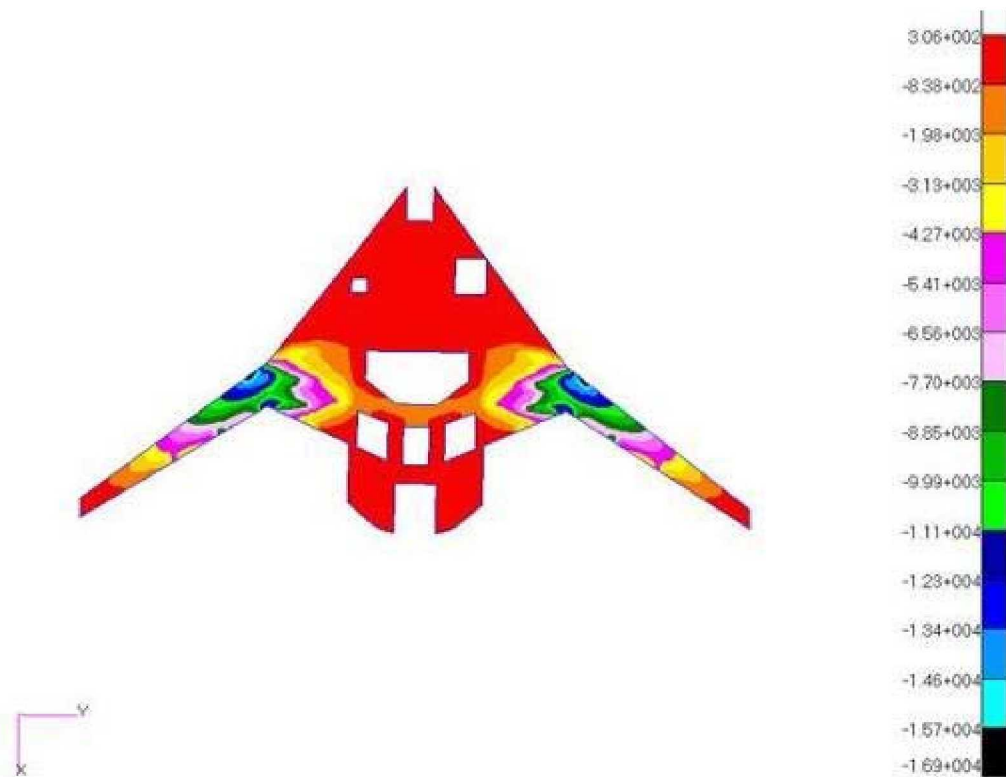
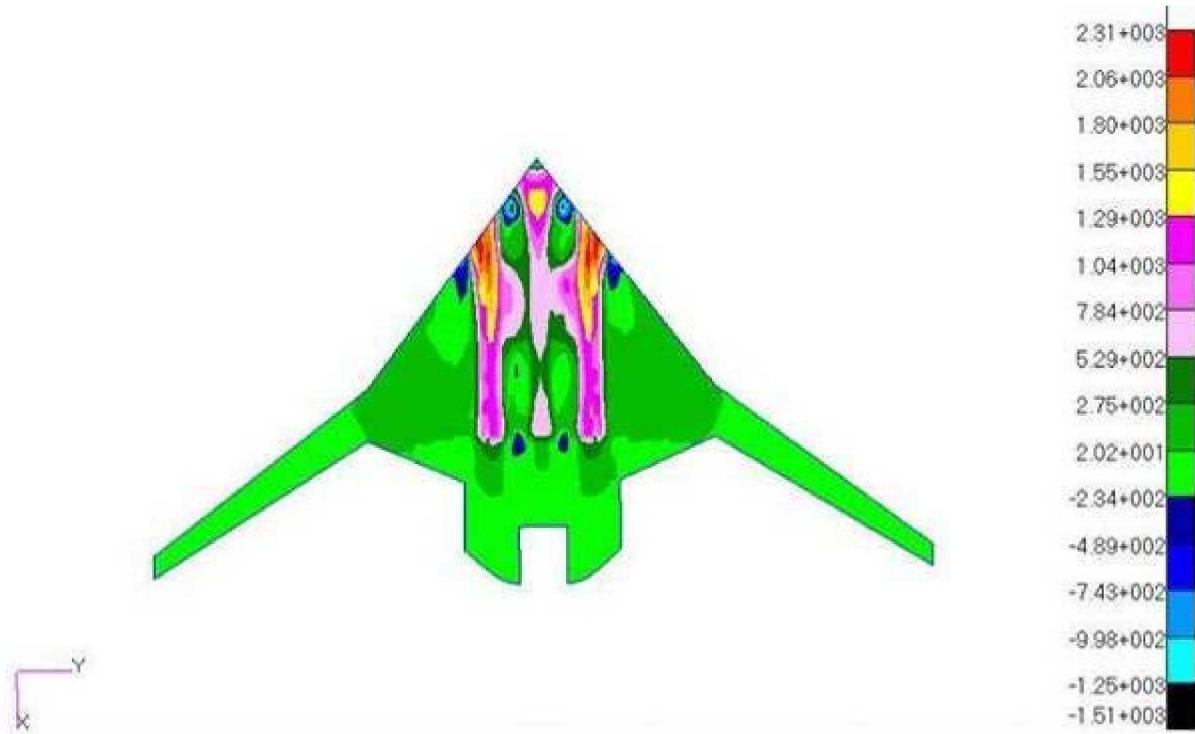


FIGURE 41. -1.0-G LIMIT LOAD SPANWISE DIRECTION (NY) LBS/IN

Upper:



Lower:

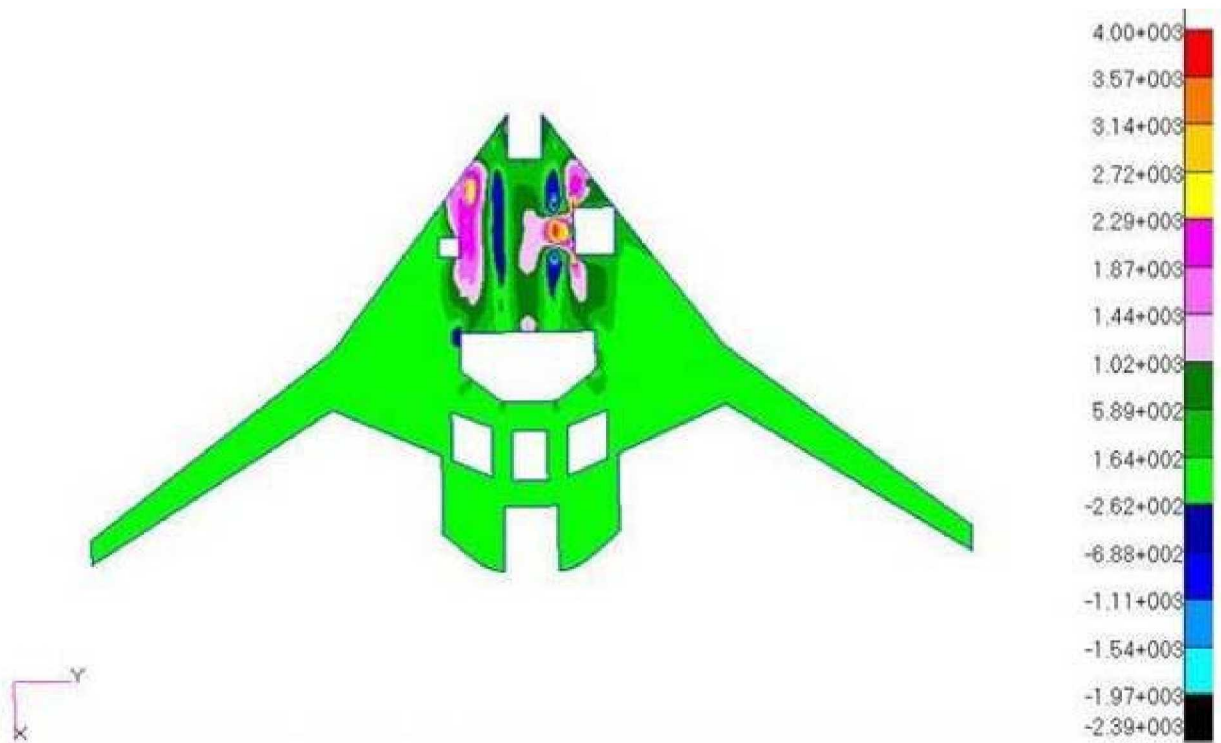
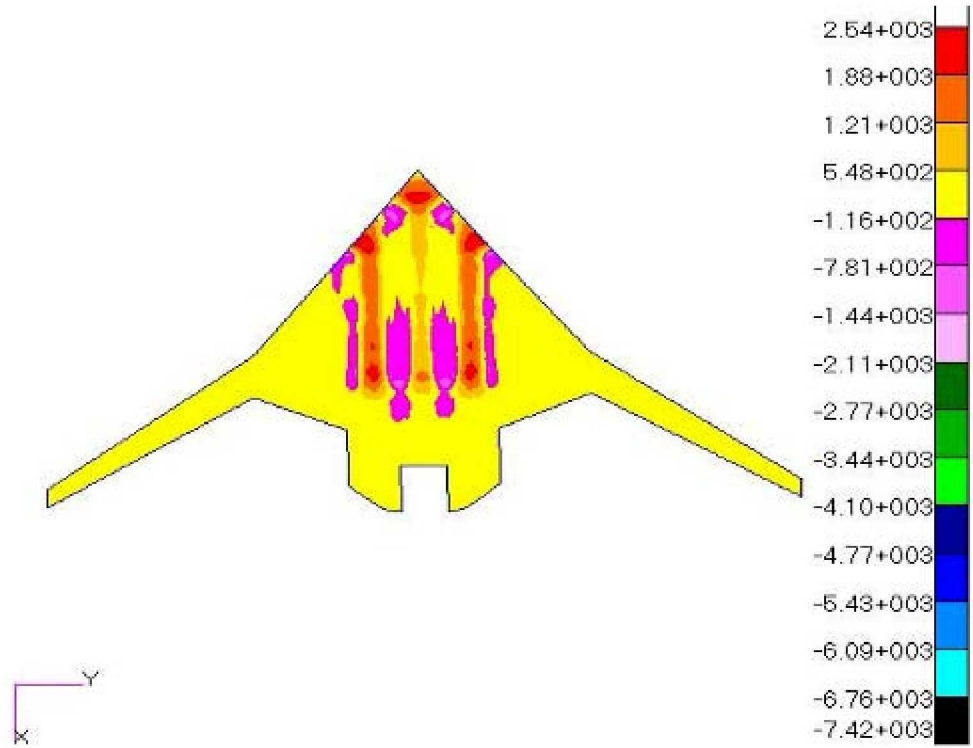


FIGURE 42. 1.33P LIMIT LOAD STREAMWISE DIRECTION (NX) LBS/IN

Upper:



Lower:

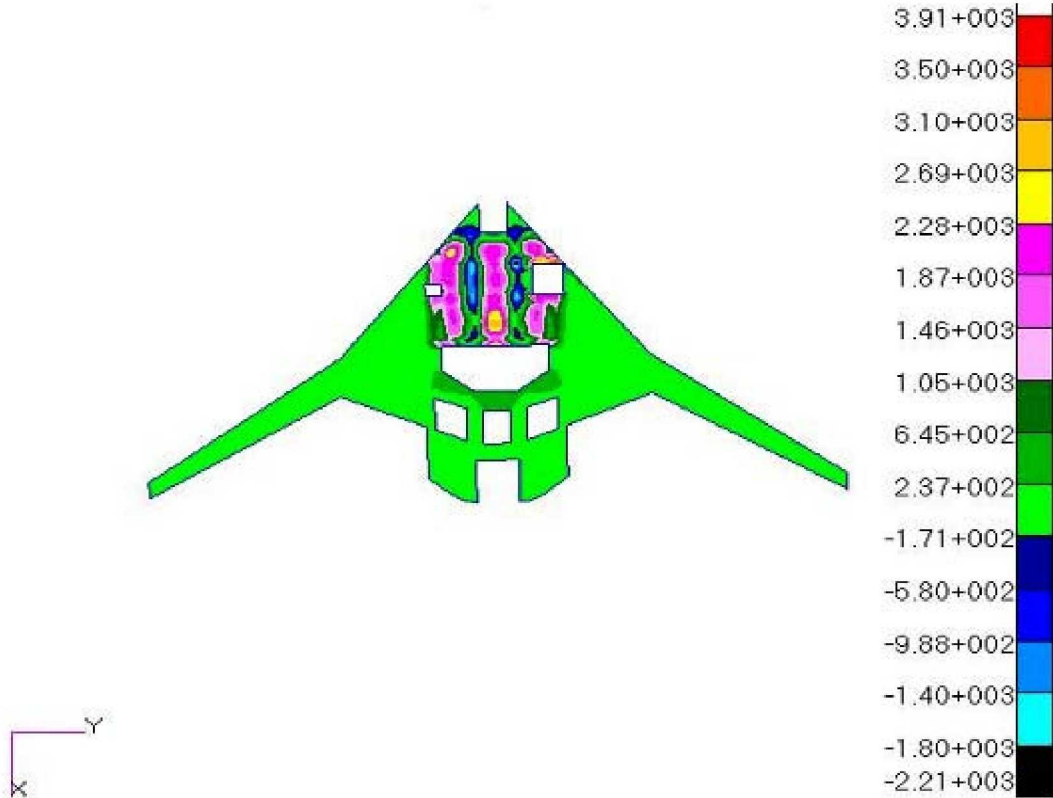


FIGURE 43. 1.33P LIMIT LOAD SPANWISE DIRECTION (NY) LBS/IN

Local Panel Sizing – The commercially available panel sizing code HyperSizer (Collier Research Corporation) was used in the global-local optimization process. It was used to automate the local airframe stiffened panel analyses and optimization using closed form, empirical-based, and state-of-the-art numerical solutions. The software code was developed based on the original NASA code ST-SIZE. Figure 44 shows the basic process flow for a HyperSizer optimization run.

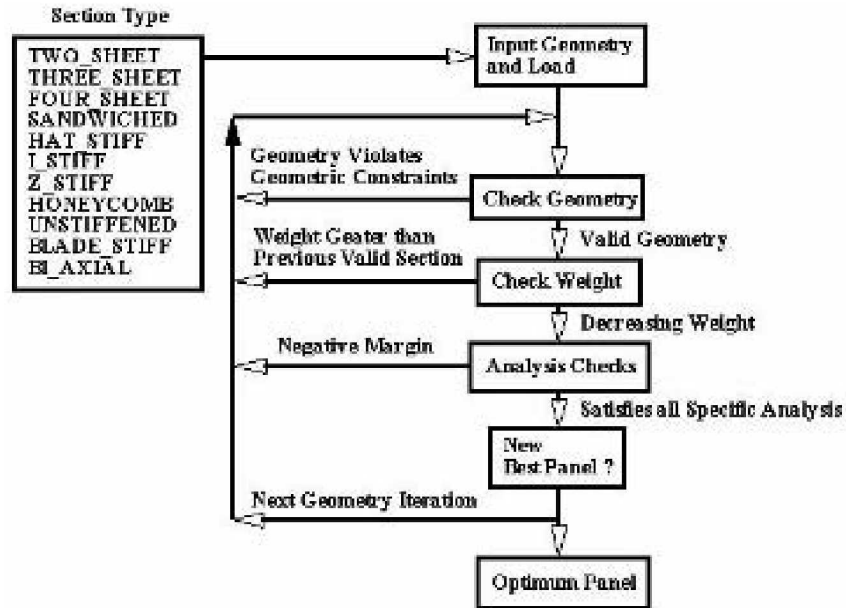


FIGURE 44. HYPERSIZER OPTIMIZATION PROCESSES

A new module called HyperFEA, was developed by Boeing in collaboration with Collier Research to integrate NASTRAN Sol200 (optimization) with HyperSizer. It allows seamless data integration and analysis iterations between the FEA and HyperSizer. With the graphical interface HyperFEA (Figure 45), users are now easily able to visualize convergence trends and other key sizing parameters after each iteration of the global-local interaction.



FIGURE 45. TYPICAL HYPERFEA

This new capability was successfully applied in this study and it significantly improved sizing accuracy and efficiency when compared to prior work. The range of analytical checks performed by HyperSizer is outlined in Table 18.

TABLE 18. HYPERSIZER MAJOR FUNCTIONS

	Detail Checks	Unstiffened	Blade	I	Z	Hat	2-Sheet	3-Sheet	Honeycomb	Bi-Axial	IsoGrid
Loads	Pressure-Induced Loads	√	√	√	√	√	√	√	√	√	√
	FEALoads	√	√	√	√	√	√	√	√	√	√
	Thermal Loads	√	√	√	√	√	√	√	√	√	√
Outer Skin Stress	X-Dir Stress	√	√	√	√	√	√	√	√	√	√
	Y-Dir Stress	√	√	√	√	√	√	√	√	√	√
	Shear Stress	√	√	√	√	√	√	√	√	√	√
	VonMises	√	√	√	√	√	√	√	√	√	√
	Tsai-Hill	√	√	√	√	√	√	√	√	√	√
	Tsai-Wu	√	√	√	√	√	√	√	√	√	√
Inner Skin Stress	Max Strain							√	√		
	X-Dir Stress							√	√		
	Y-Dir Stress							√	√		
	Shear Stress							√	√		
	VonMises							√	√		
	Tsai-Hill							√	√		
	Tsai-Wu							√	√		
Outer Flange Stress	Longitudinal Stress			√	√	√	√	√			
Web Stress	Longitudinal Stress		√	√	√	√	√			√	√
Inner Flange Stress	Longitudinal Stress		√	√	√	√	√				
Cross Web Stress	Longitudinal Stress									√	√
Budding Checks	Overall Panel	√	√	√	√	√	√	√	√	√	√
	Outer Skin Between		√	√	√	√	√	√		√	√
	Inner Skin Between Stiffeners										
	Inner Flange			√	√	√	√	√			
	Web		√	√	√	√	√	√		√	√
	Cross Web									√	√
Stiffener Crippling	Stiffener		√	√	√	√	√	√	√	√	√
Euler Johnson	Stiffener		√	√	√	√	√	√	√	√	√
Beam Column	X Direction	√	√	√	√	√	√	√		√	√
	Y Direction	√	√	√	√	√	√	√		√	√
Honeycomb Outer Skin	X-Dir Dimpling								√		
	Y-Dir Dimpling								√		
	X-Dir Wrinkling								√		
	Y-Dir Wrinkling								√		
Honeycomb Inner Skin	X-Dir Dimpling								√		
	Y-Dir Dimpling								√		
	X-Dir Wrinkling								√		
	Y-Dir Wrinkling								√		
Honeycomb Core	X-Dir Transverse Shear								√		
	Y-Dir Transverse Shear								√		
Honeycomb Panel	X-Dir Crimping								√		
	Y-Dir Crimping								√		
Composite Strength, Ply Based	Max Strain, 1,2, shear	√	√	√	√	√	√	√	√	√	√
	Tsai-Hahn	√	√	√	√	√	√	√	√	√	√
	Hoffman	√	√	√	√	√	√	√	√	√	√
	Hsein, Fiber/Matrix	√	√	√	√	√	√	√	√	√	√
	LARCO3, Fiber/Matrix	√	√	√	√	√	√	√	√	√	√
	Tsai-Wu, Strain Based	√	√	√	√	√	√	√	√	√	√
	Max Strain OHT	√	√	√	√	√	√	√	√	√	√
	Max Strain OHC, after impact	√	√	√	√	√	√	√	√	√	√
Composite Strength, Laminate Based	Max Strain, X Tension	√	√	√	√	√	√	√	√	√	√
	Max Strain, X Compression	√	√	√	√	√	√	√	√	√	√
	Max Strain, Shear	√	√	√	√	√	√	√	√	√	√
	Max Strain, OHT, OHC	√	√	√	√	√	√	√	√	√	√

Unlike other panel optimization software, HyperSizer provides a better means of modeling highly tailored structures like the PRSEUS concept. It contains the ability to independently model specific regions of a multi-element structural assembly. This aspect of the code was particularly useful in capturing the highly orthogonal behavior of the rods in the PRSEUS panel design.

A typical input template is shown in Figure 46, it demonstrates the flexibility of HyperSizer to model composite structures. Figure 47 shows how users are able to define a wide variety of

layouts, material types or laminates, and then let HyperSizer generate the optimum combination of geometries for a given set of material properties and loading conditions.

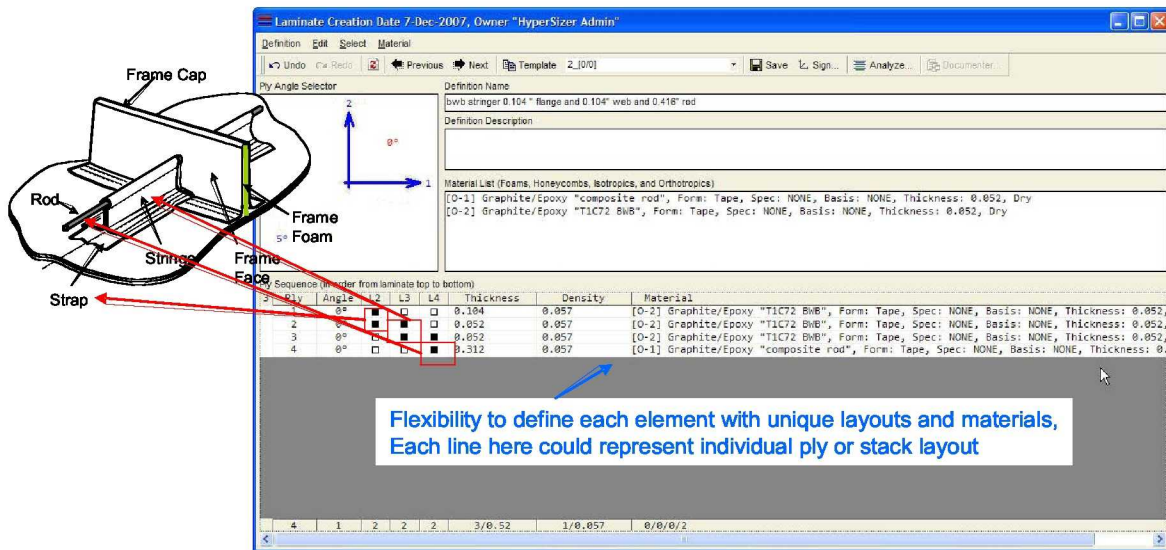


FIGURE 46. PRSEUS STRINGER MODELING

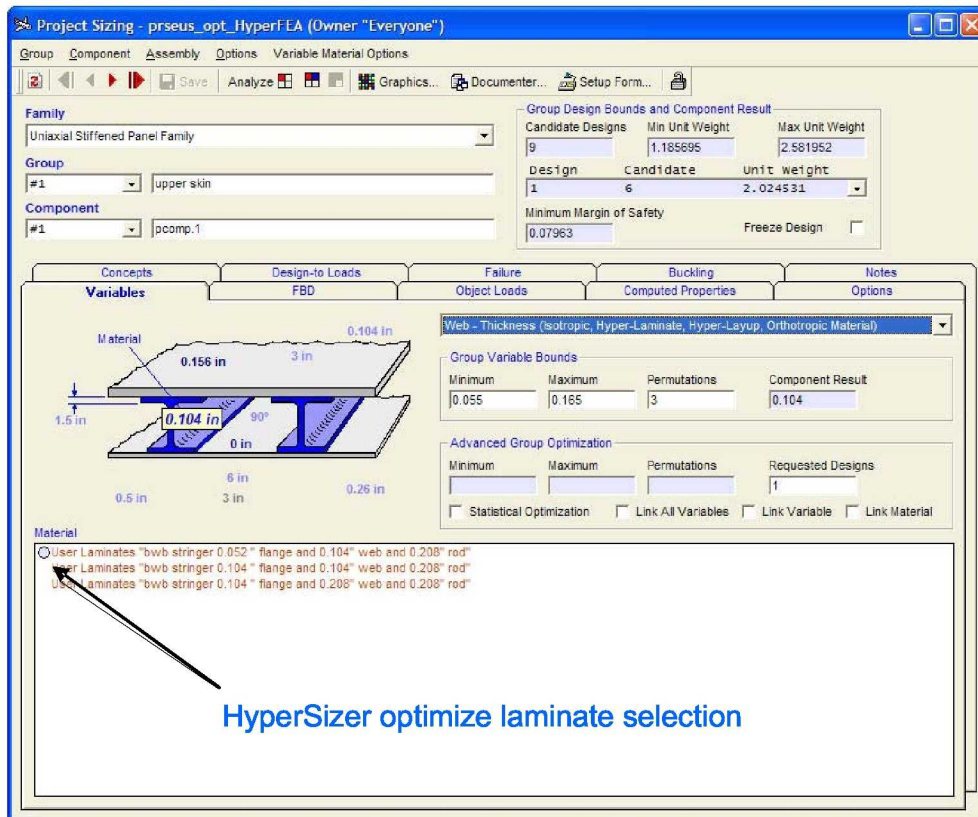


FIGURE 47. LAMINATE SELECTION INPUT SCREEN

Minimum Gauge Panel Geometry - In order to assess the benefits of a PRSEUS structural concept, the same design criteria from the prior study configuration was replicated in the sizing process, including updated load conditions and material selections. The only real difference in the two approaches was driven by the inherent attributes of each structural concept. Since the sandwich concept has no means of arresting damage propagation, the minimum skin gauge was limited to two stacks (.104-inch), whereas the PRSEUS concept was permitted a minimum skin gauge of one stack (.052-inch). This was done to account for the conventional damage-arrest design philosophy employed for the skin-stringer concept, and in particular, to demonstrate the benefit of designing beyond current no-growth design constraints for composite structures.

The starting minimum gauge stringer and frame dimensions used for the PRSEUS analysis are shown in Figure 48 and listed again in Table 19. These thicknesses are driven by either manufacturing constraints, or by a simplified 2P (18.5 psi) pressure plate analyses which determined the minimum skin thickness that would be acceptable with 6-inch stringer spacing and a 20-inch frame pitch. These dimensions established the base values from which the FEM optimization would be able iterate from to minimize the overall fuselage weight.

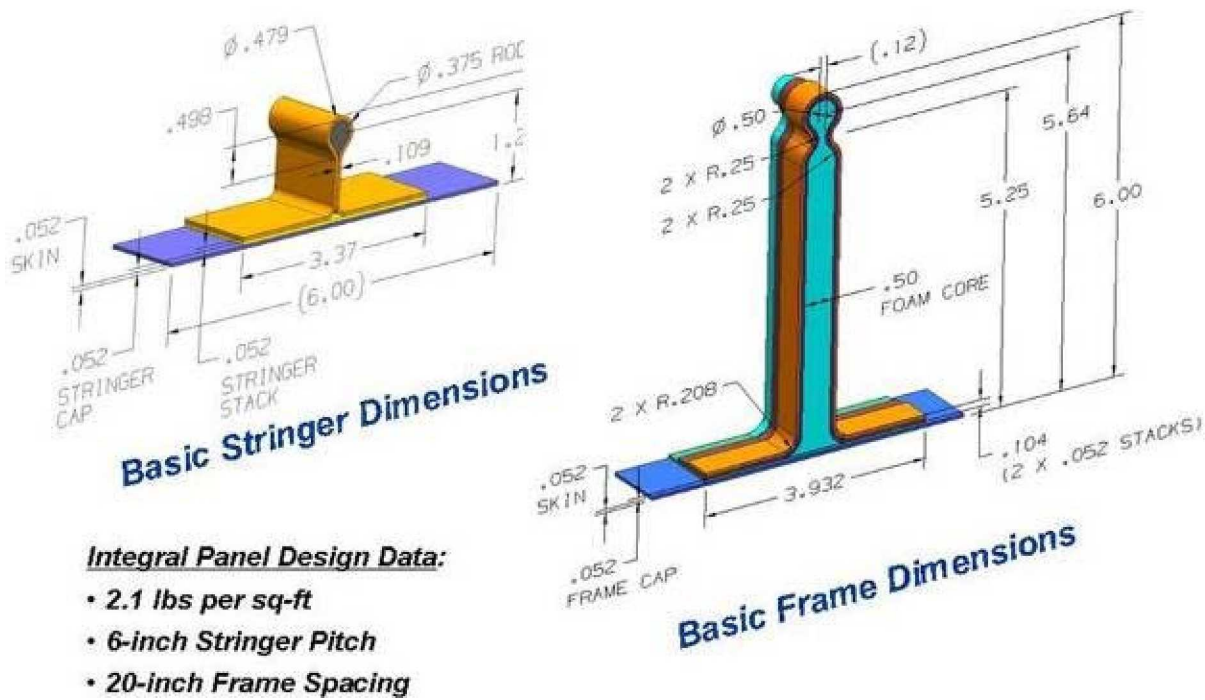


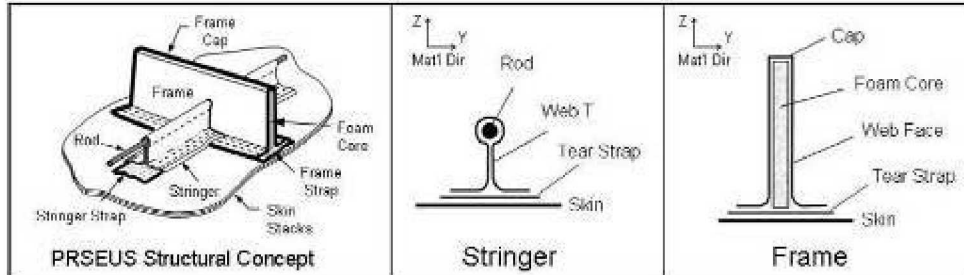
FIGURE 48. PRSEUS MINIMUM GAUGE DIMENSIONS

TABLE 19. PANEL DESIGN LIMIT & FRAME DESIGN LIMITS

Panel Design Limit		Frame Design Limit	
	Design Parameter Range		Design Parameter Range
Frame Height	6"	Panel Height	1.5"
Strap Width	3"	Skin Thickness	> 1 stack (0.052")
Strap Thickness	>1 stack (0.052")	Strap Width	3.0"
Web Foam Thickness	0.5"	Strap Thickness	>1 stack (0.052")
Web Face Sheet Thickness	> 1 stack (0.052")	Web Thickness	>0.104"
Frame Cap Area	>1 stack (0.052")	Rod Diameter	0.375"

Sizing Results - The final sizing results for the fuselage panels and frames are summarized in the following figures (Figures 49-52). The critical load conditions are 2.5-g and 2P for the upper skins, and the -1.0-g, 2.0-g Taxi Bump and 2P conditions for the lower skins. The critical failure modes for both panels and frames are primarily strength dominant.

Sizing Summary for Upper Cover Skins:



Skin T											
Design Region ID#	FEM Prop ID#	Panel H (inches)	Thickness (inches)	# Stacks	Strap W (inches)	Strap T (inches)	Web T (inches)	Rod Dia (inches)	Critical Load	Critical Design Mode	
I	1101	1.5	0.156	3	3	0.052	0.104	3/8"	2.5G	Strength	
II	1102	1.5	0.156	3	3	0.052	0.104	3/8"	2.5G	Strength	
III	1103	1.5	0.208	4	3	0.052	0.104	3/8"	2.5G	Strength	
IV	1104	1.5	0.208	4	3	0.052	0.104	3/8"	2.5G	Strength	
V	1201	1.5	0.104	2	3	0.052	0.104	3/8"	2.5G+1P	Strength	
VI	1202	1.5	0.104	2	3	0.052	0.104	3/8"	2.5G+1P	Strength	
VII	1301	1.5	0.052	1	3	0.052	0.104	3/8"	2P	Strength	
VIII	1302	1.5	0.052	1	3	0.052	0.104	3/8"	2P	Strength	
IX	1303	1.5	0.052	1	3	0.052	0.104	3/8"	2P	Strength	
X	1304	1.5	0.052	1	3	0.052	0.104	3/8"	2P	Strength	
XI	1305	1.5	0.052	1	3	0.052	0.104	3/8"	2P	Strength	
XII	1306	1.5	0.052	1	3	0.052	0.104	3/8"	2P	Strength	
XIII	1391	1.5	0.052	1	3	0.052	0.104	3/8"	2P	Strength	
XIV	1392	1.5	0.052	1	3	0.052	0.104	3/8"	2P	Strength	
XV	1501	1.5	0.052	1	3	0.052	0.104	3/8"	2P	Strength	
XVI	12010	1.5	0.104	2	3	0.052	0.104	3/8"	2.5G	Strength	
XVII	13010	1.5	0.052	1	3	0.052	0.104	3/8"	2P	Strength	
XVIII	13020	1.5	0.052	1	3	0.052	0.104	3/8"	2P	Strength	
XIX	13040	1.5	0.052	1	3	0.052	0.104	3/8"	2P	Strength	
XX	13050	1.5	0.052	1	3	0.052	0.104	3/8"	2P	Strength	
XXI	15010	1.5	0.052	1	3	0.052	0.104	3/8"	2P	Strength	

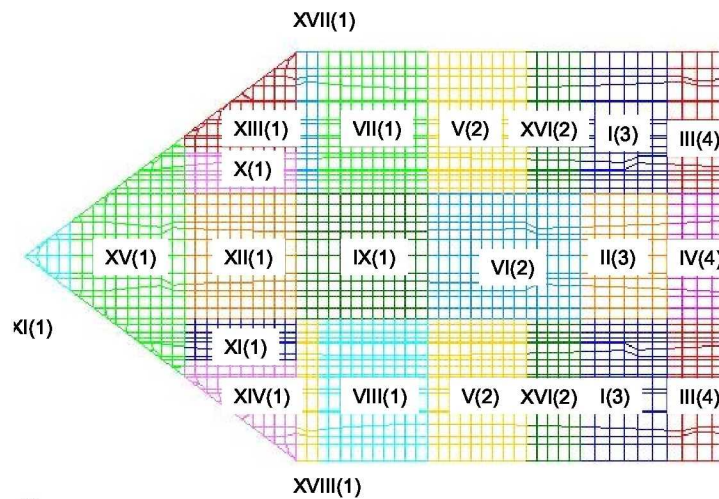
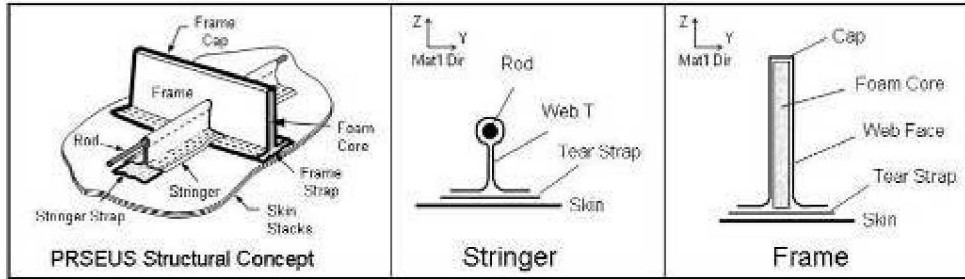


FIGURE 49. UPPER SKIN DESIGN REGIONS AND NUMBER OF SKIN STACKS

Sizing Summary for Lower Cover Skins:



Design Region ID#	FEM Prop ID#	Panel H (Inches)	Skin T			Strap W (Inches)	Strap T (Inches)	Web T (Inches)	Rod Dia (Inches)	Critical Load	Critical Design Mode
			Thickness (Inches)	# stacks							
I	2002	1.5	0.156	3	3	0.052	0.104	3/8"	-1G	Strength	
II	2101	1.5	0.104	2	3	0.052	0.104	3/8"	2G Taxi Bump	Strength	
III	2102	1.5	0.104	2	3	0.052	0.104	3/8"	2G Taxi Bump	Strength	
IV	2103	1.5	0.156	3	3	0.052	0.104	3/8"	-1G	Strength	
V	2104	1.5	0.156	3	3	0.052	0.104	3/8"	-1G	Strength	
VI	2105	1.5	0.156	3	3	0.052	0.104	3/8"	-1G	Strength	
VII	2106	1.5	0.156	3	3	0.052	0.104	3/8"	-1G	Strength	
VIII	2201	1.5	0.156	3	3	0.052	0.104	3/8"	2P	Strength	
IX	2202	1.5	0.156	3	3	0.052	0.104	3/8"	-1G	Strength	
X	2203	1.5	0.156	3	3	0.052	0.104	3/8"	-1G	Strength	
XI	2204	1.5	0.104	2	3	0.052	0.104	3/8"	2G Taxi Bump	Strength	
XII	2205	1.5	0.104	2	3	0.052	0.104	3/8"	2P	Strength	
XIII	2206	1.5	0.104	2	3	0.052	0.104	3/8"	2G Taxi Bump	Strength	
XIV	2207	1.5	0.208	4	3	0.052	0.104	3/8"	2G Taxi Bump	Strength	
XV	2208	1.5	0.156	3	3	0.052	0.104	3/8"	2P	Strength	
XVI	2209	1.5	0.208	4	3	0.052	0.104	3/8"	2G Taxi Bump	Strength	
XVII	2301	1.5	0.104	2	3	0.052	0.104	3/8"	2P	Strength	
XVIII	2302	1.5	0.104	2	3	0.052	0.104	3/8"	2P	Strength	
XIX	2303	1.5	0.104	2	3	0.052	0.104	3/8"	2P	Strength	
XX	2304	1.5	0.104	2	3	0.052	0.104	3/8"	2P	Strength	
XXI	2305	1.5	0.104	2	3	0.052	0.104	3/8"	2P	Strength	
XXII	2306	1.5	0.156	3	3	0.052	0.104	3/8"	2P	Strength	
XXIII	2501	1.5	0.104	2	3	0.052	0.104	3/8"	2P	Strength	
XXIV	2502	1.5	0.104	2	3	0.052	0.104	3/8"	2P	Strength	
XXV	21010	1.5	0.104	2	3	0.052	0.104	3/8"	2G Taxi Bump	Strength	
XXVI	21020	1.5	0.104	2	3	0.052	0.104	3/8"	2G Taxi Bump	Strength	
XXVII	22040	1.5	0.104	2	3	0.052	0.104	3/8"	2P	Strength	
XXVIII	22060	1.5	0.104	2	3	0.052	0.104	3/8"	2P	Strength	
XXIX	23010	1.5	0.26	5	3	0.052	0.104	3/8"	2P	Strength	
XXX	23020	1.5	0.104	2	3	0.052	0.104	3/8"	-1G	Strength	

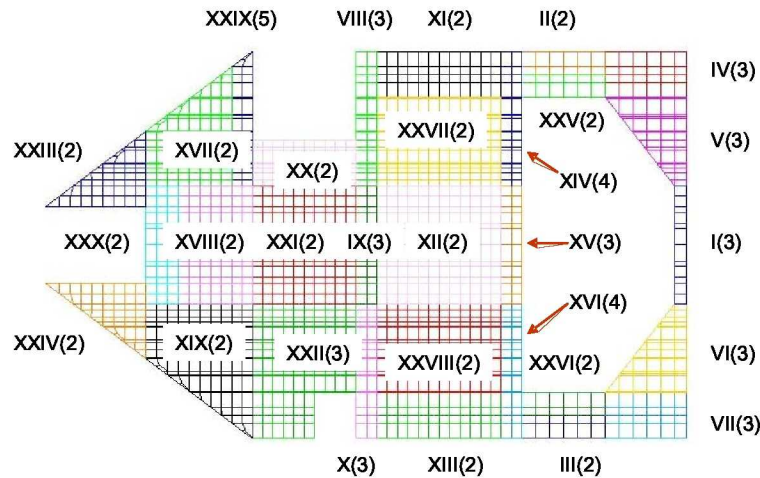
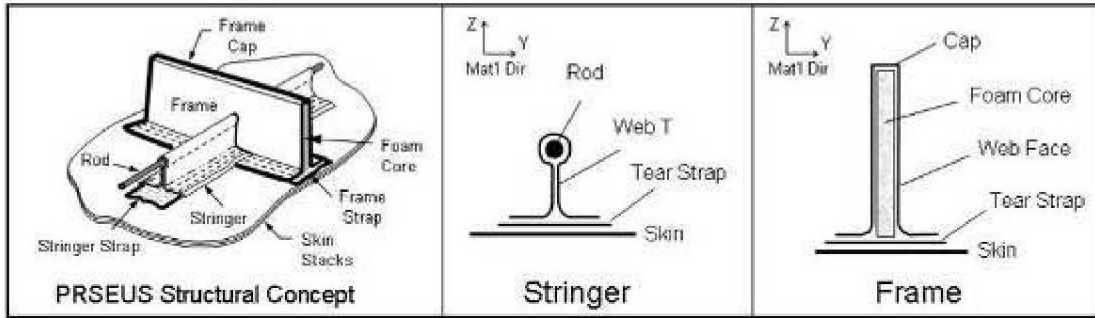


FIGURE 50. LOWER SKIN DESIGN REGIONS AND NUMBER OF SKIN STACKS

Sizing Summary for Upper Frames:



Design Region ID#	FEM Prop ID#	Frame H (inches)	Strap W (inches)	Strap T (inches)	Web Foam (inches)	Web Face T (inches)	Frame Cap Area	Critical Load	Critical Design Mode
I	5111	6	3	0.052	0.5	0.104	0.104	2.5G+1P	Strength
II	5112	6	3	0.052	0.5	0.104	0.104	2.5G+1P	Strength
III	5211	6	3	0.052	0.5	0.104	0.104	2P	Strength
IV	5311	6	3	0.052	0.5	0.104	0.104	2P	Strength
V	5312	6	3	0.052	0.5	0.104	0.104	2P	Strength
VI	5511	6	3	0.052	0.5	0.104	0.104	2P	Strength
VII	53110	6	3	0.052	0.5	0.104	0.104	2P	Strength
VIII	53111	6	3	0.052	0.5	0.104	0.104	2P	Strength

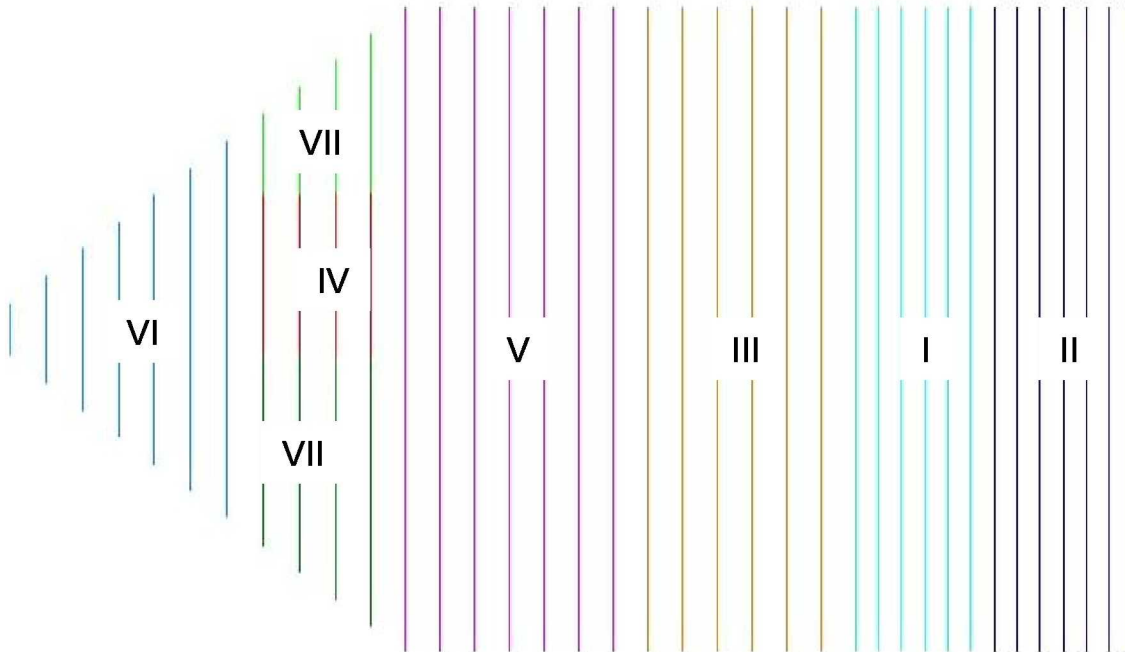
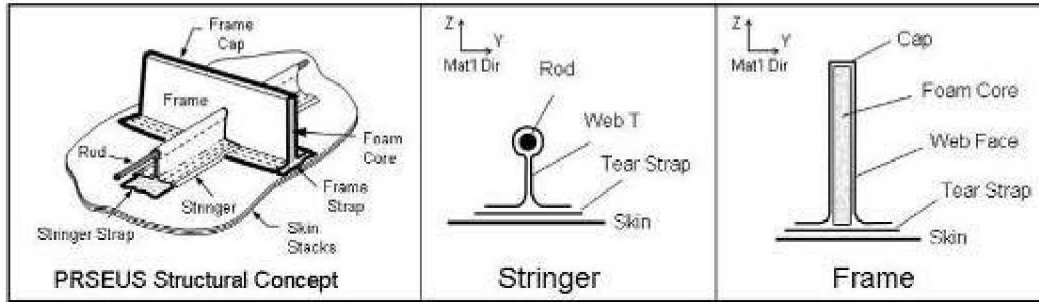


FIGURE 51. UPPER FRAME DESIGN REGIONS AND GAUGES

Sizing Summary for Lower Frames:



Design Region ID#	FEM Prop ID#	Frame H (Inches)	Strap W (Inches)	Strap T (Inches)	Web Foam (Inches)	Web Face T (Inches)	Frame Cap Area (Inches ²)	Critical Load	Critical Design Mode
I	5221	6	3	0.156	0.5	0.104	0.208	2G Taxi Bump	Strength
II	5222	6	3	0.156	0.5	0.156	0.364	2P	Strength
III	5321	6	3	0.052	0.5	0.052	0.052	2P	Strength
IV	5322	6	3	0.156	0.5	0.156	0.364	2P	Strength
V	5323	6	3	0.052	0.5	0.104	0.104	2P	Strength
VI	5521	6	3	0.052	0.5	0.052	0.052	2P	Strength
VII	6516	6	3	0.052	0.5	0.104	0.104	-1G	Strength
VIII	52210	6	3	0.052	0.5	0.104	0.104	-1G	Strength
IX	52211	6	3	0.156	0.5	0.104	0.208	-1G	Strength
X	52212	6	3	0.156	0.5	0.104	0.208	2G Taxi Bump	Strength
XI	52213	6	3	0.156	0.5	0.052	0.052	2P	Strength
XII	52214	6	3	0.052	0.5	0.104	0.104	2P	Strength
XIII	52215	6	3	0.052	0.5	0.104	0.104	2P	Strength
XIV	52216	6	3	0.156	0.5	0.104	0.208	-1G	Strength
XV	52217	6	3	0.156	0.5	0.104	0.208	2P	Strength
XVI	52220	6	3	0.156	0.5	0.104	0.208	2P	Strength
XVII	52221	6	3	0.156	0.5	0.156	0.364	2P	Strength

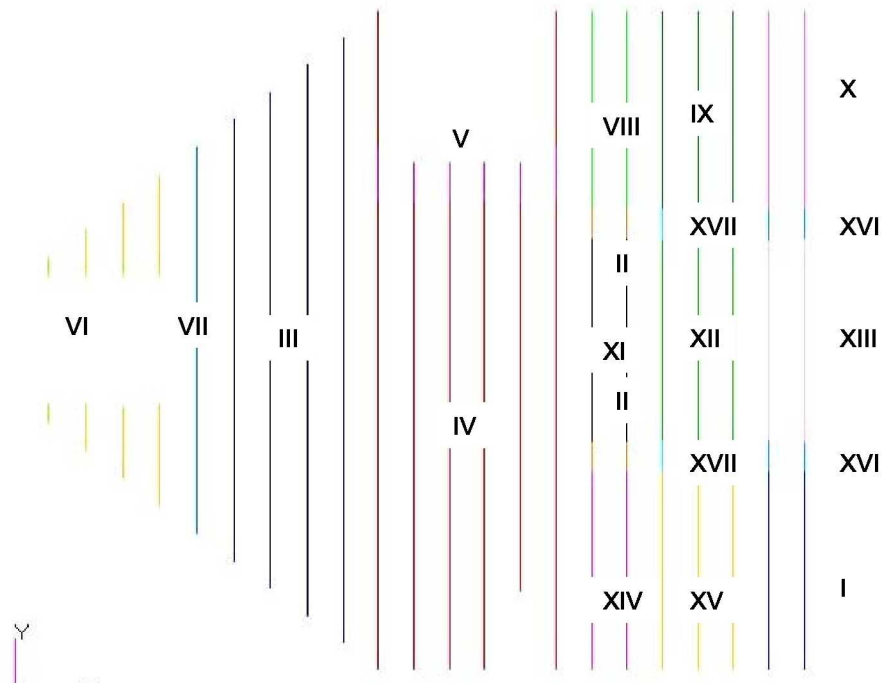


FIGURE 52. LOWER FRAME DESIGN REGIONS AND GAUGES

1.1.6 Weights Summary

The overall aircraft weights summary for the baseline BWB-5-200G configuration was further refined into a detail breakdown for the pressurized portion of the center body (Figure 53). The bottoms-up calculation methodology utilized the FEM-based sizing results which combined with a series of non-optimum factors to arrive at the final as-fabricated weight values for the airframe.

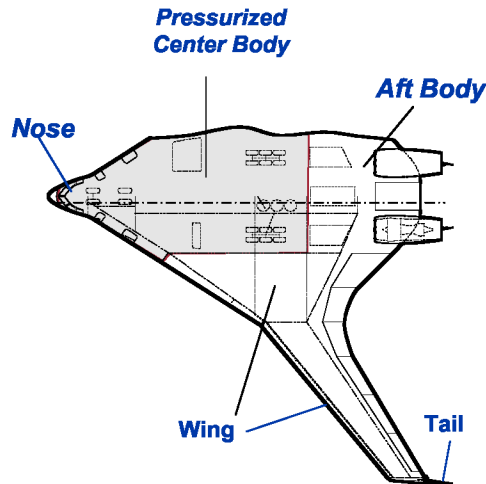


FIGURE 53. BWB PRESSURIZED REGION

The non-optimum weight factors were based on data generated from two prior studies: (1) a Boeing in-house composite structures design study (Reference: HSR Report MDC 98K0303, Weight/Size Estimate Algorithms for Global Optimization of High Speed Civil Transport Aircraft, 1998, not available for release) and, (2) the NASA TCAT Phase I Study (Reference 1). The data from these two studies was used to establish the relative weight penalty that would be assessed for each structural concept to account for factors not considered in the structural analyses.

Weight penalties for the non-optimum increments were added to the idealized structural weight values calculated by the FEM sizing task. The skin panel non-optimum factors allocated to the prior study sandwich concept was based on a 25% factor to account for the difficulty in joining and transitioning sandwich structures, whereas a 20% non-optimum factor was assessed for the PRSEUS skin-stringer concept. The 20% value is equivalent to the beaded-hat skin-stringer concept that was analyzed in the TCAT study as two skin-stringer concepts would have similar non-optimum characteristics. No further effort was completed under this study to develop or refine a specific set of non-optimum factors for the PRSEUS concept.

The detailed panel-level weights for the center body are shown for both the sandwich and PRSEUS shell concepts in Table 20. Non-optimum values were also added to the pressurized shell, frame and bulkhead structural results to generate the final as-fabricated weight components. The results represent a side-by-side vehicle-level weight comparison between the old baseline foam sandwich and the new PRSEUS shell concept. Both concepts were analyzed with consistent methodology, utilizing the same FEM geometry, loads, design requirements, and structural sizing criteria. The total pressurized body structure weight savings for PRSEUS was 10.3% relative to the old baseline sandwich design approach.

TABLE 20. PRESSURIZED CENTER BODY WEIGHT COMPARISON

Weight Item Description	Base Concept 1	Task Concept 2	Delta Weight	% Savings
Composite Skin Panel Structural Concept	Foam Sandwich	PRSEUS	Lbs / Airpl	
FEM Sized Pressurized Body Structure Weight				
Upper Skin Panel	4,793	3,903	-890	-18.6%
Lower Skin Panel	3,592	2,938	-654	-18.2%
Frames	4,448	2,439	-2,009	-45.2%
Y-Braces and Posts	2,126	2,143	18	0.8%
Internal Cabin Ribs	5,315	5,330	14	0.3%
SOB Rib	1,069	1,071	2	0.2%
Floor Panel and Beams -Upper Cabin, Lower Cargo and Bulk Cargo	5,265	5,281	16	0.3%
Internal Spars and Bulkh'ds	4,046	4,041	-4	-0.1%
Pressurized Leading Edge Structure	4,227	4,384	156	3.7%
Lower Body Press Bulkh'ds and Frames	902	904	1	0.1%
Sub Total Pressurized Body Structure Weight	35,783	32,433	-3,350	-9.4%
Non-Optimum Weight Allowance				
Skin Panel -Doublers, Cutouts, Splices and Attach	2,096	1,368	-728	-34.7%
Frame - Doublers, Cutouts, Splices and Attach	445	244	-201	-45.2%
Ribs and Floor - Doublers, Cutouts, Splices and Attach	2,051	2,051	0	0.0%
Lightning Protection	280	280	0	0.0%
Veil-Ply	233	233	0	0.0%
Paint, Primer, Sealant	651	651	0	0.0%
Sub Total Non-Optimum Weight	5,757	4,828	-929	-16.1%
Total Pressurized Body Structure Weight - lbs.	41,539	37,261	-4,279	-10.3%

To help substantiate the weight calculation methodology, two prototype PRSEUS skin panel assemblies were fabricated and weighed at the Huntington Beach stitching center. The skin panel assemblies were designed and fabricated to represent the PRSEUS minimum skin gauge geometry. The second panel that was fabricated is shown along with the fatigue test specimens that were extracted from the first panel in Figure 54.



FIGURE 54. SECOND PANEL AND SPECIMENS SHIPPED TO NASA-LARC

The first prototype panel was weighed and recorded at 2.126 lbs/ft². The panel assembly consists of the outer skin stack, 7 stringers at 6-inch spacing, and 4 frames at 20-inch intervals. The trimmed panel dimensions are 43.0-inches wide by 80.5-inches long. This data was in close agreement to the as-fabricated values used to develop the weight estimates for the vehicle-level trade study.

1.2 Compression Specimens

Eight element-level compression specimens were extracted from Panel 1 and prepared for testing. The completed specimens were sent to three different test sites: University of California at Irvine (UCI), Orange County Materials (OCM) Test Lab, and NASA-LaRC. The two single-stringer specimens statically tested by UCI are described in Section 1.2.1. The two single-frame specimens statically tested by OCM are described in Section 1.2.2. Two single-stringer and two single-frame specimens were shipped to NASA-LaRC, where they will be mechanically cycled using the loading profile described in Section 1.2.3 and then tested to failure. This portion of the test program will not be completed until the end of Phase II and therefore not included in this Phase I report.

1.2.1 Streamwise Single-Stringer Compression Panel

The general configuration for the single-stringer specimen and testing arrangement is shown in Figure 55 (detail drawing ZJ153294-1 contained in Appendix A). The integral structural panel was built using stacks of DMS 2436 Type 1, Class 72, Grade A carbon fiber (7-ply stack) material, stitched, and then infused with a DMS 2479 Type 2, Class1 VRM-34 epoxy resin. Potted ends were added for load introduction and side restraints were added to inhibit edge buckling along the panel. The specimens were identified as ZJ153294-1 Replicate 1 and Replicate 2.

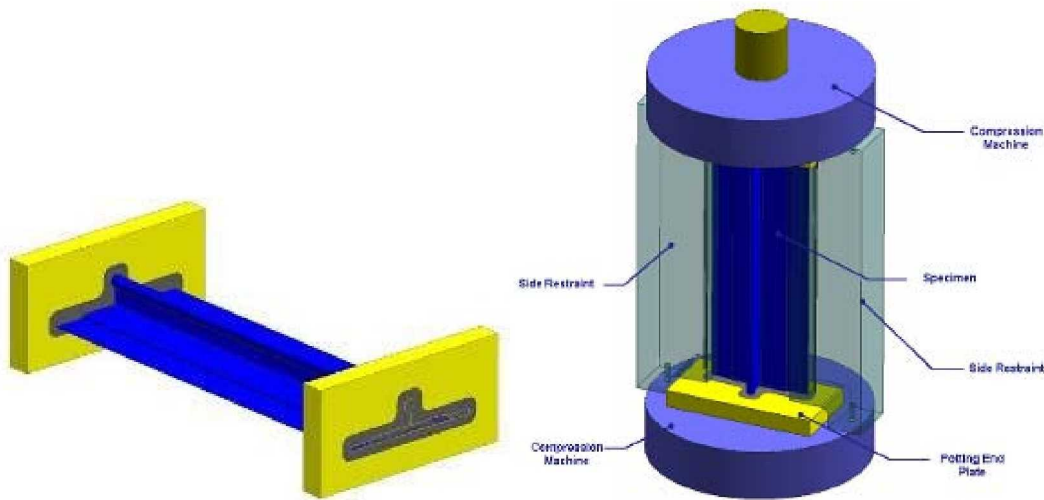


FIGURE 55. SINGLE-STRINGER COMPRESSION SPECIMEN DESIGN

The specimens were initially shipped to UCI, where after encountering alignment problems during the initial testing, the test was moved to the University of California, Santa Barbara (UCSB). The lead test investigator, Professor Lorenzo Valdevit of UCI, made arrangements to use a MTS Universal Testing Frame from the Mechanics of Materials Laboratory at UCSB (Figure 56). The frame is equipped with a 50-kip load cell, 6-inch compression platens, and an aligning device to reduce specimen rotation and movement. Alignment was performed under a proofing load of 5,000 lbs and guaranteed to 50,000 lbs. The machine was operated in displacement-control mode, at a constant displacement rate of 0.01 inch/minute. All the parameters were controlled via a custom-built computer interface.

Both specimens (Replicate 1 and Replicate 2) were statically tested to failure under laboratory environmental conditions. The load-vs-displacement plots and strain gage measurements from each test are contained in Appendix C. A summary of the results is plotted together in Figure 58. Both specimens exhibited linear behavior throughout the entire experiment, with nearly identical stiffness; usually a good indication of the dimensional accuracy and reproducibility of the manufacturing process. The relatively large difference in failure load, 48.5 vs 41.4 kips, can be explained by the Shadow Moiré results that was used to visualize the out-of-plane deflection and identify the onset of elastic buckling.

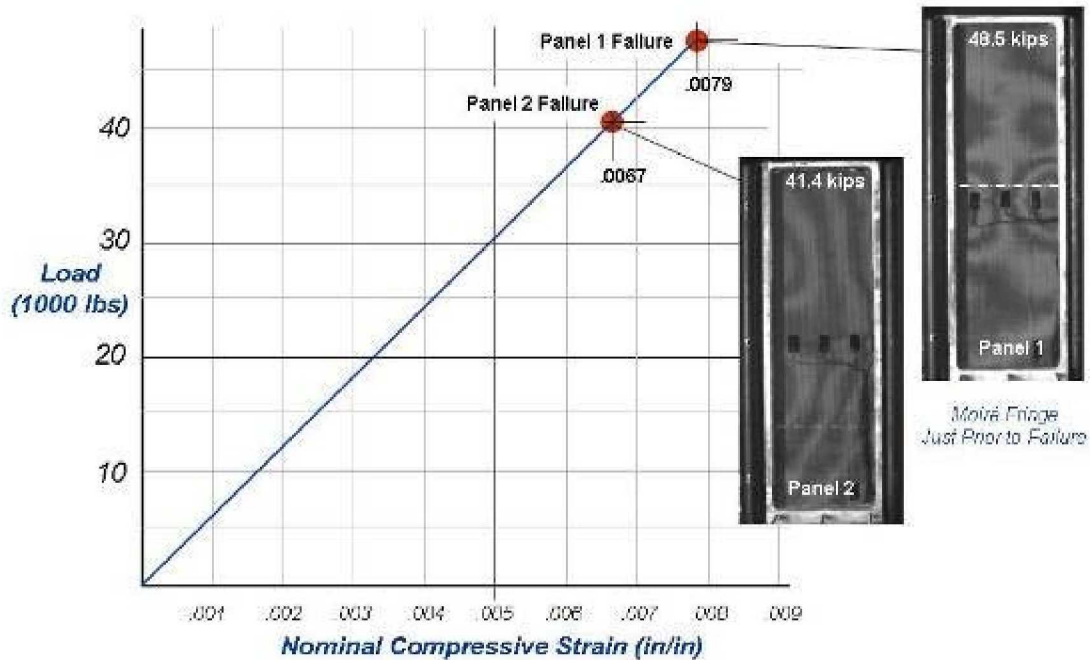


FIGURE 58. PANEL FAILURE LOAD AND SKIN BUCKLING PATTERN

Although each panel was identical, the Moiré fringe patterns were different for each replicate. Replicate 1 (48.5 kip failure load) exhibited the expected front-to-back bending mode and failed near the center of the panel (Figure 59). The fringe pattern (Figure 58) shows the alternating local skin buckling along edges that would be expected from this failure mode. The fringe pattern for Replicate 2 (41.4 kip failure load) was completely different. It suggests a side-to-side bending mode where the bending occurs across the stringer height, making the stringer member ineffective. The result is a lower failure load, at an odd location, away from the center of the panel (Figure 60). The final resting position of the tilted end plate (post-failure) is also an indication that the bending axis of Replicate 2 was side-to-side, rather than front-to-back as in Replicate 1.

In both cases, the failed sections of the panels followed the typical PRSEUS failure scenario, where skin damage initiates at an edge, the crack propagates until it is arrested by the stitching in the stringer flange, and additional load is then transferred to the rod until it fails, breaking the wrap fibers and ultimately failing the panel. The maximum strain gage readings at this point are typically in the -0.0070 in/in range depending on the gage location. This would indicate that local material failures (non-linear behavior) may have occurred and that additional load was being transferred to the rod. The average panel running load for Replicate 1 was 8,083 lbs/in and 6,900

lbs/in for Replicate 2; both of which substantially exceeded the BWB fuselage shell design requirement.

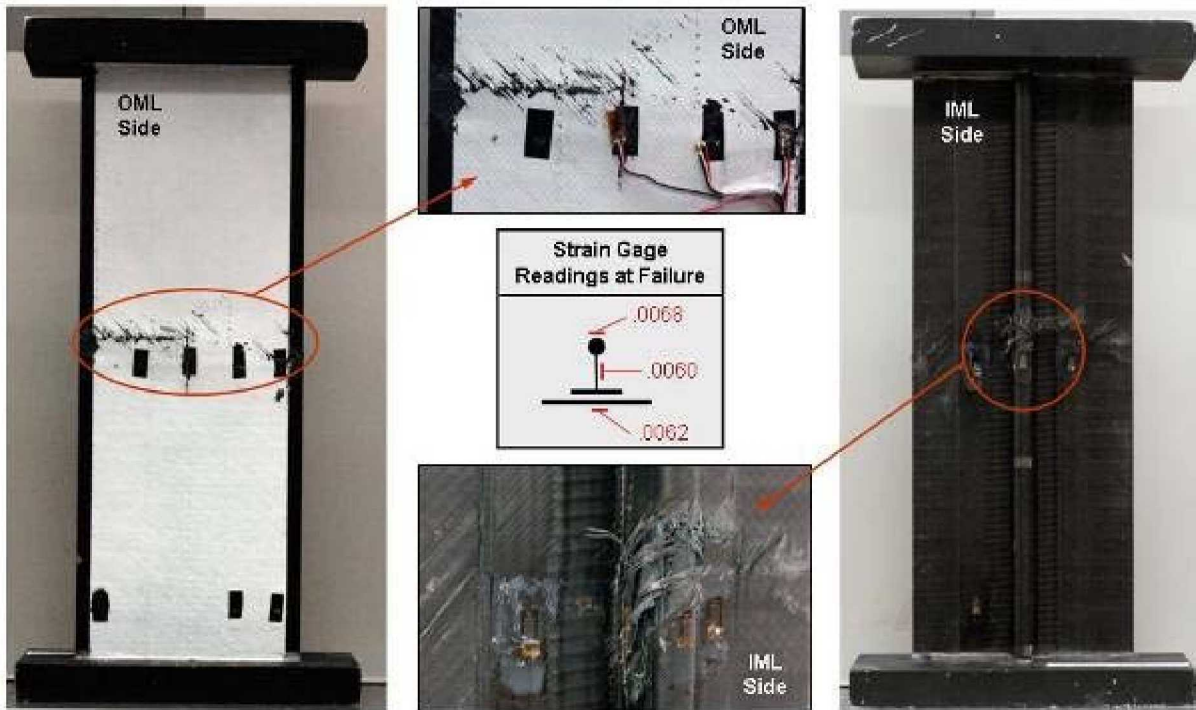


FIGURE 59. REPLICATE 1 - SINGLE-STRINGER FAILURE SUMMARY

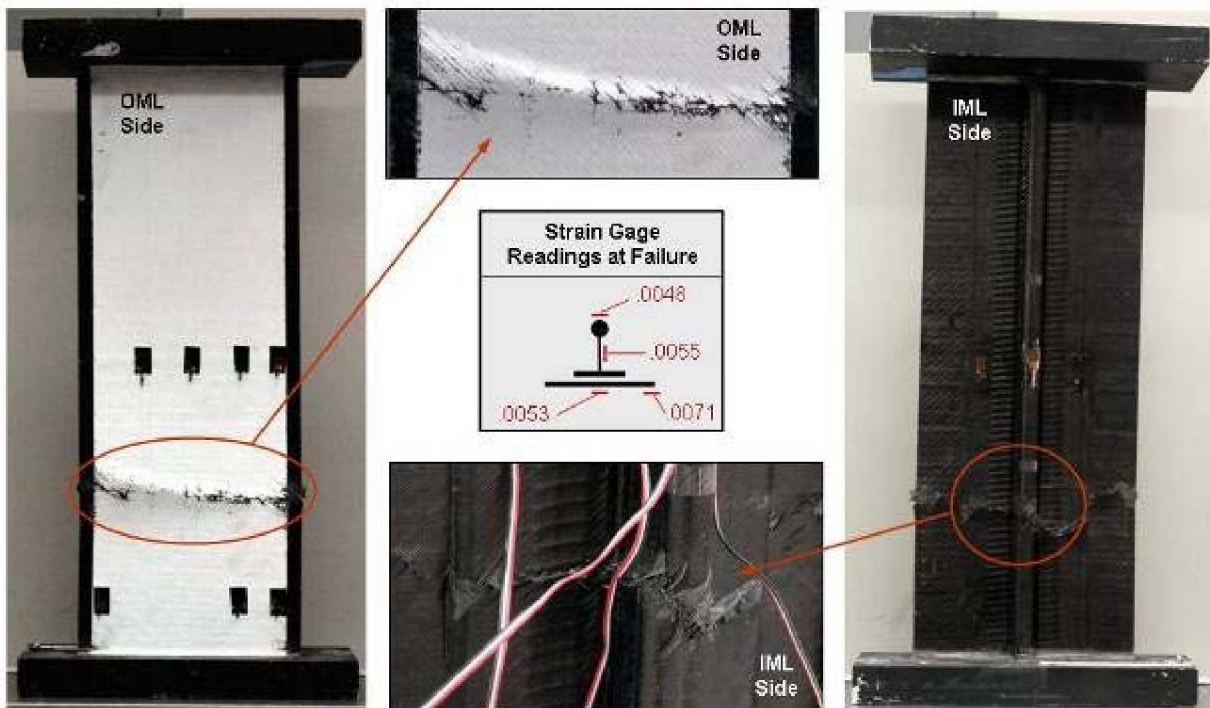


FIGURE 60. REPLICATE 2 - SINGLE-STRINGER FAILURE SUMMARY

1.2.2 Spanwise Single-Frame Compression Panel

The general configuration for the single-frame and testing arrangement is shown in Figure 61 (detail drawing ZJ153294-501 contained in Appendix A). The integral structural panel was built using stacks of DMS 2436 Type 1, Class 72, Grade A carbon fiber (7-ply stack) material, stitched, and then infused with a DMS 2479 Type 2, Class1 VRM-34 epoxy resin. Potted ends were added for load introduction and side restraints were used to inhibit edge buckling along the panel. The specimens were identified as ZJ153294-501 Replicate 1 and Replicate 2.

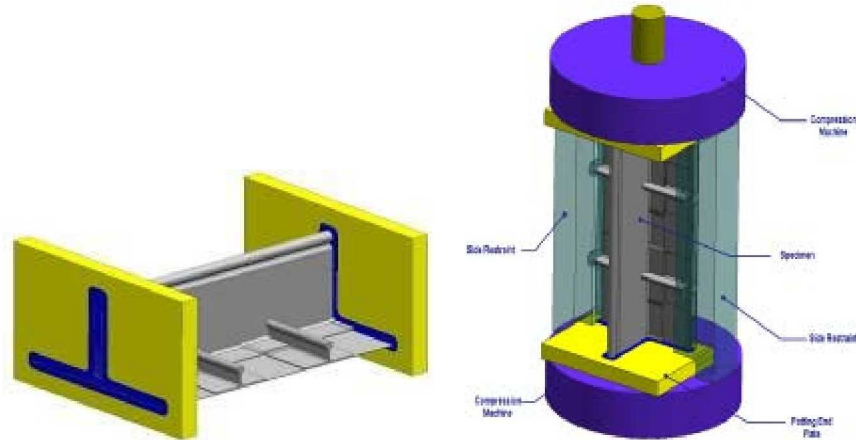


FIGURE 61. SINGLE-FRAME COMPRESSION SPECIMEN DESIGN

Further specimen preparation (Figure 62) was completed by the test lab (OCM) that included: 1) white paint application to the outside skin surface (opposite side of stiffeners) to enhance observation of fringe patterns and panel crack propagation, 2) strain gages installed to record panel strains during load application, and 3) fabrication of side restraints to inhibit panel edge buckling.

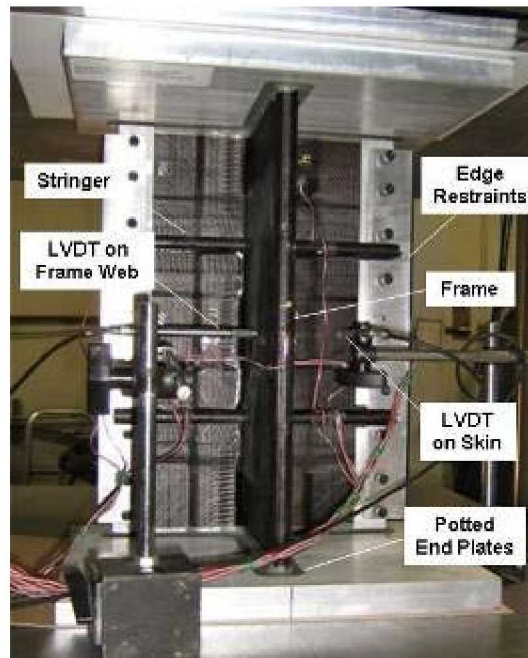


FIGURE 62. SINGLE-FRAME COMPRESSION PANEL SPECIMEN

The basic test set-up at OCM is shown in Figure 63. In addition to the equipment shown, two LVDTs were used, one was positioned on the frame web approximately mid-length between the top and bottom of the specimen, and a second LVDT was positioned on the inside surface of the skin mid way between the stringers. Photographic images were captured during testing with video and digital cameras. The fringe patterns in the photoelastic coating were photographed using a digital camera with a polarizing filter.



FIGURE 63. TEST SET-UP AT OCM

OCM instrumented both of the specimens with 12 strain gauges positioned per Figure 64. The 12 strain gages, 2 LVDT's, actuator displacement transducer and load cell were connected to a Vishay data acquisition system to collect and display all data real time.

The test articles were positioned so the center-of-gravity was located on the centerline of the load frame. Paperboard shims were used to help align the specimen. Load was applied several times while recording strain to validate uniform loading prior to the actual test. Strain gages 1 through 4 were used to balance the specimen loading within +/- 10%.

Testing of Replicate 1 was performed at a constant loading rate of 40,000 pounds per minute, but was later changed to displacement control (.02-inch per minute) for Replicate 2 after the Replicate 1 specimen was unexpectedly crushed after the failure occurred.

Both of the specimens performed and failed in a similar manner. The compressive loading was reacted in a linear fashion up to about 55 kips, then large displacements were recorded (data contained Appendix D) for the frame web and skin bay as non-visible local material failures or skin buckling may have occurred. Both specimens continued carrying load before ultimately failing at 86 and 79.5 kips (Figure 65). The failure location was the same for both specimens, the stringer pass-through cutout in the frame web.

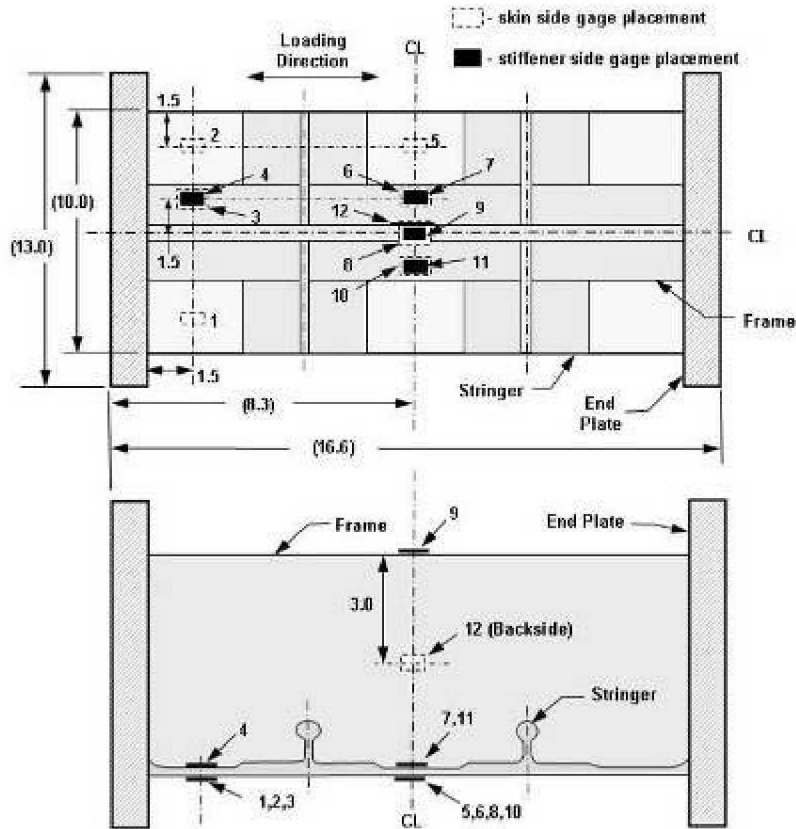


FIGURE 64. SINGLE-FRAME SPECIMEN STRAIN GAGE PLACEMENT

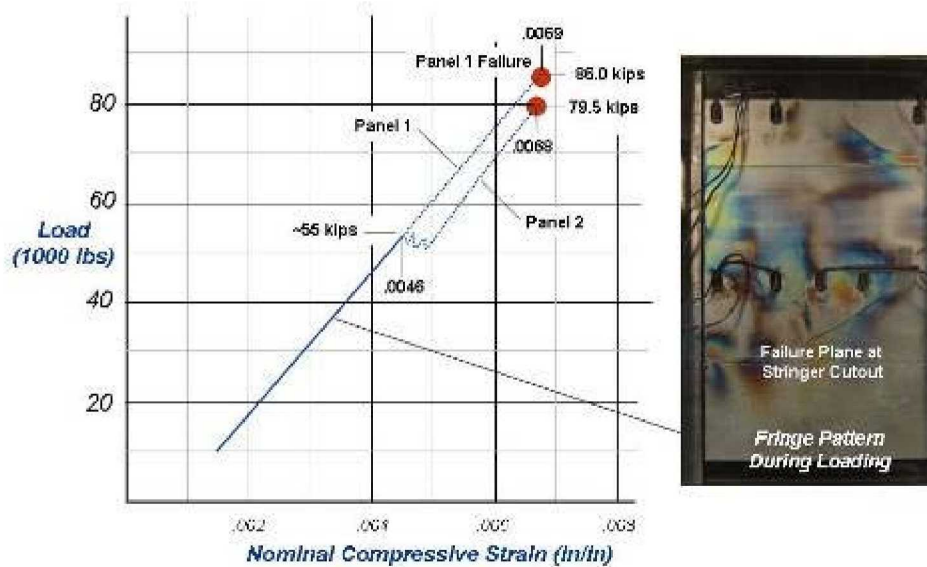


FIGURE 65. REPLICATE 1 AND 2 - SINGLE-FRAME FAILURE SUMMARY

The short column length of the specimen enforced a strength-critical failure mode, making the stringer pass-through region of the frame the most likely failure plane where the frame-plus-skin area is only 1.5 sq-inches. Using this value for the cross-sectional area, a laminate compression

modulus of 9.23×10^6 (Table 5), and a compression strain allowable of 0.004 in/in (Appendix B, Figure B1) would give the following failure load:

$$\text{Load} = (\text{Area}) \cdot (\text{Modulus}) \cdot (\text{Strain}) = (1.5) \cdot (9.23 \times 10^6) \cdot (.004) = 55,000 \text{ lbs} = 55 \text{ kips}$$

This result closely coincides with the nonlinearities observed in the strain and displacement measurements (Appendix D), and suggests that material failures or local buckling could have occurred in this region. Because there was no visible indication of failure at this point in the loading sequence, and there were no strain gages near the failure plane, the actual strains at the failure location must be assessed analytically by accounting for the difference in the cross-sectional areas (gage locations versus failure location).



FIGURE 66. REPLICATE 1 AND 2 - SINGLE-FRAME FAILURE SUMMARY

1.2.3 Fatigue Cycled Specimens

The extra set of specimens (Figure 67) extracted from Panel 1 were shipped to NASA-LaRC for future testing that will be completed during Phase II. These specimens will be fatigue cycled two life times before being statically tested to failure. The results will then be compared to the static test results achieved during Phase I to assess the potential end-of-life material degradation caused by mechanical fatigue.



FIGURE 67. FATIGUE SPECIMENS SHIPPED TO NASA-LARC

Fatigue Spectrum - A simplified compression-compression loading profile was developed to simulate the end-of-life fatigue damage that would be expected for compression dominated regions of the BWB pressurize shell. In creating this profile (Figure 68) the following assumptions were used:

- 1 Service Life = 55,000 cycles = 11 times one Block
- 1 Block = Sum of Flight Types A-E = 5,000 GAG cycles
- Flight Types are applied sequentially
- Each flight represents equivalent damage of 1 GAG cycle
- Relative exceedance/frequencies based on SOA testing
- Peak compressive strains were reduced for pressurization
- Max compressive strains based on material capability
- Loading magnitudes are panel specific
- Use for BWB PRSEUS single-stack min gauge panels
- Maintain min compression-compression loading (200 lbs)

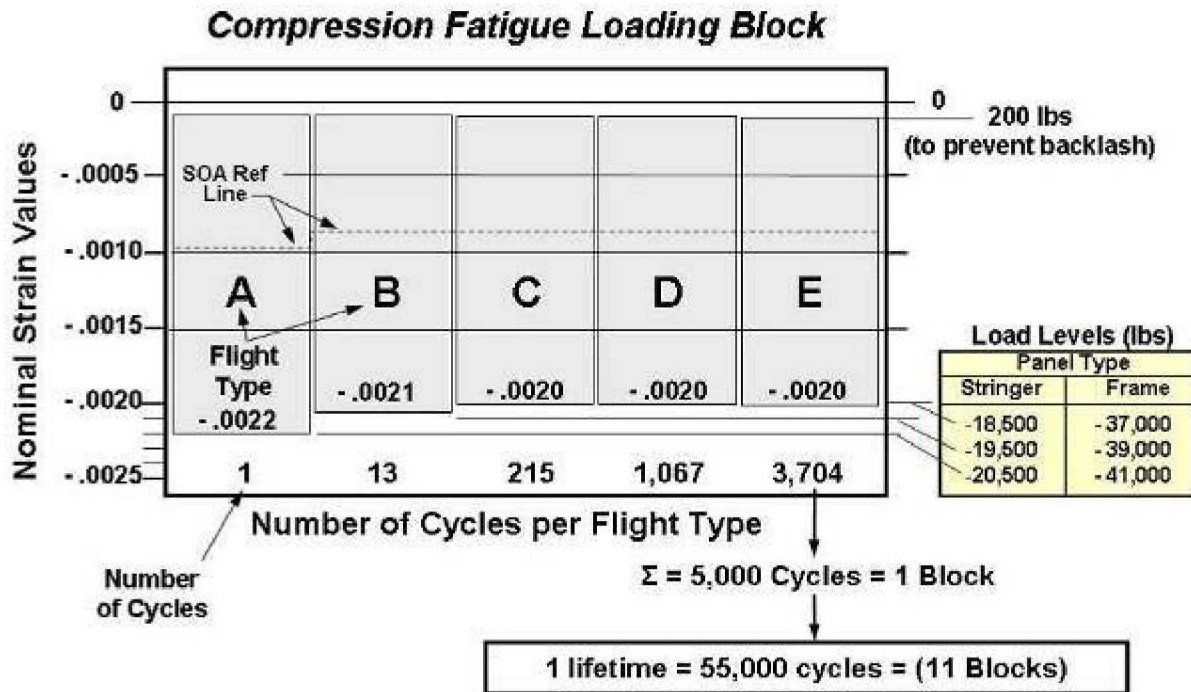


FIGURE 68. COMPRESSION FATIGUE SPECTRUM FOR ELEMENT PANELS

This profile will be used to precondition the fatigue specimens prior to statically testing them to failure. The results will then be compared with the static-only specimen results to assess whether internal cracking in, or around, the PRSEUS-specific features (stitching, transitions, rod-to-wrap interface, etc.) can affect the overall compression strength or buckling behavior of the panel.

1.3 Phase I Conclusions and Metrics

Overall, the sizing results and weight estimates matched our initial expectations of achieving a substantial weight-savings over the old baseline sandwich concept. Because PRSEUS is a highly engineered solution that moves beyond traditional composite design practices to offer an orthogonally-tailored skin-stringer-frame design that can also be operated beyond conventional no-growth design constraints, it resulted in a very efficient solution that was able to maintain residual load-carrying capabilities under a variety of damage scenarios in all three primary loading directions (X, Y, and Z planes). This attribute not only enabled higher operating loads (Metric B), it also provided efficient load paths that resulted in a 10.3% lighter pressure cabin (Metric A) for the BWB configuration evaluated in this study.

The highly integrated nature of the PRSEUS concept was most evident in the large weight savings that was achieved for the frame members (45%) and skin panels (18%). The arrangement of dry warp-knit fabric, precured rods, and foam-core materials are assembled and then stitched together to create the optimal structural geometry for the bi-directional loading environment of the BWB pressure cabin. Because the load path continuity is maintained at the stringer-frame intersection in both directions, and the frame elements are placed directly on the IML skin surface instead of offset, a higher structural efficiency was achieved for the PRSEUS concept relative to a sandwich panel design where the load transfer between the skin panel and frame become awkward.

In its entirety, the integral panel design is intended to first exploit the orthotropic nature of carbon fibers, and then to suppress the out-of-plane failure modes with through-the-thickness stitching. Taken together, these two features enable the application of a new damage-arrest design approach for composite structures that is capable of overcoming the noncircular pressure vessel weight penalty inherent in the BWB airplane configuration.

To measure these attributes, two key metrics were established at the outset of Phase I:

- Metric A - PRSEUS pressure shell will be 10% lighter than the a sandwich design.
- Metric B - Buckling load for the single-stringer compression specimen will exceed the design strength-critical load, as defined by the notched material property.

The selection of these two particular measures was done to provide a direct means of assessing the relative merits of the PRSEUS design approach compared to the presumed strengths of the old baseline sandwich design approach. Because sandwich concepts are often shown to be the lightest weight solution, at least during the preliminary design phases of a program, a metric that captures airframe weight was selected, Metric A, and because sandwich concepts are also very efficient under pressure and axial compressive loading scenarios, Metric B was selected to demonstrate that a highly-tailored geometrically-efficient post-buckled panel configuration, like PRSEUS, is more effective than a non-buckled sandwich design under axial compression loading.

1.3.1 Metric A

The data for this metric comes from the airframe weights statement generated during the vehicle-level airframe sizing exercise described in Section 1.1 of this report. When the pressurized shell elements only (skin panels and frames added together) are compared, a large 28% weight savings was realized with the PRSEUS concept. This was due mainly to the advantages of the skin-

stringer-frame design with respect to damage arrestment (results in higher tension design values), post-buckling of the skins (permits thinner gauges), and an integral frame design (more efficient in spanwise compression loading).

The advantages of better structural integration are particularly evident when the frame weights are considered in isolation. The 45% weight savings for the frames using the PRSEUS concept serves to highlight the integration weight penalty incurred with the sandwich design approach. In this case, the pad-ups regions required at each frame station to transfer loads between the sandwich skin panel and frame member contributed very little to the overall bending stiffness of the frame member and resulted in a large weight penalty.

Such a disparity is particularly discriminating within the BWB design environment, where the combined loading of internal pressure (out-of-plane) and axial compression (along the frame direction) produce large secondary-bending effects in the skin panels that can only be efficiently reacted by tall frame members. Structural concepts without an efficient frame or beam-type element straddling the spanwise direction of the pressure cabin (between rib bulkheads), as well as, possessing an effective means of transferring out-of-plane loads between the skin and frame elements will be less effective than integral design solutions like PRSEUS that integrate the skin, stringer, and frame element into a harmonized design solution capable of efficiently reacting loads in all three directions.

When the remaining structural elements that were not changed in the sizing exercise (bulkheads, floors, etc.) and the non-optimum were added to the weights statement, the final overall weight savings attributed to the PRSEUS shell concept is reduced to 10.3%, which slightly exceeded the 10% goal established for Metric A. This result is shown plotted relative to normalized data from the NASA TCAT Phase I Study (Reference 1) in Figure 69.

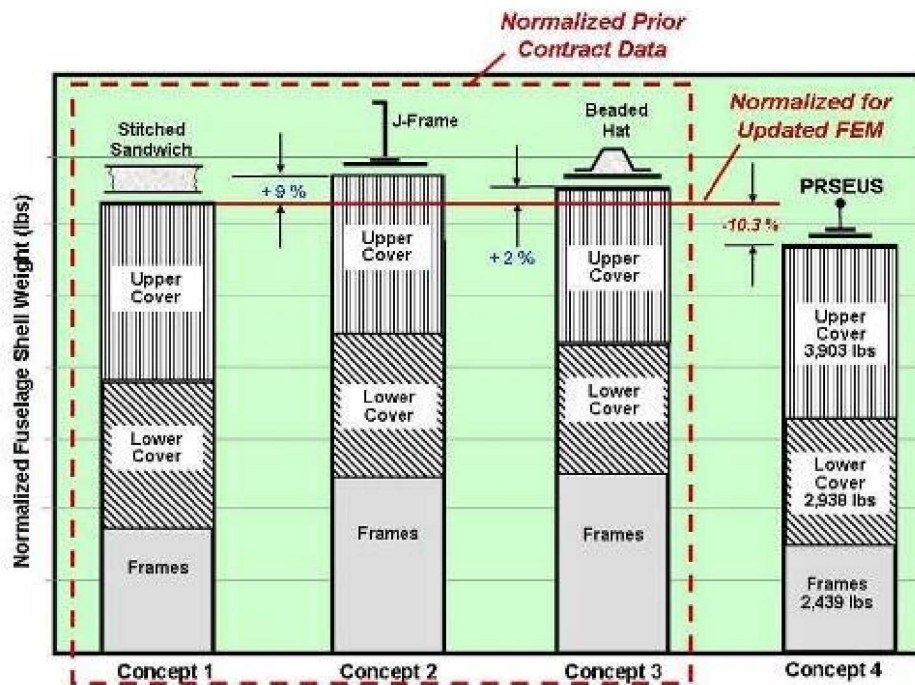


FIGURE 69. METRIC A - NORMALIZED WEIGHT COMPARISON

The data was normalized using the prior sandwich concept results produced in that study (Reference 1) in combination with the sandwich panel results developed in this study. This was done to account for the changes and improvements made to the FEM since those initial results were published in 2004. The resulting normalized plot provides a direct comparison of the prior study concepts and shows the relative improvements that can be achieved using the PRSEUS design approach.

1.3.2 Metric B

The data for this metric comes from the single-stringer compression testing described in Section 1.2.1 of this report. The purpose of this metric was to demonstrate the superior buckling capability of the PRSEUS skin-stringer structural concept relative to a highly efficient sandwich panel design approach. By taking advantage of the stitched-on stringer and higher percentage of 0-degree fiber tailoring that is possible (because stitching is used to suppress interlaminar failures at the transition regions between the hard and soft fiber orientations), the skin-stringer panel can be driven further into the post-buckled design regime to reduce weight. The fundamental argument then becomes, is a post-buckled skin-stringer panel more efficient than a nonbuckled sandwich panel?

To answer this question without conducting an actual sandwich panel test, one must consider that the optimum sandwich panel design is a strength-constrained design, whereby the facesheets can easily be moved further apart to satisfy stability criterion without materially affecting panel weight. The advantage of the sandwich panel design is that stability concerns are not violated until after strength design limits are typically reached. For such a strength-constrained design under compressive loading, the critical design parameter then becomes the material compression strength (typically compression-after-impact, or open-hole compression). The objective then simplifies down to the design of an efficient panel geometry whereby the stability design constraints are not exceeded until after the strength-design constraints are reached. Typically, achieving these objectives simultaneously results in the lightest weight sandwich panel. With this in mind, the Metric B goal was established so that the skin-stringer PRSEUS panel would also achieve a similar result; the PRSEUS panel would not become stability critical prior to reaching the strength-constrained design allowable.

The result of this assessment is graphically depicted in the load-vs-strain plot in Figure 70. Here, the data from the single-stringer testing was plotted to show the Panel 1 (ZJ153294-1 Replicate 1) and Panel 2 (ZJ153294-1 Replicate 2) failure loads relative to the nominal compressive strains in the panels. The goal established for Metric B was for the test panels to exceed the compression strength design allowable (.0040 in/in in this case) prior to failure. In both cases this was achieved. Panel 1 was 2.0 times higher, and Panel 2 was 1.7 times higher. These high margins give a good indication of the structural efficiency of the PRSEUS structural concept and indicate that post-buckled designs that push further into the post-buckled range are possible because stitching prevents stiffener separation. Such a capability will become even more important as the combined axial-plus-pressure load cases of BWB design environment are assessed in future studies.

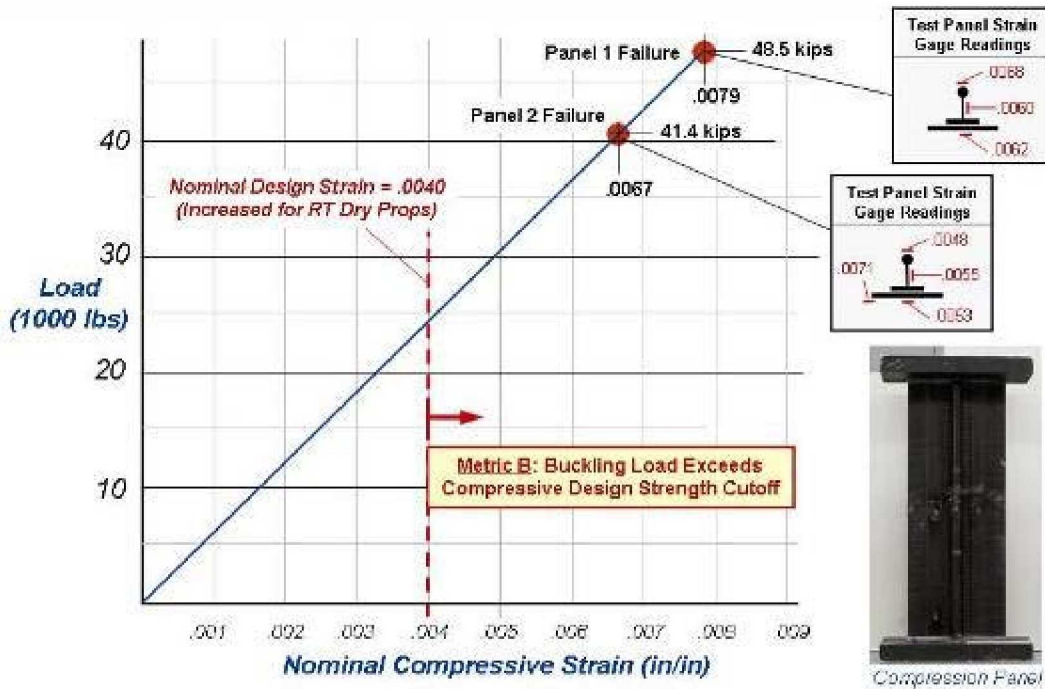


FIGURE 70. METRIC B - COMPARISON OF COMPRESSION DESIGN PARAMETERS

2.0 PHASE II PROPOSAL

There are two key aspects of shaped-vehicle design that will have a large impact on fuselage weight. First, the combined axial-and-pressure loads that lead to secondary panel bending and pre-buckled panel shapes, and second, the damage-arrest design philosophy that must be employed to react against the severe out-of-plane loading environment.

The complex interaction between the axial and pressure load components in the BWB shell represents a difficult challenge for the structural analyst. These near-flat panels experience combined secondary-bending and nonlinear effects that exacerbate panel buckling under compressive loads. To quantify the effects of this problem, a series of compression, tension, and pressurized subcomponent specimens will be analyzed and tested in Phase II to provide the foundation needed for a large-scale combined-loads testing in the future.

2.1 Phase II Plan

The Phase II plan maintains the continuity of Phase I activities by extending the building-block development approach to encompass more technically demanding analysis and testing tasks (Figure 71). Over the course of Phase II, three large subcomponent specimens will be fabricated and tested to understand the structural responses for axial and pressure-type loadings. Further analytical work will also be undertaken to improve the panel-level sizing methods that were used during Phase I. All the Phase II data will then be compiled in a final vehicle-level trade study to assess the benefits of the Phase II activities (Figure 72)

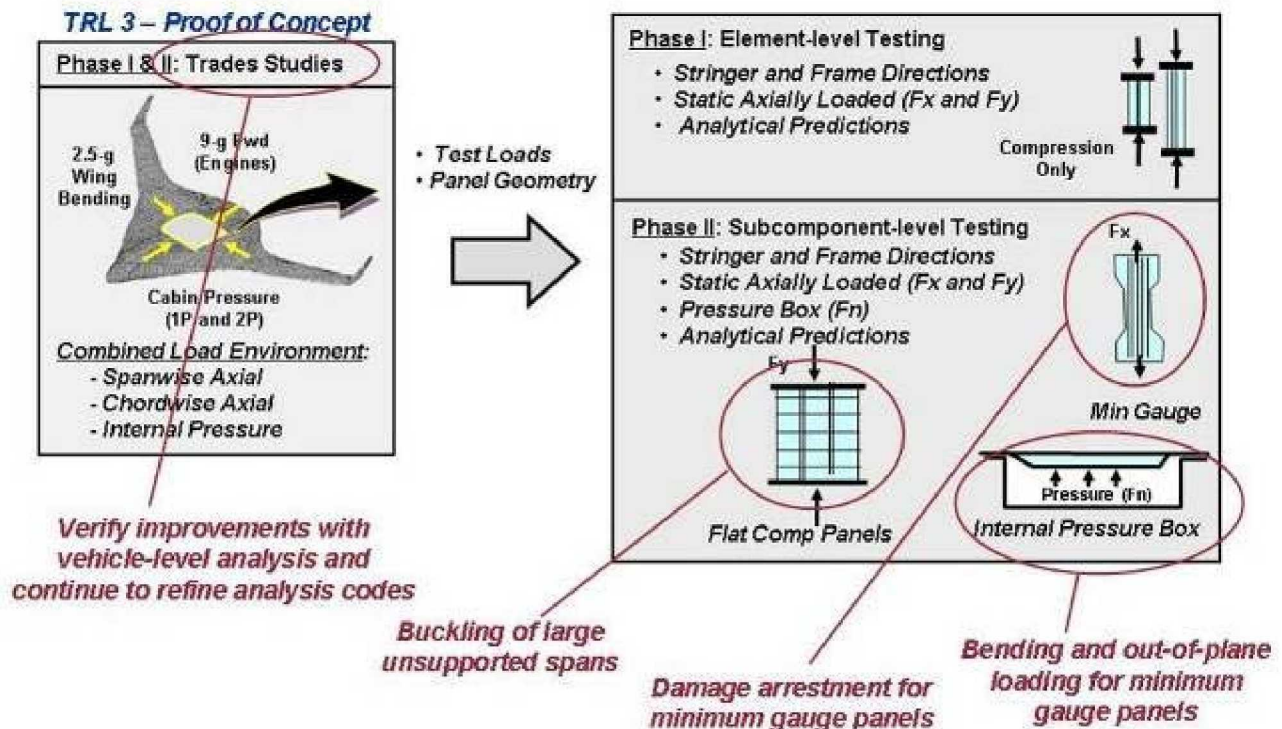


FIGURE 71. KEY ELEMENTS OF PHASE II PLAN

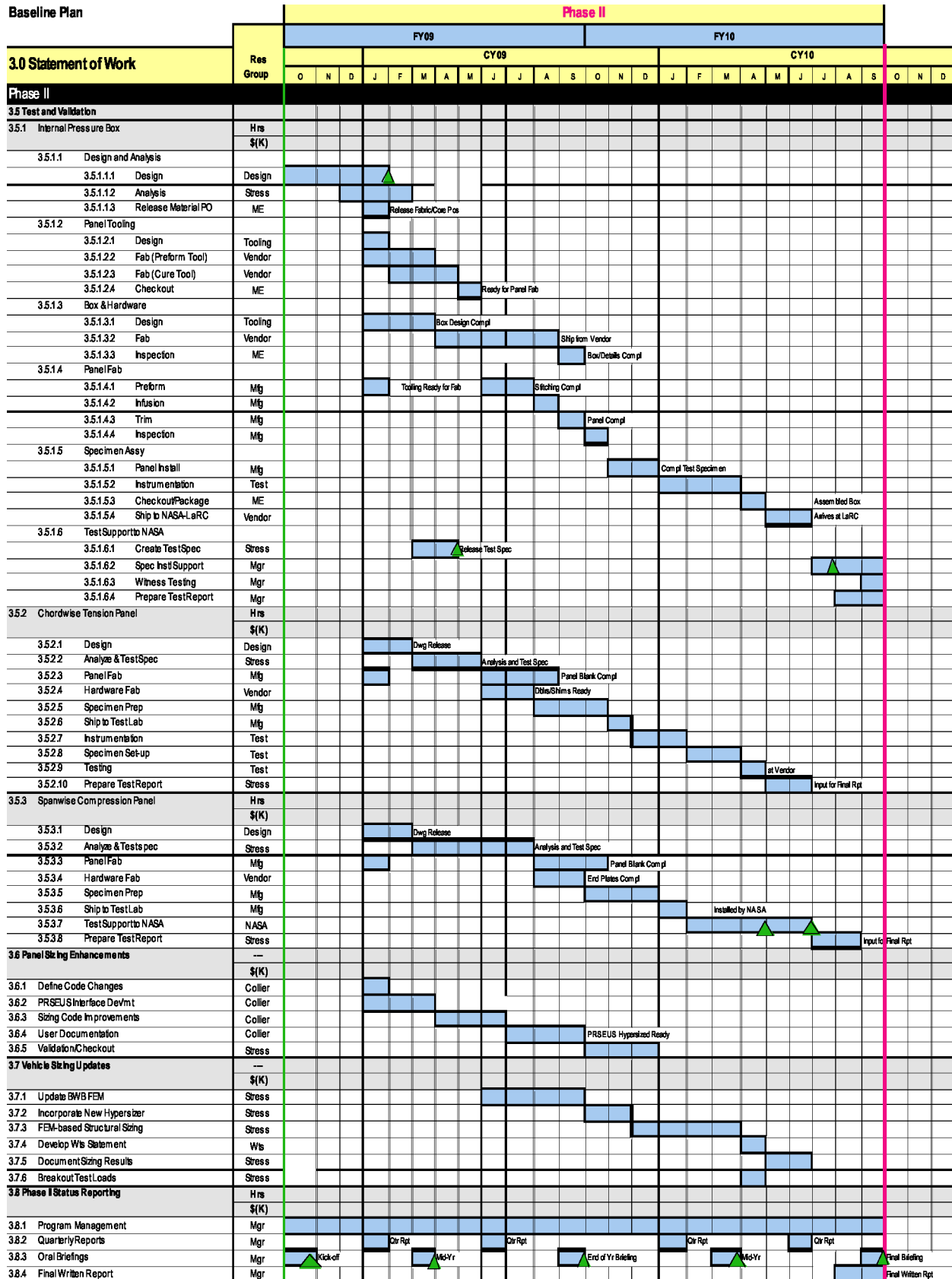


FIGURE 72. PHASE II WORK STATEMENT

WBS 3.5 Test and Validation – Three different subcomponent specimens (WBS 3.5.1 Internal Pressure Box, WBS 3.5.2 Streamwise Tension Panel, and WBS 3.5.3 Spanwise Compression Panel) will be designed, analyzed, and fabricated by Boeing. Two of the specimens (WBS 3.5.1 and WBS 3.5.3) will be tested at NASA-LaRC and one specimen (WBS 3.5.1) will be tested by an outside test lab under subcontract to Boeing. Boeing will provide on-site engineering support during specimen set-up and testing for all tests, as well as write test specification documents that dictate the overall test procedure and data requirements (instrumentation, loading sequence, load levels, data recording, etc.).

WBS 3.5.1 Internal Pressure Box - The large pressure box subcomponent (Figure 73) represents the first step in isolating the secondary-bending effects experienced in the BWB pressure shell. It is, in fact, the first time that a PRSEUS test panel will be subjected to internal pressure loading. Because the 2P loading condition drives much of the BWB minimum gauge skin and stringer spacing design requirements for the shell region, this is a critical test in establishing the overall structural viability of the airframe design approach.

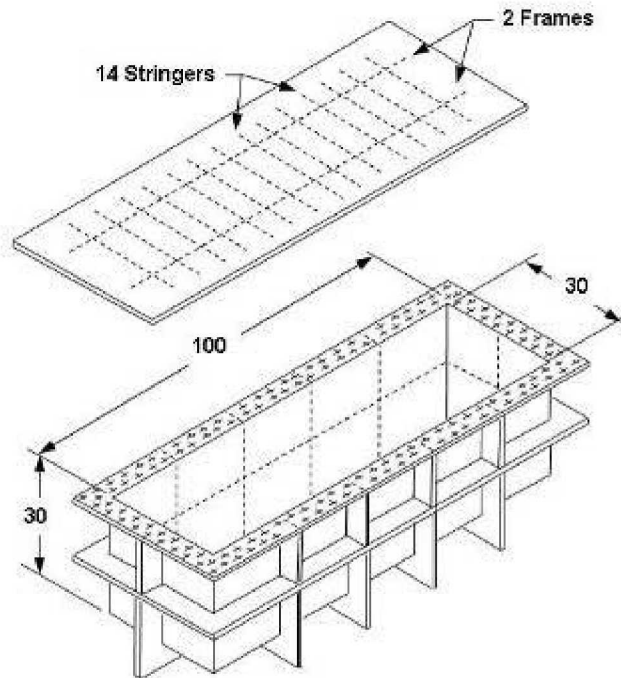


FIGURE 73. PRESSURE BOX TEST SPECIMEN

An FEM-based analysis will be used to properly predict failure loads and structural deformations for the test panel and pressure box.

WBS 3.5.1.1 Design and Analysis – Detail design definition will be created for the test panel and box structure hardware. The panel will be sized using a set of internal loads derived from the vehicle-level trade studies and designed to satisfy minimum gauge requirements.

WBS 3.5.1.2 Panel Tooling - A flat 3-ft x 9-ft stitching frame and a 4-ft x 10-ft cure tool will be designed by Boeing and then fabricated by an outside supplier.

WBS 3.5.1.3 Box & Hardware – A low-cost metallic pressure box structure, as well as all the related load introduction hardware will be designed by Boeing and then fabricated by an outside supplier.

WBS 3.5.1.4 Panel Fabrication – One 3-ft x 9-ft specimen panel blank will be stitched, cured, and rough-cut. Additional labor and material costs will not be carried in the estimate to provide back-up panels. In the event problems are encountered during fabrication, then hours and dollars will be reprogrammed from other tasks to support additional panel fabrication.

WBS 3.5.1.5 Specimen Assembly – All the specimen details and loading hardware fabricated in the prior tasks will be assembled into the final specimen configuration, and then shipped to the COLTS facility at NASA-LaRC.

WBS 3.5.1.6 Test Support to NASA – Design, analysis, and management hours will be set aside to help support the specimen set-up and testing that will be conducted by NASA personnel at the NASA-LaRC COLTS test facility. (Actual specimen set-up and testing costs are not included in this proposal and will be covered by NASA in-house budgets.)

WBS 3.5.2 Streamwise Tension Panel - The primary purpose of this subcomponent test is to demonstrate the distinctive damage-arrest design advantages of the PRSEUS concept for the particular minimum-gauge fuselage geometry calculated for the BWB shell. Because the primary fiber axis of the skin is parallel to the frame direction (instead of the stringer) to accommodate the bi-directional loading environment of the BWB, it will be more difficult to turn-the-crack and maintain fail-safety without the aid of the fiber-splitting phenomena that normally occurs in a skin laminate under loading parallel to the 0-deg dominated fiber axis. This concern will be investigated using the 3-stringer dog-bone tension specimen geometry shown in Figure 74.

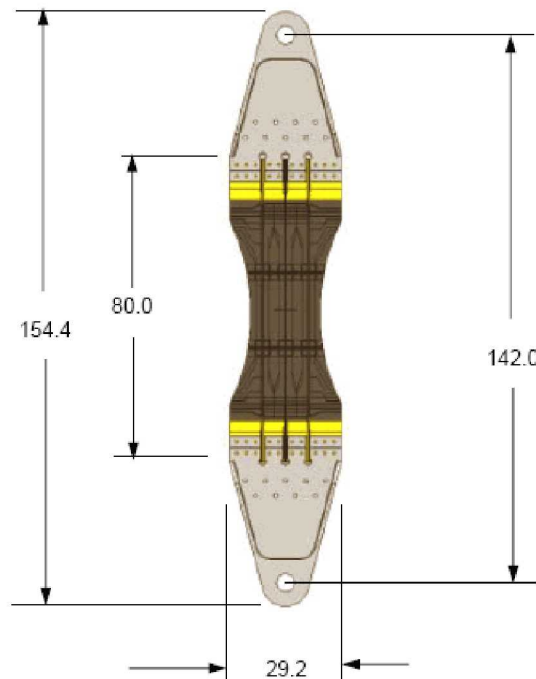


FIGURE 74. STREAMWISE TENSION PANEL GEOMETRY (INCHES)

WBS 3.5.2.1 Design – Two detail design drawings will be created, one for the specimen blank (cured PRSEUS panel prior to edge trim) and another that details the final test specimen configuration with the end grips installed.

WBS 3.5.2.2 Analyze – An FEM-based analytical task will be performed to predict failure loads, modes, and determine the optimum strain gage placement for testing. A detailed test specification document will also be prepared that describes the test set-up, instrumentation locations, and data recording requirements.

WBS 3.5.2.3 Panel Fabrication – A flat 4-ft x8-ft PRSEUS panel will be fabricated using an existing stitching and cure tool. Additional labor and material costs will not be carried in the proposal estimate to enable additional panel fabrication. If an additional panel is required, then the hours and dollars will be reprogrammed subtask WBS 3.7.3 FEM-based Structural Sizing.

WBS 3.5.2.4 Hardware Fabrication – Small shims and end doublers will be fabricated by an outside supplier. A set of existing end grip plates will be refurbished readied for panel assembly.

WBS 3.5.2.5 Specimen Prep – The specimen blank will be final machined to the dog-bone shape and prepared for doubler bonding, shimming, and end plate assembly. The completed specimen will then be impacted and inspected.

WBS 3.5.2.6 Ship to Test Lab – Boeing will fabricate a small shipping container and ship the test specimen to the outside test lab.

WBS 3.5.2.7 Instrumentation – Approximately 30 strain gages will be installed on the panel by outside test lab personnel per the instructions given in the test specification document.

WBS 3.5.2.8 Specimen Set-up – The outside test lab will install the test specimen into their tension test equipment, connect gages, and perform pretest checkout.

WBS 3.5.2.9 Testing – The outside test lab will perform a static loading to failure in room temperature dry conditions and record data per instructions given in the test specification generated in Task 3.5.2.2.

WBS 3.5.2.10 Prepare Test Report – A final write-up of the test will be prepared by Boeing and included in the final report. It will describe the pre- and post-test activities and data.

WBS 3.5.3 Spanwise Compression Panel - The primary purpose of this subcomponent test is to assess the buckling stability of the PRSEUS integral frame feature. Because the frame and skin stacks are infused as a singular element, without shear clips or fasteners, the ensuing panel geometry is a highly effective component under compressive loading. This test will simulate the spanwise compression loads that are imparted on the upper portion of the pressure shell by the positive maneuver wing bending loads. The 2-frame compression specimen geometry shown in Figure 75 will be used for this test.

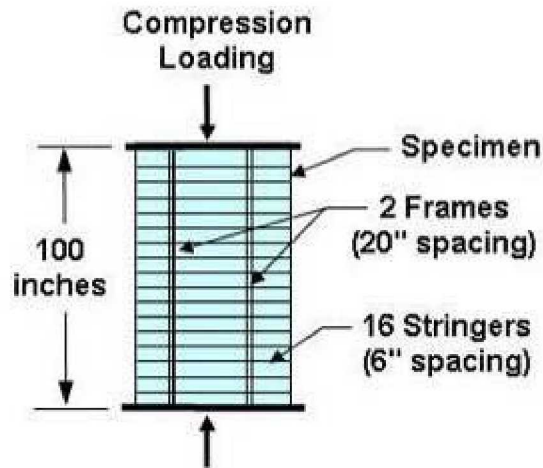


FIGURE 75. SPANWISE COMPRESSION PANEL GEOMETRY (INCHES)

WBS 3.5.3.1 Design – Two detail design drawings will be created, one for the specimen blank (cured PRSEUS panel prior to edge trim) and another that details the final test specimen configuration with the potted in plates installed.

WBS 3.5.3.2 Analyze – An FEM-based analytical task will be performed to predict failure loads, modes, and determine the optimum strain gage placement for testing. A detailed test specification document will also be prepared that describes the test set-up, instrumentation locations, and data recording requirements.

WBS 3.5.3.3 Panel Fabrication – A flat PRSEUS panel will be fabricated using the pressure box panel tooling created under WBS 3.5.1.2. Additional labor and material costs will not be carried in the proposal estimate to enable additional panel fabrication. If an additional panel is required, then the hours and dollars will be reprogrammed subtask WBS 3.7.3 FEM-based Structural Sizing.

WBS 3.5.3.4 Hardware Fabrication – Two end plates will be fabricated by an outside supplier.

WBS 3.5.3.5 Specimen Prep – The specimen blank will be final machined and prepared for end plate potting. After potting, the end plates will be ground flat and parallel. The completed specimen will then be impacted and inspected.

WBS 3.5.3.6 Ship to Test Lab – A small shipping container will be fabricated and the specimen will be ship to NASA for instrumentation and static testing.

WBS 3.5.3.7 Test Support to NASA – Hours will be set aside to help support the specimen set-up and testing that will be conducted by NASA personnel at their test facility. (Actual specimen set-up and testing costs are not included in this proposal and must be covered by NASA in-house budgets.)

WBS 3.5.3.8 Prepare Test Report – A final write-up of the test will be prepared by Boeing and included in the final report. It will describe the pre- and post-test activities and data.

WBS 3.6 Panel Sizing Enhancements - During the Phase I trade studies several opportunities were identified to improve the interoperability of the HyperSizer analysis code and the PRSEUS structural concept. Such changes are necessary due to the unique structural features of the rod-stiffened design and its ability to operate well into the post-buckled design regime. The goal of such changes is twofold: 1) more accurately reflect the actual structural response, and 2) simplify the user interface to permit novice users to conduct trade studies using the PRSEUS structural concept.

WBS 3.6.1 Define Code Changes – Based on the Phase I trade study results, an initial set of software changes and analytical enhancements will be written up for HyperSizer analysis code by Collier Research. The proposed changes will be negotiated by telecon with Boeing and NASA-LaRC present until a final agreement is reached.

WBS 3.6.2 PRSEUS Interface Development – Boeing will supply PRSEUS design requirements and materials properties to Collier Research for incorporation into the HyperSizer code. Collier Research will develop and add a PRSEUS input screen into the HyperSizer code.

WBS 3.6.3 Sizing Code Improvements – Collier Research will rewrite software code within HyperSizer to incorporate the changes structural sizing changes outlined in WBS 3.6.1.

WBS 3.6.4 User Documentation – Collier Research will write a set of user instructions specific to the PRSEUS-related modifications which will be included as a chapter in the final written report.

WBS 3.6.5 Validation/Checkout – Collier Research will deliver the updated HyperSizer package to Boeing where it will be run and checked against the Phase I and II sizing results.

WBS 3.7 Vehicle Sizing Updates - The vehicle-level analysis work completed in Phase I will be updated during the Phase II period of performance. In addition to the updated PRSEUS interface, a higher level of analytical fidelity will be achieved through the incorporation of a more accurate sizing methodology based on the results of the Phase I testing.

WBS 3.7.1 Update BWB FEM - The existing Phase I BWB-5-200G FEM will be updated to reflect the latest vehicle-level program requirements.

WBS 3.7.2 Incorporate New Hypersizer - The input deck for PRSEUS material properties and geometry constraints will be updated to correspond to the new HyperSizer interface.

WBS 3.7.3 FEM-based Structural Sizing - The structure will be sized using a two-stage process (global then local optimizations). Global sizing optimizes vehicle-level stiffness and load distributions to satisfy vehicle-level design requirements. Local optimization models various panel-level design constraints that address local panel strength and stability checks.

WBS 3.7.4 Develop Weights Statement – A detailed weights statement will be developed that breaks down the individual structural assemblies by major sections of the airplane.

WBS 3.7.5 Document Sizing Results – The detailed analyses performed under WBS 3.7 will be written up in the final report and available for public release.

WBS 3.7.6 Breakout Test Loads – Additional global FEM modeling tasks will be undertaken to breakout local internal loading distributions to support the subcomponent test program.

WBS 3.8 Phase II Status Reporting – Boeing will continue to use the program management best practices established during Phase I to manage the proposed program.

WBS 3.8.1 Program Management – There will be weekly internal status meetings in which program cost, schedule, staffing, risk, and technical issues will be coordinated, planned, managed, and tracked using standard government Earned Value Management (EVM) techniques.

WBS 3.8.2 Quarterly Reports – Program status reports will be prepared on a quarterly basis (except in periods where a mid-year or year-end oral briefing occurs) to report program progress and issues.

WBS 3.8.3 Oral Briefings – Oral technical briefings of progress will be conducted at NASA’s facility in Langley, Virginia. There will be briefings in Phase II consisting of a project kickoff meeting, two mid-year updates and two year-end briefings. In addition to these progress briefings, meetings are also planned to support test coordination or to witness a test.

WBS 3.8.4 Final Written Report – A Phase II final report will be submitted that summarizes activities, results, findings, and recommendations.

REFERENCES

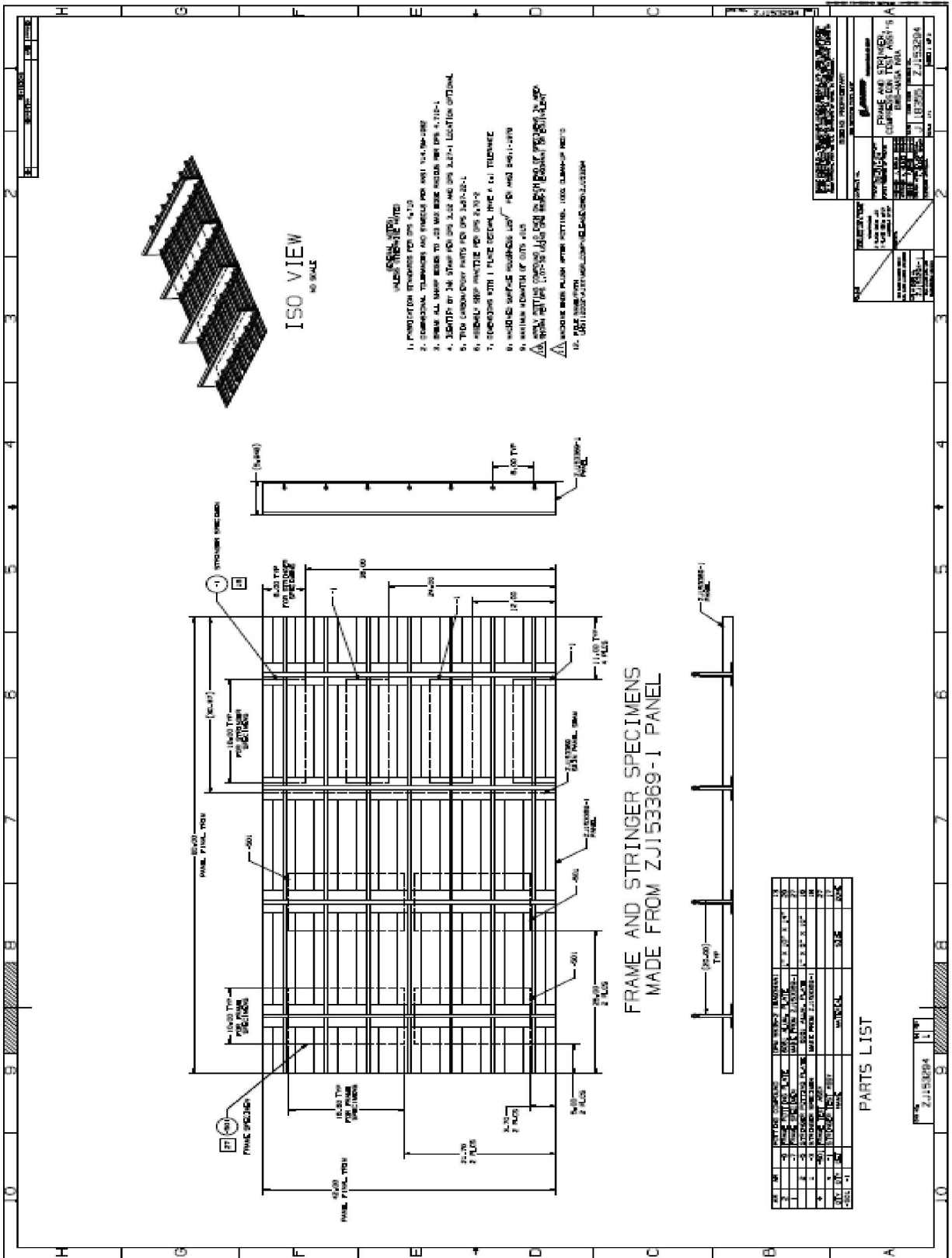
¹ NASA TCAT Phase I Study (Novel Blended Wing Body Structural Concepts), Velicki, A., Contract NNL04AA36C CLIN 0001, July 2004.

² AIR VEHICLE TECHNOLOGY INTEGRATION PROGRAM (AVTIP), Delivery Order 0059: Multi-role Bomber Structural Analysis, AFRL-VA-WP-TR-2006-3067, Krishna Hoffman, MAY 2006, Final Report for 14 December 2004 – 08 May 2006, AFRL-VA-WP-TR-2006-3067.

³ Karal, M., “AST Composite Wing Study – Executive Summary”, NASA/CR-2001-210650, Prepared for NASA, Langley Research Center under Contract NAS1-20546, March 2001.

⁴ Velicki, A. and Thrash, P.J., “Advanced Structural Concept Development Using Stitched Composites”, 49th AIAA/ASME/ASCE/SHS/ASC Structures, Structural Dynamics, and Materials Conference, 7-10 April 2008, Schaumburg, IL, AIAA Paper 2008-2329.

APPENDIX A – PANEL AND SPECIMEN DRAWINGS



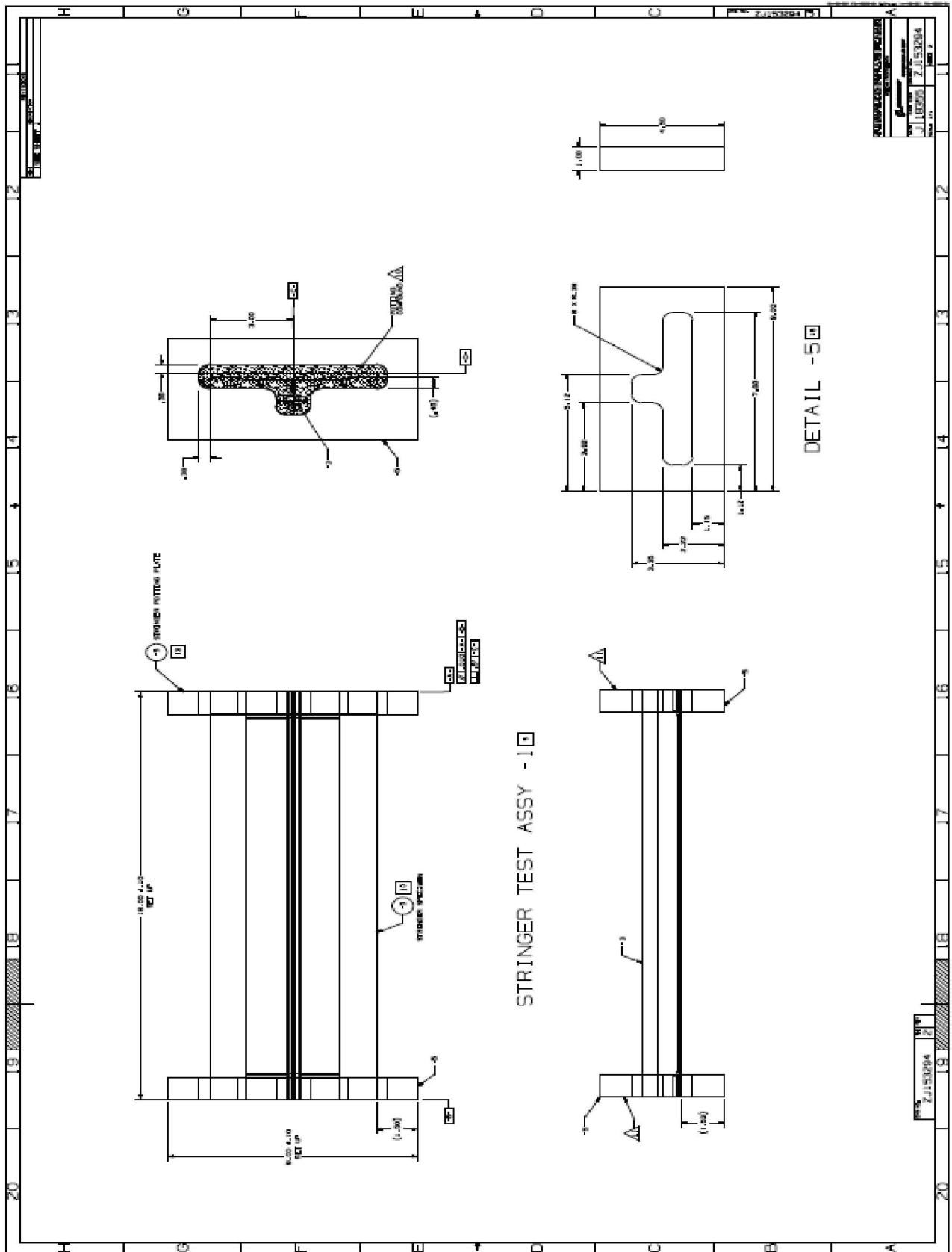


FIGURE A2. SINGLE-STRINGER SPECIMEN DRAWING

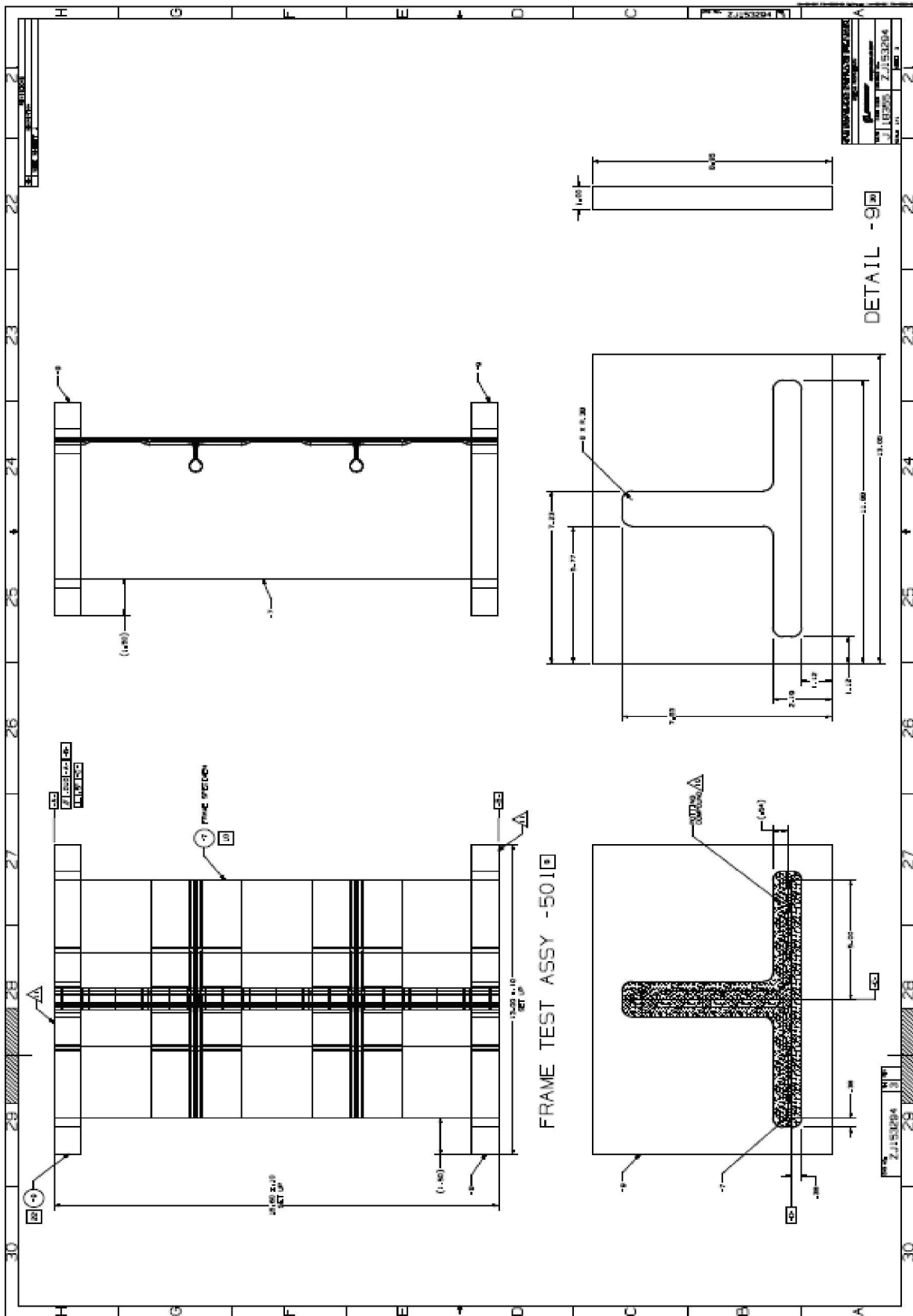


FIGURE A3. SINGLE-FRAME SPECIMEN DRAWING

APPENDIX B – FATIGUE PROFILE DEVELOPMENT NOTES

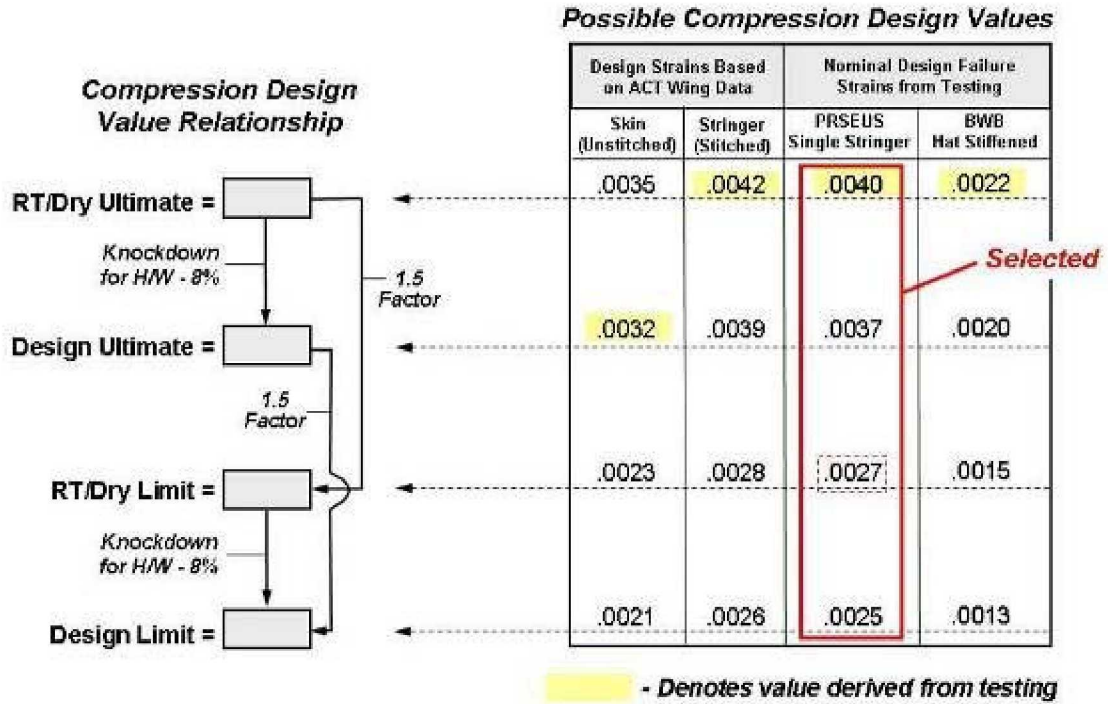


FIGURE B1. AVAILABLE STRAIN DATA – FOUR OPTIONS

Based on Maximum Capability of Material Structural Concept to Carry Axial Loading

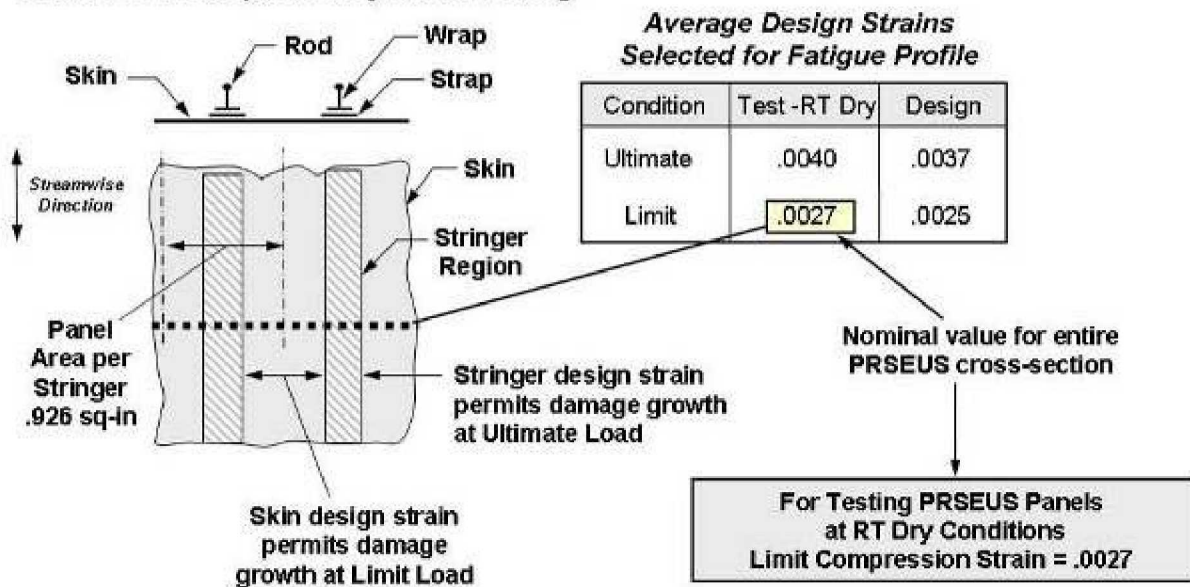


FIGURE B2. AXIAL COMPRESSION STRAIN FROM MANEUVER

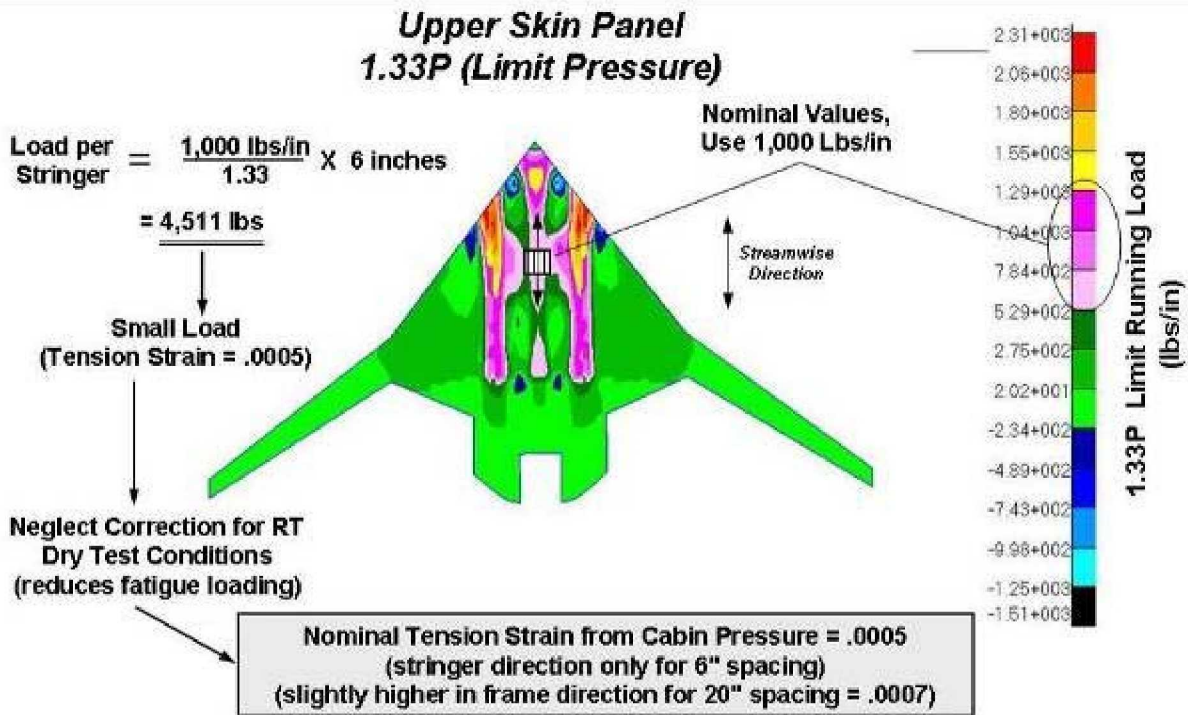


FIGURE B3. AXIAL TENSILE STRAIN FROM 2P LOAD CASE

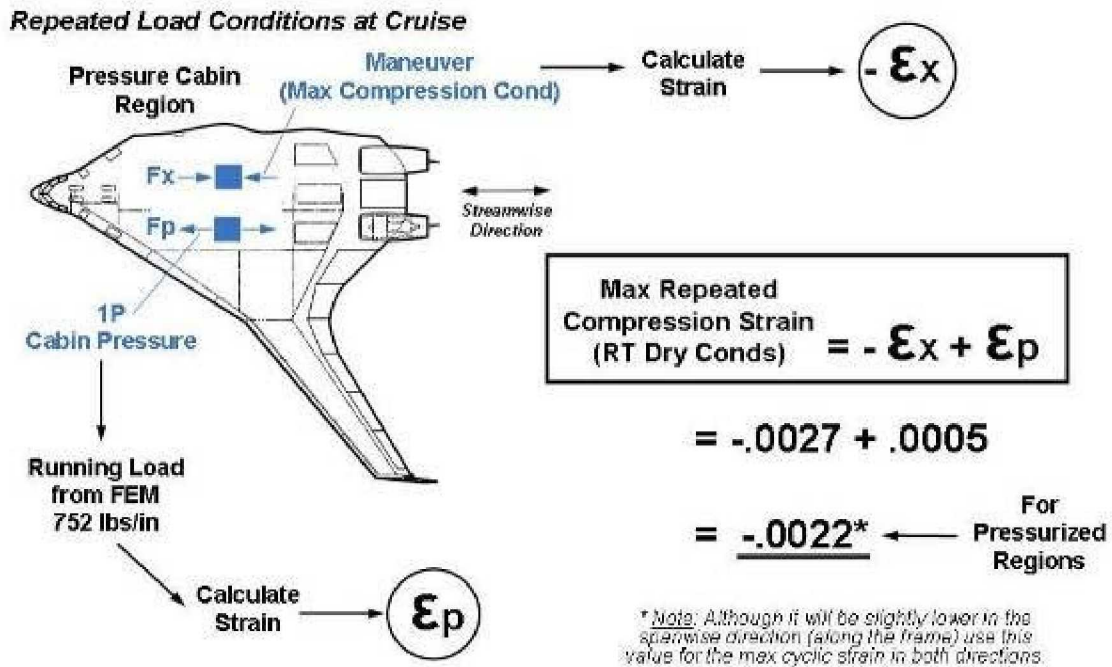


FIGURE B4. MAXIMUM REPEATED COMPRESSION STRAIN CALCULATION

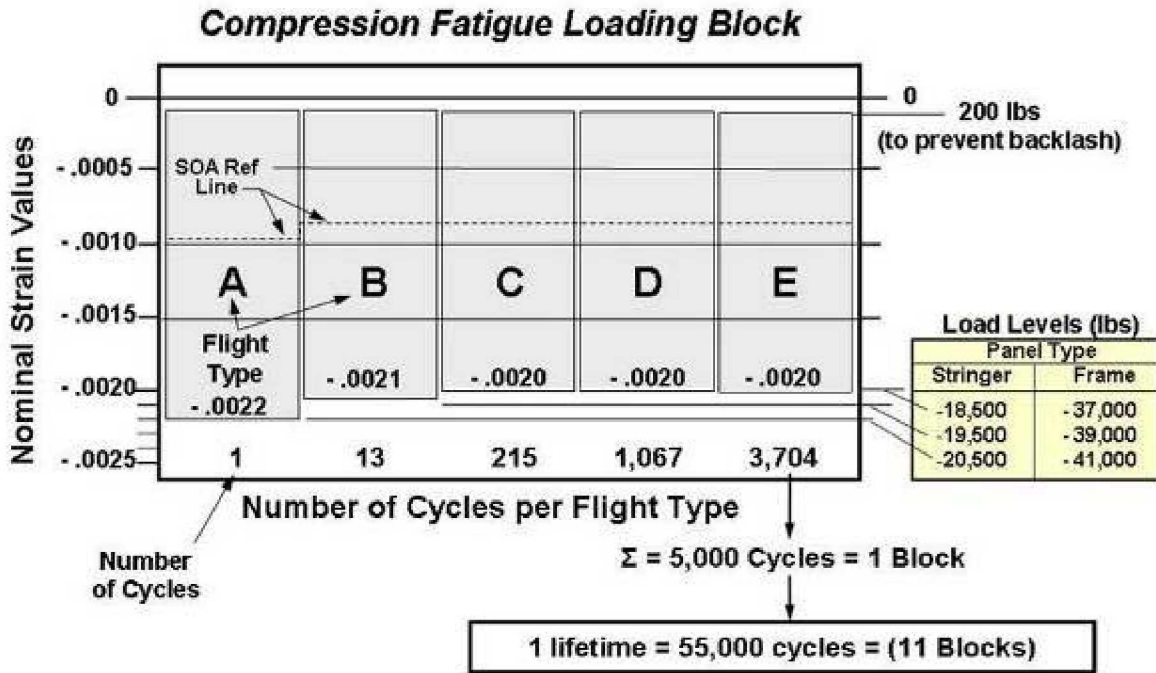


FIGURE B5. FATIGUE LOADING PROFILE FOR SPECIMENS

APPENDIX C – SINGLE-STRINGER SPECIMEN TEST DATA

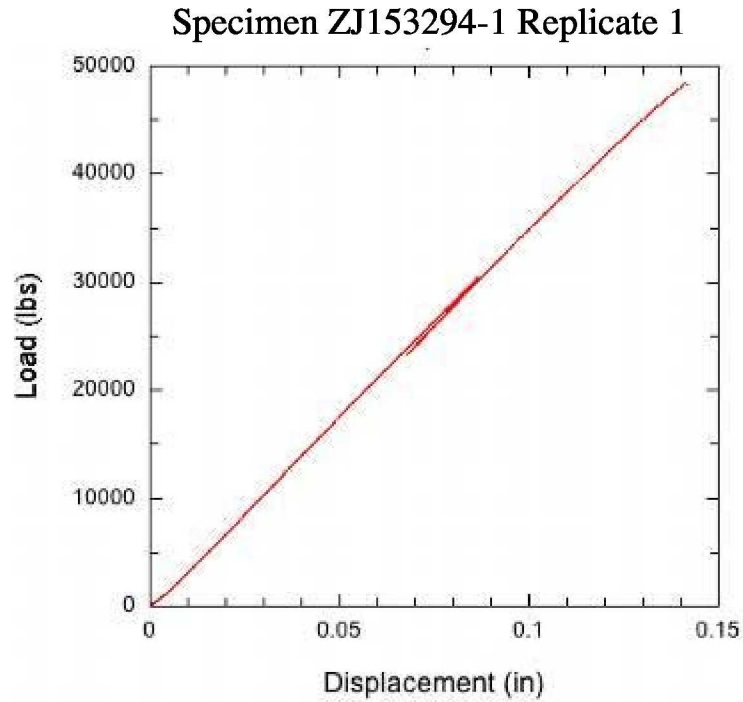


FIGURE C1. LOAD-VS-DEFLECTION PLOT - SINGLE-STRINGER REPLICATE 1

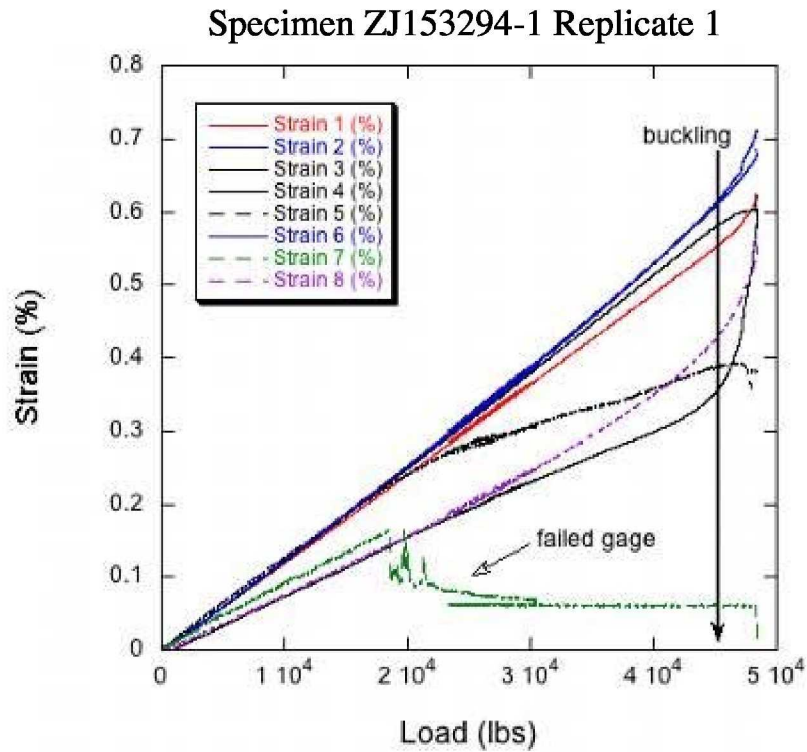


FIGURE C2. STRAIN GAGE READINGS - SINGLE-STRINGER REPLICATE 1

Specimen ZJ153294-1 Replicate 2

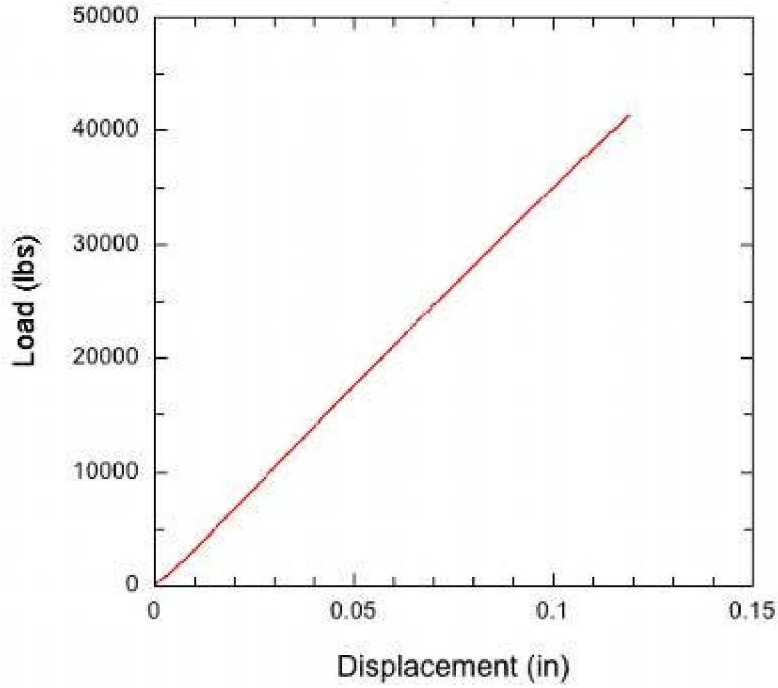


FIGURE C3. LOAD-VS-DEFLECTION PLOT - SINGLE-STRINGER REPLICATE 2

Specimen ZJ153294-1 Replicate 2

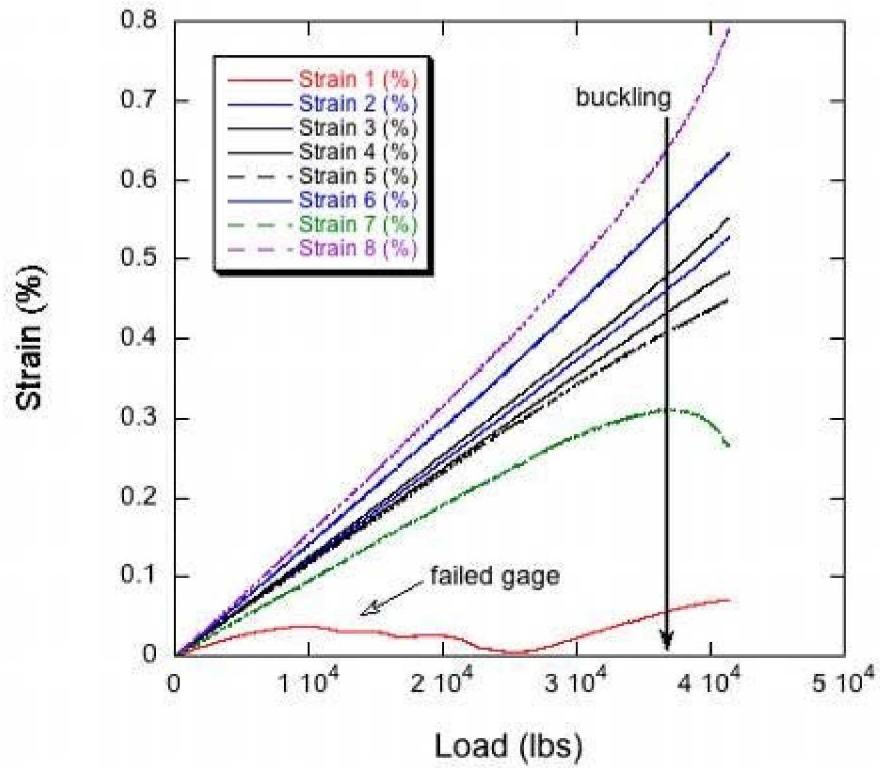


FIGURE C4. STRAIN GAGE READINGS - SINGLE-STRINGER REPLICATE 2

APPENDIX D - SINGLE-FRAME SPECIMEN TEST DATA

Specimen ZJ153294-501 Replicate 1

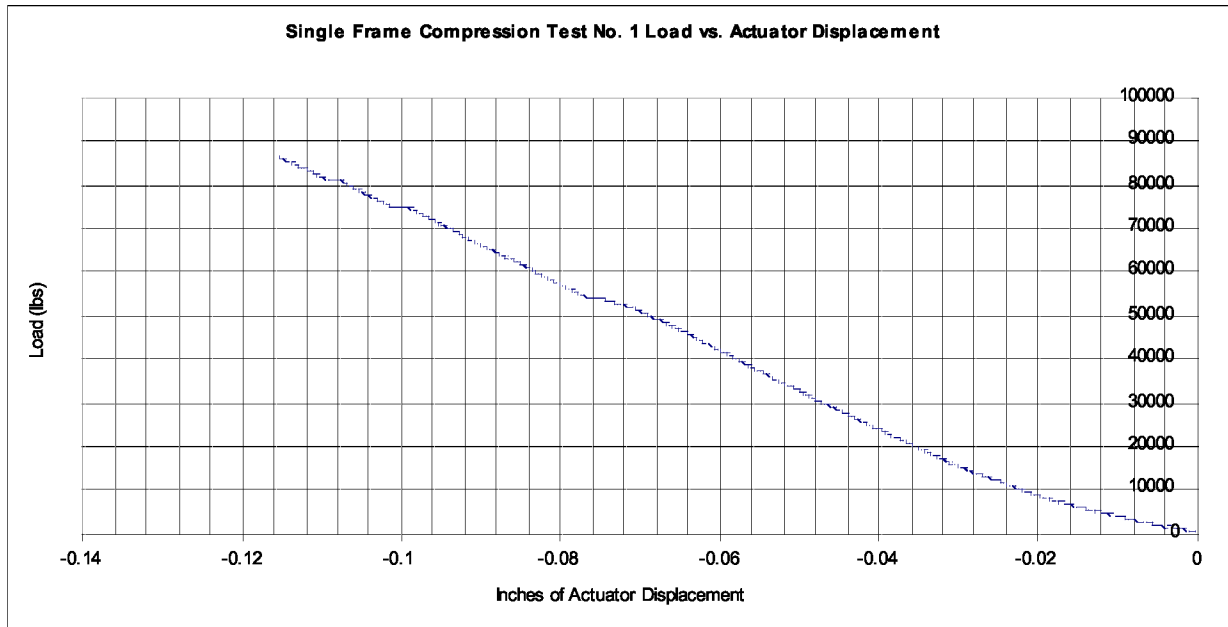


FIGURE D1. LOAD-VS-DEFLECTION PLOT - SINGLE-FRAME REPLICATE 1

Specimen ZJ153294-501 Replicate 1

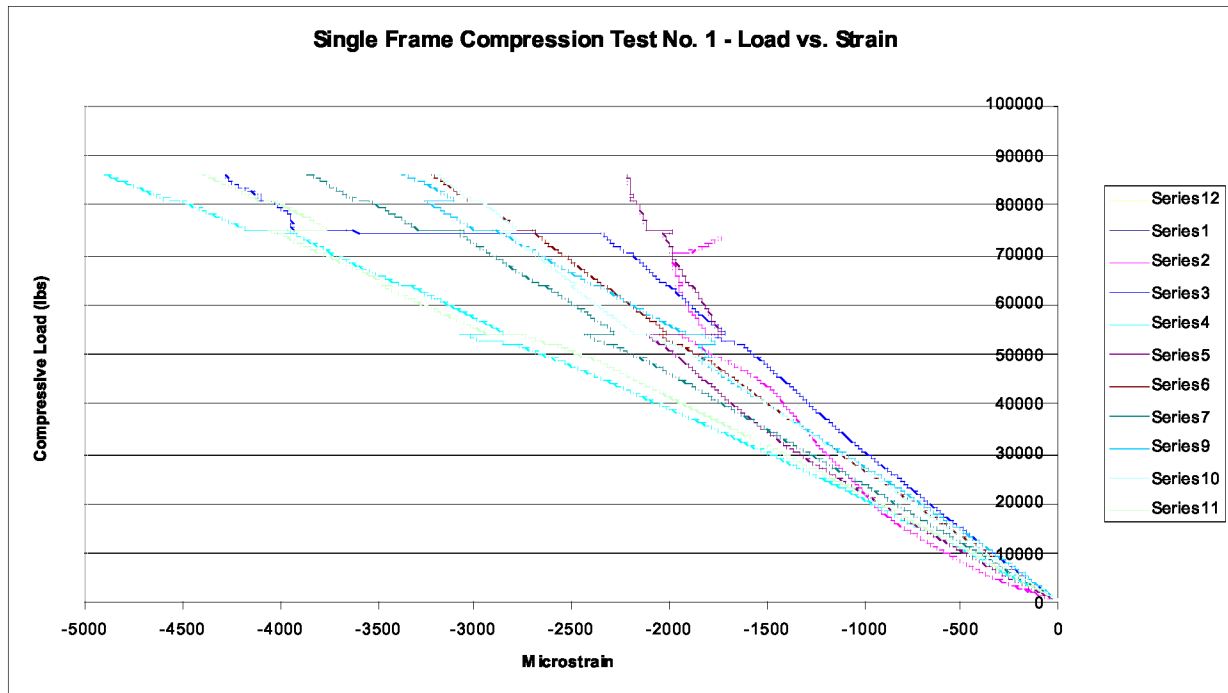


FIGURE D2. STRAIN GAGE READINGS - SINGLE-FRAME REPLICATE 1

Specimen ZJ153294-501 Replicate 1

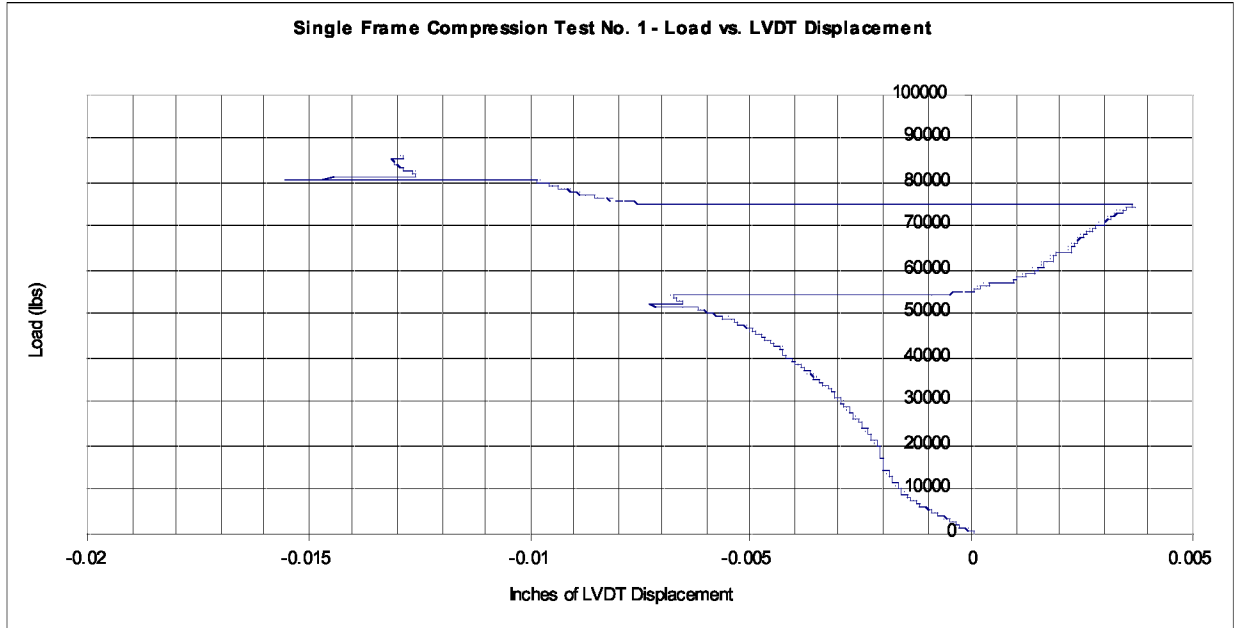


FIGURE D3. LDVT DISPLACEMENT – FRAME WEB

Specimen ZJ153294-501 Replicate 1

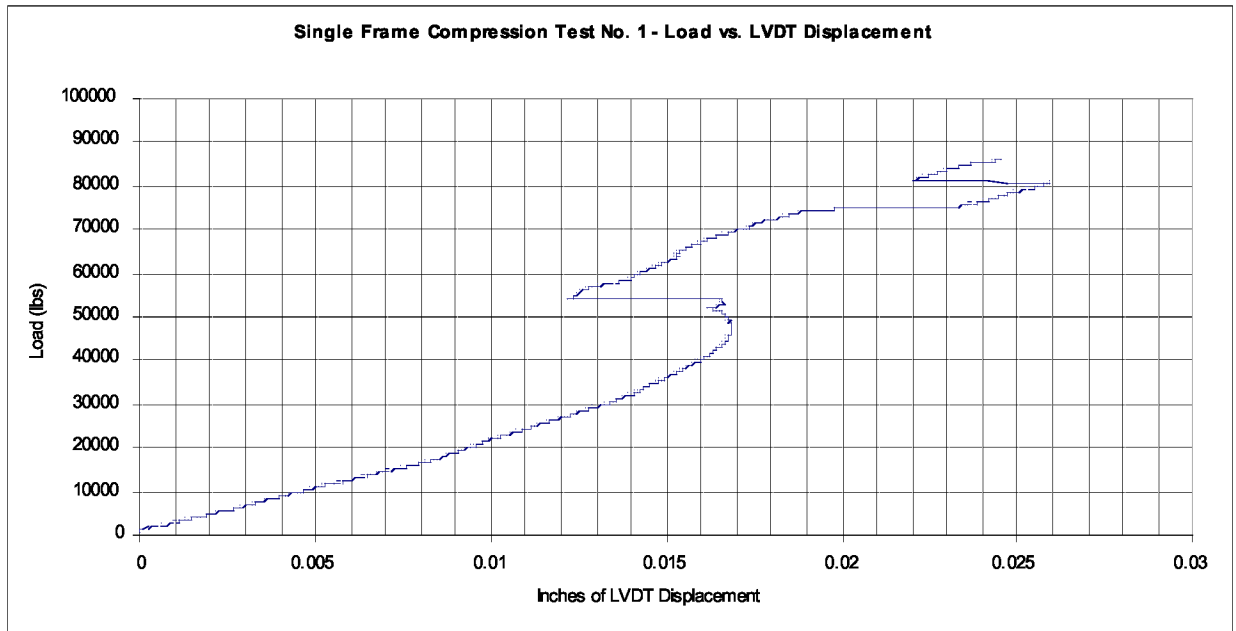


FIGURE D4. LDVT DISPLACEMENT - SKIN

Specimen ZJ153294-501 Replicate 2

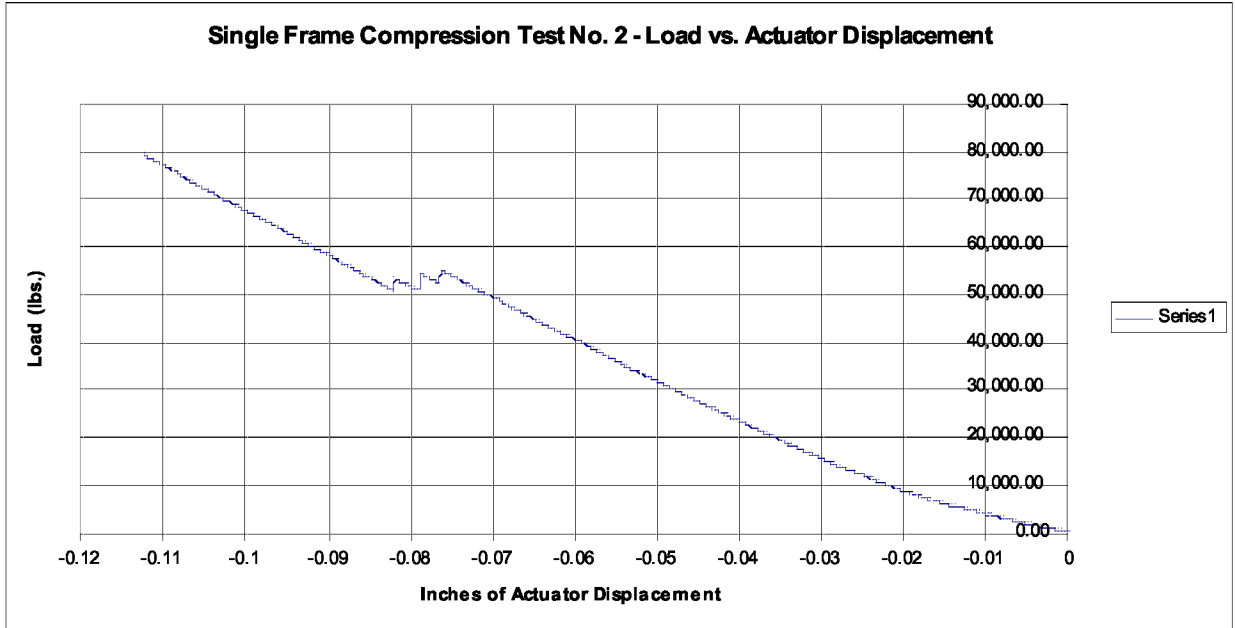


FIGURE D5. LOAD-VS-DEFLECTION PLOT - SINGLE-FRAME REPLICATE 2

Specimen ZJ153294-501 Replicate 2

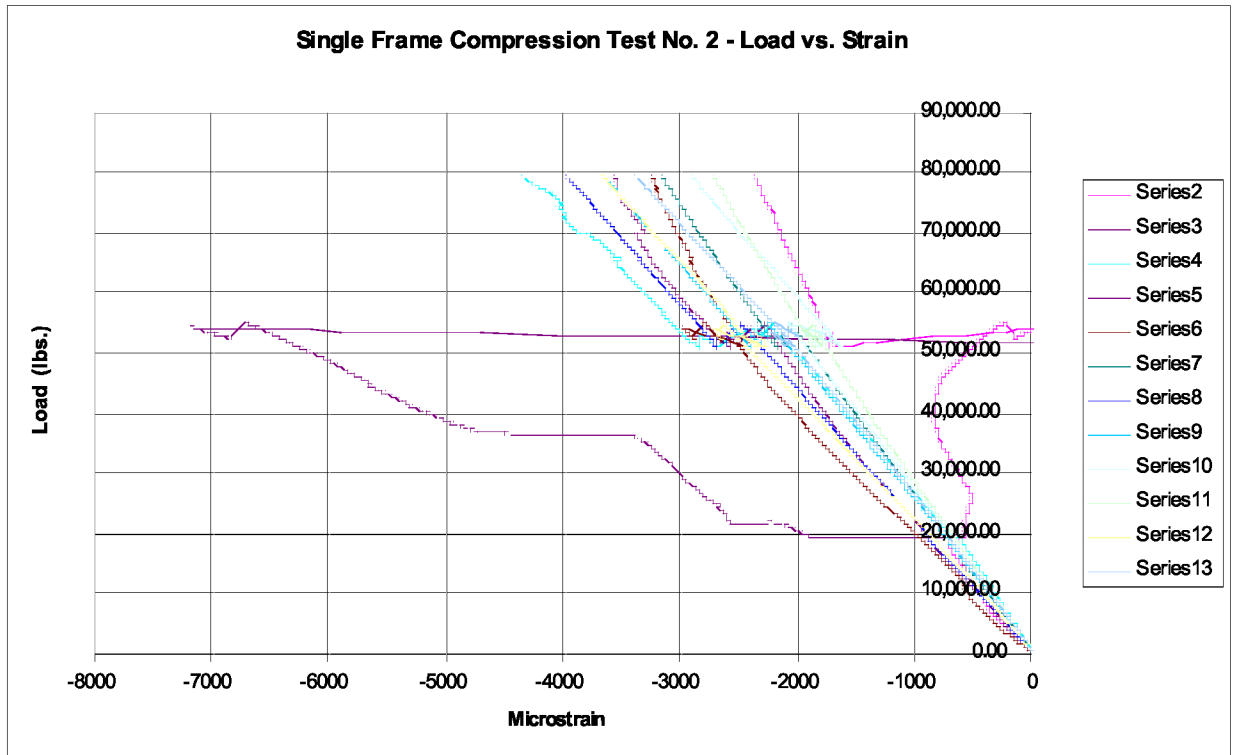


FIGURE D6. STRAIN GAGE READINGS - SINGLE-FRAME REPLICATE 2

Specimen ZJ153294-501 Replicate 2

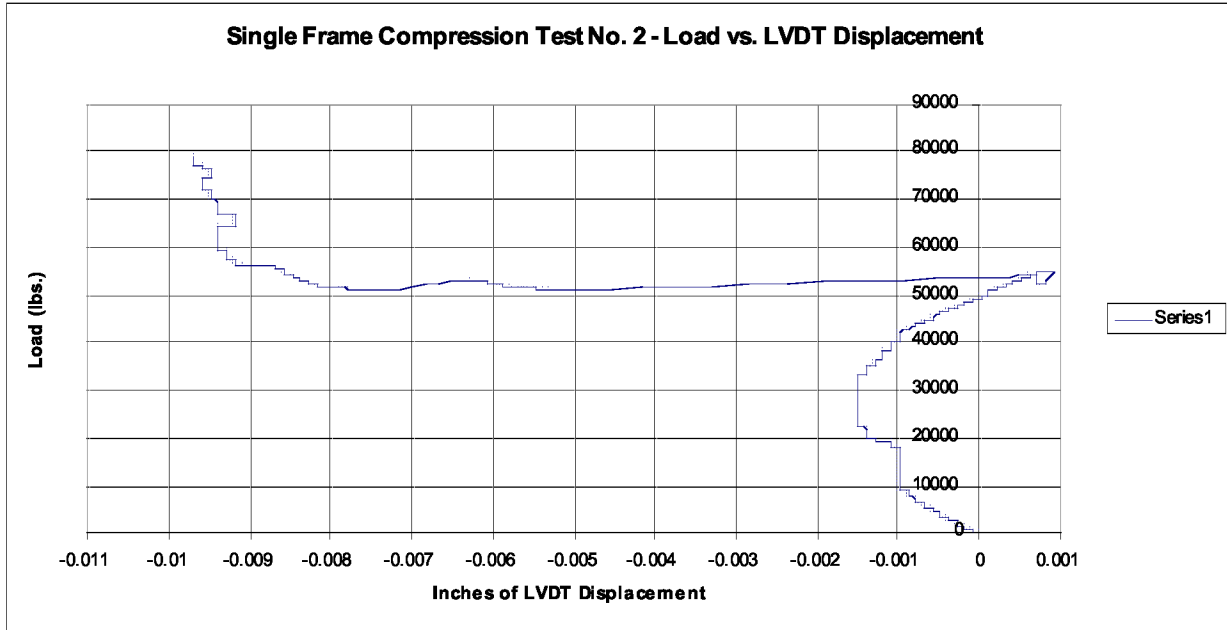


FIGURE D7. LDVT DISPLACEMENT – FRAME WEB

Specimen ZJ153294-501 Replicate 2

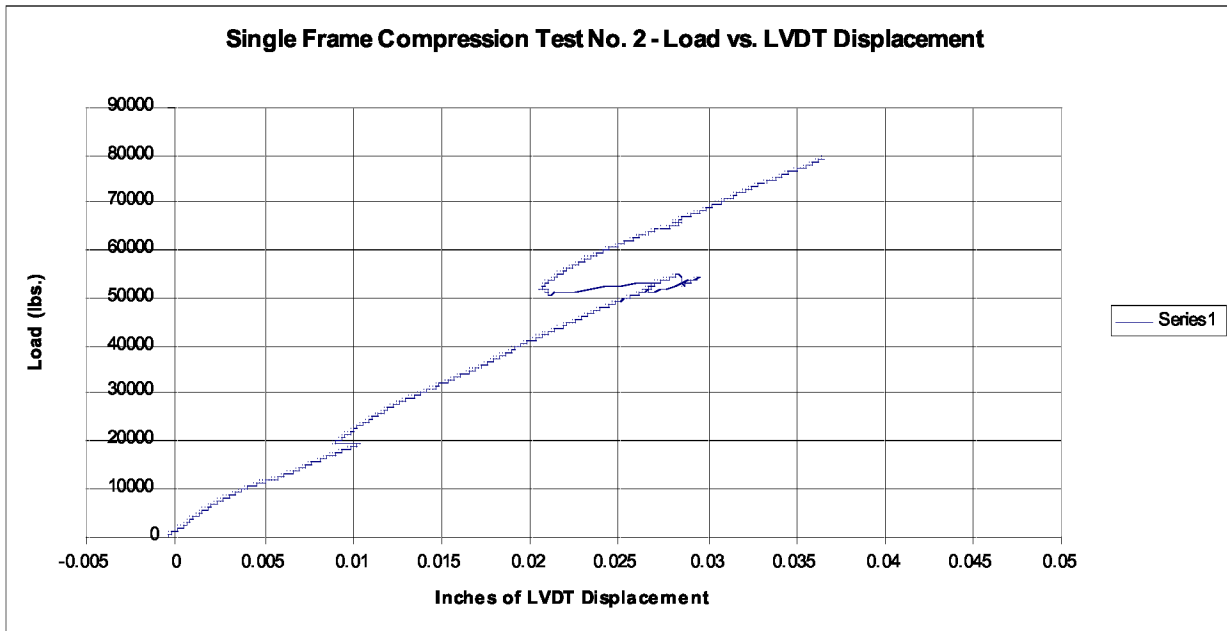


FIGURE D8. LDVT DISPLACEMENT - SKIN

REPORT DOCUMENTATION PAGE			Form Approved OMB No. 0704-0188		
<p>The public reporting burden for this collection of information is estimated to average 1 hour per response, including the time for reviewing instructions, searching existing data sources, gathering and maintaining the data needed, and completing and reviewing the collection of information. Send comments regarding this burden estimate or any other aspect of this collection of information, including suggestions for reducing this burden, to Department of Defense, Washington Headquarters Services, Directorate for Information Operations and Reports (0704-0188), 1215 Jefferson Davis Highway, Suite 1204, Arlington, VA 22202-4302. Respondents should be aware that notwithstanding any other provision of law, no person shall be subject to any penalty for failing to comply with a collection of information if it does not display a currently valid OMB control number. PLEASE DO NOT RETURN YOUR FORM TO THE ABOVE ADDRESS.</p>					
1. REPORT DATE (DD-MM-YYYY) 01-09 - 2009		2. REPORT TYPE Contractor Report		3. DATES COVERED (From - To)	
4. TITLE AND SUBTITLE Damage Arrersting Composites for Shaped Vehicles - Phase 1 Final Report			5a. CONTRACT NUMBER NNL07AA48C		
			5b. GRANT NUMBER		
			5c. PROGRAM ELEMENT NUMBER		
6. AUTHOR(S) Velicki, Alex			5d. PROJECT NUMBER Project No. 4200208122		
			5e. TASK NUMBER		
			5f. WORK UNIT NUMBER 561581.02.08.07.15.03		
7. PERFORMING ORGANIZATION NAME(S) AND ADDRESS(ES) NASA Langley Research Center Hampton, VA 23681-2199			8. PERFORMING ORGANIZATION REPORT NUMBER		
9. SPONSORING/MONITORING AGENCY NAME(S) AND ADDRESS(ES) National Aeronautics and Space Administration Washington, DC 20546-0001			10. SPONSOR/MONITOR'S ACRONYM(S) NASA		
			11. SPONSOR/MONITOR'S REPORT NUMBER(S) NASA/CR-2009-215932		
12. DISTRIBUTION/AVAILABILITY STATEMENT Unclassified - Unlimited Subject Category 39 Availability: NASA CASI (443) 757-5802					
13. SUPPLEMENTARY NOTES Langley Technical Monitor: Dawn C. Jegley					
14. ABSTRACT This report describes the development of a novel structural solution that addresses the demanding fuselage loading requirements for the Hybrid Wing or Blended Wing Body configurations that are described in NASA NRA subtopic A2A.3, "Materials and Structures for Wing Components and Non-Circular Fuselage." The phase I portion of this task includes a comprehensive finite element model-based structural sizing exercise performed using the BWB airplane configuration to generate internal loads and fuselage panel weights for an advanced Pultruded Rod Stitched Efficient Unitized Structure (PRSEUS) structural concept. An accompanying element-level test program is also described which substantiates the analytical results and calculation methods used in the trade study. The phase II plan for the continuation of this research is also included herein.					
15. SUBJECT TERMS BWB structure; CAPRI; VARTM; Buckling; Composites; Integrated structure; Pultruded rod; Stitched structure; Warp-knit fabric					
16. SECURITY CLASSIFICATION OF:			17. LIMITATION OF ABSTRACT	18. NUMBER OF PAGES	19a. NAME OF RESPONSIBLE PERSON
a. REPORT	b. ABSTRACT	c. THIS PAGE			STI Help Desk (email: help@sti.nasa.gov)
U	U	U	UU	97	19b. TELEPHONE NUMBER (Include area code) (443) 757-5802